UNDERSTANDING COASTAL MORPHODYNAMIC PATTERNS FROM DEPTH-AVERAGED SEDIMENT CONCENTRATION

F. Ribas[1], A. Falqués[1], H.E. de Swart[2], N. Dodd[3], R. Garnier[4], and D. Calvete[1]

Corresponding author: F. Ribas, Department of Applied Physics, Universitat Politècnica de Catalunya, Barcelona, Spain. (francesca.ribas@upc.edu)

[1]Department of Applied Physics, Universitat Politècnica de Catalunya, Barcelona, Spain
[2]Institute for Marine and Atmospheric research, Utrecht University, Utrecht, the Netherlands
[3]Faculty of Engineering, University of Nottingham, Nottingham, UK
[4]Instituto de Hidráulica Ambiental IH Cantabria, Universidad de Cantabria, Santander, Spain

This review highlights the important role of the depth-averaged sediment concentration (DASC) to understand the formation of a number of coastal morphodynamic features that have an alongshore rhythmic pattern: beach cusps, surf zone transverse and crescentic bars, and shoreface-connected sand ridges. We present a formulation and methodology, based on the knowledge of the DASC (which equals the sediment load divided by the water depth), that has been successfully used to understand the characteristics of these features. These sand bodies, relevant for coastal engineering and other disciplines, are located in different parts of the coastal zone and are characterized by different spatial and temporal scales, but the same technique can be used to understand them. Since the sand bodies occur in the presence of depth-averaged currents, the sediment transport approximately equals a sediment load times the current. Moreover, it is assumed that waves essentially mobilize the sediment and the current increases this mobilization and advects the sediment. In such conditions, knowing the spatial distribution of the DASC and the depth-averaged currents induced by the forcing (waves, wind, and pressure gradients) over the patterns allows inferring the convergence/divergence of sediment transport. Deposition (erosion) occurs where the current flows from areas of high to low (low to high) values of DASC. The formulation and methodology are especially useful to understand the positive feedback mechanisms between flow and morphology leading to the formation of those morphological features, but the physical mechanisms for their migration, their finite-amplitude behavior and their decay can also be explored.

1. INTRODUCTION

Coastal zones are highly valued worldwide for their natural beauty, the recreational opportunities they offer and the economic benefits that result from tourism, shipping, and fishing industries. As a result, more than half the world's population (and the percentage is growing) has settled along this narrow strip of the world's surface [*Komar*, 1998] and its preservation has turned out to be important for social, economic and ecological reasons. Sandy coasts, which are about 25% of the coasts on a global scale [*Short*, 1999], are highly dynamic, and increasing our knowledge of such complex systems is necessary to build more reliable engineering tools. Field data collected in the *swash and surf zones* and on the continental shelf of sandy coasts often reveal the presence of undulations in the sandy bed and the shoreline (hereafter referred to as *morphodynamic patterns*), indicating that they are an integral part of the coastal system. (Italicized terms are defined in the glossary, after the main text.) Many of these morphodynamic patterns show a remarkable spatial periodicity along the shore (Figure 1). Understanding the dynamics of these alongshore rhythmic patterns is important to increase our general knowledge about coastal processes and, thereby, our capacity to predict the short/long-term evolution (erosion/accretion) of the coastal system.

Crescentic bars (also called *rip-channel systems*, Figure 1a) are well known examples of alongshore rhythmic morphologic patterns that commonly occur in the surf zone [*van Enckevort et al.*, 2004, and references therein]. A crescentic bar consists of an alongshore sequence of shallower and deeper sections alternating shoreward and seaward (respectively) of a line parallel to the shore in such a way that the bar shape is undulating in plan-view. In some cases the undulation is quite subtle, the bar being almost straight, but occasionally it features pronounced crescent moons with the horns pointing shoreward and the bays (deeps) located seaward. The deeper sections are called *rip channels* because strong seaward directed currents called *rip currents* [*Dalrymple et al.*, 2011] are concentrated there. Patches of transverse bars are other distinct morphologic features observed in the surf zone [*Gelfenbaum and Brooks*, 2003; *Wright and Short*, 1984; *Ribas and Kroon*, 2007; *Pellón et al.*, 2014, and references therein] (Figures 1b,c). They consist of several sand bars that extend perpendicularly to the coast or with an oblique orientation and the alongshore distance between bars can be remarkably constant. They are typically attached to the shoreline but they have been occasionally observed attached to a *shore-parallel bar*. Patches of shoreface-connected sand ridges are examples of larger scale features that occur on the *inner shelf*. They consist of several elongated sandy bodies of a few kilometers, oriented at an angle with respect to the shoreline, and separated an approximately constant alongshore distance [*Dyer and Huntley*, 1999, and references therein]. Beach cusps are well known morphologic features with an alongshore rhythmicity that occur at the swash zone (Figure 1d). Beach cusps can be described as lunate embayments (lowered areas of beach level) separated by relatively narrow shoals or horns (raised areas of beach level) [*Coco et al.*, 1999, and references therein]. These four features are located in different parts of the coastal zone (i.e., at different water depths), and are characterized by different spatial and temporal scales, as shown in Table 1 and Figure 2.

The relevance of these alongshore rhythmic patterns for coastal engineering is being increasingly recognized for several reasons. Firstly, studying their dynamics allows identification of important physical mechanisms that control coastal evolution. In particular, it increases our understanding of the effective sediment transport in areas of the coastal zone where there is still a significant lack of knowledge on such important process (e.g., swash zone and inner surf zone) [*Soulsby*, 1997]. Secondly, these alongshore rhythmic morphodynamic patterns have a direct impact on the shoreline by creating areas of erosion and deposition [*Komar*, 1998; *MacMahan et al.*, 2006]. The presence of beach cusps and transverse bars implies an erosion of the shoreline in their embayments, and crescentic bars and shoreface-connected ridges affect wave refraction and breaking, creating patterns in the nearshore flow circulation that can cause erosional hot spots [*Sonu*, 1973; *Wright and Short*, 1984; *Benedet et al.*, 2007]. Furthermore, beach cusps are notable morphodynamic features because they occur in the swash zone, a region whose dynamics are not yet well understood but which forms the physical interface between the land and the sea, where the effects of erosion/deposition are most clearly seen. In the surf zone, sandy bars are a natural protection of the beach: waves dissipate part of their energy on the bars and the bars can also provide sand to the beach as they can migrate onshore. Furthermore, the alongshore migration of surf zone bars can cause (additional) erosion/deposition patterns near coastal structures that are generally not considered in engineering projects. It is also important to understand the horizontal circulation induced by surf zone bars since the associated currents enhance transport and exchange of pollutant or floating matter [*Castelle and Coco*, 2013]. Further, although surfers take advantage of rip currents occurring in between sand bars to move offshore, such currents are dangerous for swimmers, being one of the most lethal natural hazards worldwide [*Dalrymple et al.*, 2011]. On the continental shelf, shoreface-connected ridges are of interest to coastal engineering as sources for extraction of sand (e.g., for beach nourishment or for the construction industry) and because they are located in areas where wind turbine fields are present or planned [*van* *de Meene and van Rijn*, 2000]. Also, due to their alongshore migration, they can produce the infilling of navigation channels and affect pipeline burial. Shoreface-connected ridges also have an interest for biologists since they provide favorable conditions for benthic life and fish [*Slacum et al.*, 2010], in particular on their sheltered landward side (where grain size is smaller). From a geologic point of view, all these morphodynamic features are of interest because they lead to depositional rhythmic patterns that can be detected in the stratigraphy, and thus provide insight into the long-term evolution of the coast. In particular, shoreface-connected ridges, having evolved over thousands of years, can be traced in and dated from cores [*McBride and Moslow*, 1991].

Rhythmic morphodynamic patterns are the result of waves and currents that erode and transport sediment by exerting *shear stresses* at the sandy sea bed. The convergence/divergence of sediment transport produces bed level changes, which feedback into the wave and current fields. Rhythmic morphologic patterns grow very often due to *feedback mechanisms* (the so-called self-organization theory), without a corresponding spatial pattern in the hydrodynamic forcing (the latter being essential in the so-called template theories) [*Coco and Murray*, 2007]. The key message of the present contribution is that, despite the fact that beach cusps, surf zone bars and shoreface-connected ridges have different scales and occur in different areas of the coastal zone, they nevertheless have one important aspect in common: their formation, migration and long-term evolution can be explained by the *advection* of the *depth-averaged sediment concentration (DASC)* by the *depth-averaged current*. As each feature is associated with different types of water motion, each has its own typical spatial distribution of sediment concentration. The aim of this contribution is to highlight the important role of the spatial distribution of the DASC in the development of these alongshore rhythmic coastal morphodynamic patterns. Previous studies focusing on these distinct features will be reviewed and linked, thereby showing that, by using a specific formulation of the equations, the convergence/divergence of sediment transport can be understood in a remarkably simple way, from the joint action of the gradients in the DASC and the current perturbations produced by the evolving morphologic pattern. This formulation is a powerful tool to get insight into the underlying feedback mechanisms that explain why features with a specific spatial pattern (e.g., *up-current orientation* of shoreface-connected ridges and transverse bars, see Figure 2) grow and migrate [e.g., *Falqués et al.*, 2000; *Calvete et al.*, 2001; *Caballeria et al.*, 2002; *Ribas et al.*, 2003; *Calvete et al.*, 2005; *Dodd et al.*, 2008; *Ribas et al.*, 2012]. The physical mechanisms for the saturation of the growth of the features or for their decay can also be explored with this technique [e.g., *Garnier et al.*, 2006, 2008; *Vis-Star et al.*, 2008; *Garnier et al.*, 2013].

The first step is to present and discuss the formulation and methodology, based on the DASC, which have been successfully used to understand and model the characteristics of coastal patterns. In existing publications, different versions of this formulation were presented, corresponding to the specific morphodynamic features being studied. Here we will present the overall theory, the underlying hypotheses and the physical interpretation of the equations. The model framework and most important physical laws and processes governing the dynamics of the currents, the waves and the sediment at the coast are presented in section 2. Since this contribution focuses on the morphologic evolution, some technical details of the hydrodynamic processes will be given in appendices. The formulation of the equations, with the DASC being the main focus, is derived in section 3, and the methodology that allows understanding rhythmic pattern formation is described. The second step is to review the key studies that apply this formulation to the development of the four specific morphologic patterns mentioned above (Figure 2): crescentic bars (section 4), transverse bars (section 5), shoreface-connected sand ridges (section 6) and beach cusps (section 7). A physical and transparent explanation, based on the DASC, will be provided of why alongshore rhythmic patterns of a certain shape grow and sometimes migrate. Each of these four sections can be read independently of the others. Finally, the most important conclusions are summarized in section 8 and a list of important open issues for future research is included in section 9.

The four selected patterns have in common the presence of a coastline and an underlying topography with a cross-shore slope (sloping beach, sloping shelf), which clearly distinguishes an alongshore and a cross-shore coordinate. Also, they occur on wave-dominated sandy coasts (without vegetation) that are uninterrupted in the alongshore direction at the length scale of the studied feature. We do not cover other coastal morphodynamic patterns such as ripples, megaripples, tidal sand waves, tidal sand banks, sorted bedforms, cuspate shorelines and km-scale shoreline sand waves. A review on ripples, tidal sand banks and tidal sand waves can be found in *Blondeaux* [2001]. *Gallagher* [2011], and references therein, studied the formation of megaripples. A review on sorted bedforms (or rippled scour depressions, related to a physical mechanism based on sediment sorting) and large-scale cuspate shorelines was presented by *Coco and Murray* [2007]. Km-scale shoreline sand waves have been studied by *van den Berg et al.* [2012] and references therein.

2. COASTAL MORPHODYNAMICS, THE MODEL FRAMEWORK

Coastal morphodynamics is the research field that studies the mutual interactions between the sea bed morphology and coastal hydrodynamics through sediment transport [*Wright and Thom*, 1977]. These interactions are included in the process-based coastal area models [*Amoudry and Souza*, 2011] (Figure 3). The sea bed level and the shoreline of sandy coasts change due to the divergence/convergence of sediment transport, which itself is driven by the bed shear stresses exerted by the flow velocities related to the currents, the incoming waves and the *turbulence*. Changes in bed level in turn affect these hydrodynamic processes, so feedback mechanisms occur.

It is important to keep in mind that those processes can occur at several time scales so that the corresponding variables and equations are commonly time-averaged to just keep the dynamics at the scale of interest. In particular, each morphological feature has its own morphodynamic time scale, T_m, defined as that at which significant morphological changes occur. This scale is roughly $T_m = O(10^4 s)$ for beach cusps, $T_m = O(10^5 s)$ for surf zone bars and rip channels and $T_m = O(10^{10} s)$ for shoreface-connected sand ridges.

Figure 4 shows the frame of reference commonly used in coastal morphodynamic models. The domain represents a sea that is bounded by an alongshore uniform coast. The y-axis is oriented in the alongshore direction, the x-axis is perpendicular to it, with x the distance to the coastline and the z-axis is vertical.

2.1. Coastal sediment transport and bed evolution

Conservation of sediment mass is the key equation of coastal morphodynamics and, after some assumptions that are described in Appendix A, can be cast into

$$(1-p)\frac{\partial h}{\partial t} + \vec{\nabla} \cdot \vec{q} = 0 \ . \qquad (1)$$

Here $\vec{\nabla} = (\partial/\partial x, \partial/\partial y)$ is the horizontal nabla operator, $\vec{q}(x, y, t)$ is the *net* transport of sediment per unit width (total volume of sediment crossing the horizontal unit length per unit time, $m^2 s^{-1}$), $h(x, y, t) = z_b(x, y, t) - z_{b0}(x)$ is the bed elevation with respect to an alongshore uniform background bathymetry, $z = z_{b0}(x)$, and p is *sediment porosity* (typically $p \sim 0.4$). The adjective *net* means that $\vec{q}(x, y, t)$ results from a time-average on a time interval that is short enough with respect to the morphological time scale we are interested in. Equation (1) states that the bed level rises ($\partial h/\partial t > 0$) at the locations where sediment transport converges ($\vec{\nabla} \cdot \vec{q} < 0$) and vice versa (Figure 7).

To evaluate bed level changes sediment transport must therefore be computed. Sediment transport in the coastal environment is a complex process that depends on the mechanics of sediment grains subject to forces exerted by waves and currents. It takes place both in suspension (*suspended load*) and in contact with the bed (*bed load*, which may include *sheet flow*) [*Soulsby*, 1997]. Sediment transport is still poorly understood and hard to predict accurately [*Amoudry and Souza*, 2011], due to the complexity of the processes involved. On the other hand, field observations suggest that the dynamics of beach cusps, rhythmic surf zone bars and shoreface-connected ridges is associated to the action of intense currents involving net water mass flux. These observations motivate the working hypothesis that the net sediment transport, $\vec{q}$, depends on the *depth-averaged current*, $\vec{v}$, (net water volume flux per unit width divided by net water depth, see section 2.2) through the formula

$$\vec{q} = \alpha \vec{v} \ , \tag{2}$$

where α is the total sediment load (including bedload and suspended load). This formula is inspired by the case of suspended load transport with a vertically uniform concentration, in which case the expression is exact and α is the depth-integrated volumetric sediment concentration (m^3/m^2). As is further explained in Appendix A, additional sediment transport occurs in the cross-shore direction due to a number of sources including gravity combined with bottom slope, *wave nonlinearities* and *undertow*. Here it is assumed that the joint action of the various cross-shore sediment transport sources, not described by equation (2), determines an equilibrium cross-shore beach and inner shelf profile. This profile is chosen as the background bathymetry, $z_{b0}(x)$, and in the absence of current, $\vec{v}$, it is assumed to be stable. The possible unbalance in cross-shore sediment transport due to any deviation, $h(x, y, t)$, just tends to drive the bathymetry back to equilibrium. This is represented by a slope term that is added to equation (2), which becomes

$$\vec{q} = \alpha \vec{v} - \gamma \vec{\nabla} h \ . \tag{3}$$

The rationale behind equation (3) is that oscillatory motions mobilize (or *stir*) the sediment, due to either the orbital velocities at the bed or the turbulent vortices created by breaking waves, without producing a transport. The current increases the stirring and transports the sediment (as illustrated in Figure 6). The stirring is represented by the *sediment load* α and the slope coefficient γ, which can depend (nonlinearly) on local quantities such as the current magnitude $|\vec{v}|$, the amplitudes of the wave orbital velocity and the turbulence-induced velocity, the sediment properties and the water depth D. If the velocities at the bed are smaller than a critical value, α and γ are zero. This formulation works reasonably well, in the sense that it captures the overall characteristics of the processes [*Fredsoe and Deigaard*, 1992; *Soulsby*, 1997; *Camenen and Larroudé*, 2003]. However, it has important limitations that are discussed in detail in Appendix A. The most important are that cross-shore sediment transport plays a passive role, driving the bathymetry to the alongshore uniform equilibrium and that the sediment transport is in equilibrium with the local hydrodynamics so that possible lags are neglected.

The sediment load α in the first term of equation (3) is the total volume of sediment in motion per horizontal area unit (m^3/m^2), and can also be interpreted as a 'stirring function' [e.g., *Falqués et al.*, 2000] if this term is understood as describing sediment being stirred (by waves and currents) up to load α and then being transported by the current. Characteristic values of α range from 10^{-5} m^3/m^2, for bedload conditions, to 10^{-3} m^3/m^2, for total load conditions [*Soulsby*, 1997]. Table 2 shows examples of the α function for six standard sediment transport formulas that can be cast in the form of equation (3), all of them described in detail in *Soulsby* [1997]. An illustration of the applicability of many of these different sediment transport parameterizations (and others) is given in *Camenen and Larroudé* [2003]. As described in *Soulsby* [1997], the existing formulas have been extensively calibrated, although mostly in *wave flumes* or outside the surf zone. Under breaking waves, the strong turbulent vortices can have a significant amplitude at the bed and add to the sediment stirring by the current and the wave orbital velocity [*Voulgaris and Collins*, 2000; *Butt et al.*, 2004]. This process is not included in any of the standard sediment transport formulas (Table 2) but can be included with an adequate expression of the α function. For example, *Reniers et al.* [2004] added this process in the α of the Soulsby and van Rijn formula and *Ribas et al.* [2011] modified it and showed its importance for the dynamics of rhythmic surf zone bars. In the surf zone applications the stirring by turbulent vortices as implemented by *Ribas et al.* [2011] will be included.

2.2. Coastal hydrodynamic processes

As explained in the previous section, to calculate the sediment transport some hydrodynamic variables, such as the current, the water depth and the wave orbital velocity, must be computed. Water motion in the coastal zone occurs at different time scales. On the coasts studied here, incoming waves are the most obvious motion to the eye. The characteristic time scale of waves is provided by their period, T_w, which typically ranges between 1 and 20 s. At shorter time scales turbulent motions take place. Since the relative amount of sediment carried by the water motion is small (volumetric concentration of sediment hardly reaches $O(10^{-2})$) the bed level typically changes at a characteristic time scale (morphodynamic time scale), $T_m \gg T_w$. Therefore, it is sufficient to consider time-averaged hydrodynamic variables and thus filter out the fast dynamics at the time scales of waves and turbulence. This means that the hydrodynamics is decomposed into two components: a) mean motions and b) "fast" fluctuating motions. Of course, waves and turbulence affect the dynamics of the system but their effects are considered only through averages that are described by the corresponding hydrodynamic forces on the mean motions. Therefore, all hydrodynamic variables are time-averaged on a time scale T_w. An exception will be made when describing the dynamics of the *swash zone*, where the time average needs to be made on a shorter time scale, filtering only the turbulent motions but not the waves.

Another important assumption is that we focus on morphodynamic features located in shallow waters and the horizontal scales involved in these features are at least one order of magnitude larger than the vertical scales. It is therefore reasonable to expect that their dynamics can be understood within the framework of the depth-integrated shallow water approximation [*Phillips*, 1977; *Mei*, 1989; *Svendsen*, 2006]. Thus, the hydrodynamic variables describing the mean hydrodynamic motions (i.e., the dynamics of the water columns) are the depth-averaged current, i.e., the time-averaged water volume flux per unit width divided by the time-averaged water depth, $\vec{v}(x, y, t)$ (hereinafter simply referred to as current), and the time-averaged free surface level, $z_s(x, y, t)$.

Conservation of water mass is one of the fundamental laws for the mean hydrodynamic motions. Its depth-integrated formulation reads

$$\frac{\partial D}{\partial t} + \vec{\nabla} \cdot (D\vec{v}) = 0 \ , \tag{4}$$

where $D = z_s - z_b$ is the time-averaged water depth. The quantity $D\vec{v}$ is the volumetric flux of water per unit width entering a water column [*Svendsen*, 2006]. Equation (4) states that if there is convergence of water flux (i.e., $\vec{\nabla} \cdot (D\vec{v}) < 0$, meaning that a net quantity of water flows into the water column) an increase in water depth will occur (i.e., $\partial D/\partial t > 0$, for instance by increasing the free surface level z_s, see Figure 5a). Note that, in the swash zone, an extra term may appear on the right hand side (RHS) of equation (4), related to the infiltration of water into the bed [*Dodd et al.*, 2008].

The momentum balance for time and depth-averaged currents

$$\frac{\partial \vec{v}}{\partial t} + \vec{v} \cdot \vec{\nabla} \vec{v} = -g\vec{\nabla} z_s + \frac{\vec{\tau}_b}{\rho D} + \frac{\vec{\tau}_w}{\rho D} + \frac{1}{\rho D}\vec{\nabla} \cdot (\mathbf{R} - \mathbf{S}) \ , \tag{5}$$

is the other fundamental law governing the mean motions. The LHS (left hand side) is the horizontal acceleration of the water columns and the RHS consists of the forces per mass unit acting on them. The first term on the RHS represents the pressure gradient force per unit mass due to gradients of the free surface level. The second term involves the net bed shear stress, $\vec{\tau}_b$, which produces frictional forces on the flow and also the wind can produce forces described through the free surface shear stresses, $\vec{\tau}_w$. The turbulent

Reynolds stress tensor, **R**, and the wave radiation stress tensor, **S**, are 2D second order symmetric tensors that describe the net depth-integrated transfer of momentum that are due to turbulence and waves, respectively. Their divergence, whose x- and y-components are (e.g., $\vec{\nabla} \cdot \mathbf{S}$)

$$\frac{\partial S_{xx}}{\partial x} + \frac{\partial S_{xy}}{\partial y} \quad , \quad \frac{\partial S_{yx}}{\partial x} + \frac{\partial S_{yy}}{\partial y} \quad , \tag{6}$$

results in a force acting on the water columns. For beach cusps **S** is absent since the time average is made on a time scale shorter than T_w, filtering the turbulent motions but not the waves. Moreover, for large scale features O(1-10 km), appearing on the continental shelf, the Coriolis volumetric force is added on the RHS of equation (5).

Knowing the bed level $z_b(x, y, t)$, the system of the hydrodynamic equations (4) and (5) is not closed mainly because the stress tensors depend on the fast fluctuating hydrodynamic components, i.e., turbulence and waves. Turbulent stresses play a secondary role and are modeled with the standard eddy viscosity approach [*Svendsen*, 2006] so that they are proportional to $\nabla\vec{v}$ components through a mixing coefficient that depends on wave energy dissipation. However, wave radiation stresses are crucial in the surf zone as they provide the main driving force for the currents. They depend on *wave energy density*, on the propagation direction and on the ratio c_g/c (c_g, c being the group and phase celerities) [*Longuet-Higgins and Stewart*, 1964; *Svendsen*, 2006]. Essentially, when waves approach the coast and feel the sea bottom they start *refracting*, *shoaling* and breaking, varying their energy density and direction. These changes cause in turn gradients in the radiation stresses producing net forces on the water column. The net bed shear stresses in equation (5), τ_{bi}, are parameterized in terms of $\vec{v}$, the wave orbital velocity at the edge of the boundary layer and a friction coefficient that depends on D, sediment size and unresolved small bedforms. This is not straightforward and different options can be used [e.g., *Feddersen et al.*, 2000]. The specific equations and parameterizations used to describe the different features can be found in *Caballeria et al.* [2002] (surf zone bars), *Calvete et al.* [2001] (shoreface-connected ridges), and *Dodd et al.* [2008] (beach cusps).

Although the individual wave motions are not resolved in the present formulation, the knowledge of the time-averaged properties of waves is nevertheless crucial. These include wave energy density, energy dissipation, orbital velocity amplitude, angle and wavenumber. In fact, all these quantities can be computed in terms of the root-mean-square height, $H(x, y, t)$, the wavenumber, $k(x, y, t)$, and the wave angle, $\theta(x, y, t)$ (Figure 4) and these three variables can be evaluated using the dispersion relation, the wavenumber irrotationality and the wave energy balance. The details and the corresponding set of equations, which are subsequently coupled to equations (4) and (5), are described in Appendix B.

A common assumption regarding coastal morphodynamics is the so-called *quasi-steady approximation*. It consist of dropping out all the time derivatives from the hydrodynamic equations (4) and (5) but not from the bed evolution equation (1). It is not an essential step for the methodology explained in this contribution but it facilitates the physical interpretation of the equations. For instance, the mass conservation equation (4) becomes $\vec{\nabla} \cdot (D\vec{v}) = 0$, which means that there is no net water transport into or out from the water column. A gradient in D then implies a change in $\vec{v}$ (Figure 5b shows a 1D example of a current increase due to a decreasing water depth).

The quasi-steady assumption means that the hydrodynamics is in equilibrium with the morphology all the time, i.e., the hydrodynamic variables are assumed to adapt instantaneously to the bed level so that the former vary only when the latter changes. This assumption suppresses any oscillatory solution of equations (4) and (5) like *infragravity waves*, *shear waves*, *low frequency eddies* and tidal waves. The first three types of motion occur with periods ranging from about 20 s to O(10^3 s) [*Reniers et al.*, 2004] while tides occur at periods of O(10^4 s). The quasi-steady approximation can be applied if the oscillatory water motions do not affect significantly the morphologic evolution. This is not the case for beach cusps, which are in fact closely linked to the unsteady wave motion as it is expressed in the uprush and backwash of the waves. On the other hand, despite low frequency eddies may affect crescentic bar dynamics [*Reniers et al.*, 2004] and infragravity waves (edge waves) had earlier been thought to be the primary cause of rhythmic surf zone features (*Holman and Bowen* [1982] and others, see sections 4.2 and 5.2), it is nowadays accepted that these low-frequency oscillatory motions are not essential for the formation of rhythmic bars in the surf zone [*Blondeaux*, 2001; *Coco and Murray*, 2007]. Similarly, although tidal oscillations mildly affect the evolution of shoreface-connected sand ridges, they are not essential for explaining their formation [*Walgreen et al.*, 2002]. The quasi-steady assumption is therefore applied to understand the dynamics of surf zone rhythmic bars and shoreface-connected sand ridges.

3. FORMULATION AND METHODOLOGY BASED ON THE DEPTH-AVERAGED SEDIMENT CONCENTRATION

3.1. Bed evolution equation

A formulation of the bed evolution equation based on the *depth-averaged sediment concentration* is now derived. For this, we substitute $\vec{q}$ from equation (3) into equation (1) to obtain the so-called bed evolution equation (BEE),

$$(1-p)\frac{\partial h}{\partial t} = -D\vec{v}\cdot\vec{\nabla}\mathcal{C} - \mathcal{C}\,\vec{\nabla}\cdot(D\vec{v}) + \vec{\nabla}\cdot(\gamma\vec{\nabla}h)\ , \qquad (7)$$

where $\mathcal{C} = \alpha/D$ is the total sediment load divided by the water depth. In the present contribution, $\mathcal{C}$ is interpreted as a depth-averaged sediment concentration (DASC) and it includes both bedload and suspended load. Some authors [*Falqués et al.*, 2000] have called it 'potential stirring' but here we use the name DASC because it is related to a variable that can be measured. In the outer surf zone and the continental shelf, bottom changes occur at depths larger than O(1 m). In the inner surf zone and the swash zone, water depths range between $0.1 - 1$ m. Given that $\alpha \leq 10^{-3}$ m^3/m^2 (see section 2.1), characteristic values of $\mathcal{C}$ range from 10^{-7} to 10^{-2} m^3/m^3 ($\mathcal{C}$ could be higher only in the very shallow swash zone). The left hand side (LHS) of equation (7) quantifies the bottom changes. The first term on the RHS describes the erosion/deposition produced due to the advection of $\mathcal{C}$ by the depth-averaged current $\vec{v}$ when there are gradients of $\mathcal{C}$ (section 3.2 is devoted to explain in depth the physical interpretation of this term). The second term on the RHS describes the deposition (erosion) that occurs when water flux converges (diverges). The third term on the RHS is a slope-induced diffusive term and tends to damp the gradients in bed level.

If the quasi-steady hypothesis can be assumed (i.e., for surf zone and inner shelf features), the mass conservation equation (4) becomes $\vec{\nabla} \cdot (D\vec{v}) = 0$ (see section 2.2) and the BEE becomes

$$(1-p)\frac{\partial h}{\partial t} = -D\vec{v} \cdot \vec{\nabla}\mathcal{C} + \vec{\nabla} \cdot (\gamma \vec{\nabla} h) \ . \qquad (8)$$

In the application at the swash zone (beach cusp development), where the quasi-steady hypothesis does not hold, equation (7) is used, with an additional term related to water infiltration into the bed (see section 7). An equation similar to equation (8) was first derived and used for the nearshore by *Caballeria et al.* [2002].

3.2. Erosion/deposition processes

Equation (8) gives the time evolution of the bed level deviations at any location as a function of the water depth, D, the depth-averaged current, $\vec{v}$, and the gradient of the DASC, $\mathcal{C}$. It is not a closed equation since it needs the knowledge of $\vec{v}$ and the distribution of $\mathcal{C}$. The powerful advantage of equation (8), with respect to the original equation (1), is that it allows for an interpretation of the erosion/deposition processes, in terms of $\vec{v}$ and $\vec{\nabla}\mathcal{C}$, which might be known from field observations, from numerical simulations or just qualitatively from physical reasoning.

According to equation (8), $\vec{v} \cdot \vec{\nabla}\mathcal{C} > 0$ will tend to induce bed erosion ($\partial h/\partial t < 0$) and $\vec{v} \cdot \vec{\nabla}\mathcal{C} < 0$ will tend to induce bed accretion ($\partial h/\partial t > 0$). In words, *any current with a component in the direction of the gradient in $\mathcal{C}$ will produce erosion and any current with a component that opposes this gradient will cause accretion* (Figure 8). This behavior can be physically understood from the fact that $\mathcal{C}$ is in local equilibrium with the flow, i.e., it is the depth-averaged sediment concentration of the water column corresponding to the stirring by the local hydrodynamics (section 2.1 and Appendix A). If $\mathcal{C}$ increases along the flow ($\vec{v} \cdot \vec{\nabla}\mathcal{C} > 0$), water with little amount of $\mathcal{C}$ will move to places where the stirring by the hydrodynamics allows for larger $\mathcal{C}$. Therefore, more sediment will be picked up from the bed underneath the water column, which will hence be eroded (Figure 8a). The contrary will happen if $\mathcal{C}$ decreases along the flow (Figure 8b).

3.3. Linearized bed evolution equation

In order to understand the dominant mechanisms involved in the initial formation of the features of interest, it is convenient to assume that the state of the system is a superposition of an initially alongshore uniform steady state (the equilibrium state already defined in section 2.1) and a perturbed state, with small amplitude perturbations that evolve from the equilibrium state [*Dodd et al.*, 2003]. The equilibrium state represents the mean dynamic balance in the absence of rhythmic features. It consists of an alongshore uniform equilibrium profile $z_{b0}(x)$ (already mentioned in section 2.1), a depth-averaged sediment concentration $\mathcal{C}_0(x)$, a water depth $D_0(x)$ that includes the wind- or wave-induced set-up/set-down, and often an *alongshore current* $V_0(x)$. The set-up (set-down) is an over-elevation (under-elevation) of the free surface level in the coastal zone forced by the cross-shore transfer of momentum after waves break or by wind-induced cross-shore forces. The alongshore current is forced by the alongshore momentum transfer produced after oblique waves break, by wind-induced alongshore forces or by free surface gradients. A schematic representation of the alongshore current and the wave-induced set-up can be seen in Figure 4.

Small perturbations in bed level, $h(x, y, t)$ (the bed level deviations defined in section 2.1, but now assumed to be small), concentration, $c(x, y, t)$, depth, $d(x, y, t)$, and current, $(u(x, y, t),\ v(x, y, t))$, are added to the equilibrium. The total variables then read

$$z_b = z_{b0} + h \ , \quad \mathcal{C} = \mathcal{C}_0 + c \ , \quad D = D_0 + d \quad \text{and} \quad \vec{v} = (0, V_0) + (u, v) \ . \tag{9}$$

Substituting these expressions into equation (8) and only retaining the terms that are linear in the small quantities (u, v, c, d and h), yields the linearized BEE,

$$(1-p)\frac{\partial h}{\partial t} = -D_0 u \frac{d\mathcal{C}_0}{dx} - D_0 V_0 \frac{\partial c}{\partial y} + \frac{\partial}{\partial x}\left(\gamma_0 \frac{\partial h}{\partial x}\right) + \frac{\partial}{\partial y}\left(\gamma_0 \frac{\partial h}{\partial y}\right) \ . \tag{10}$$

Here γ_0 is the equilibrium value of the γ coefficient in equation (8).

Equation (10) shows that the small bed level changes of a known equilibrium state can be analyzed just from the perturbations that the bottom produces in the cross-shore component of the current, u, and the alongshore gradients of the perturbation of the DASC, $\partial c/\partial y$. The first RHS term of equation (10) leads to deposition (erosion) if $u\, d\mathcal{C}_0/dx$ is negative (positive). The second RHS term of equation (10) leads to deposition (erosion) if $V_0\, \partial c/\partial y$ is negative (positive). Note that if $V_0 = 0$, the second RHS term disappears and erosion/deposition processes only depend on u and the cross-shore gradient of the equilibrium DASC, $d\mathcal{C}_0/dx$. The last two RHS terms of equation (10) have a diffusive effect on the bed perturbations. The first derivation of a linearized BEE similar to equation (10) for the nearshore was made by *Falqués et al.* [1996].

3.4. Erosion/deposition patterns: global analysis

The equations and analysis of the previous sections, based purely on equations (8) or (10), are local in the sense that these equations describe the bed level evolution in one location due to local convergence/divergence of the sediment transport. Since this contribution aims at understanding the development of morphologic patterns that grow and migrate on the whole domain, it is essential to understand the erosion/deposition patterns occurring on the whole domain. As an example, given a morphological feature consisting of alongshore alternating bars and troughs, Figure 9 shows what erosion/deposition patterns would produce (a) pure growth, (b) growth and down-drift migration, (c) pure down-drift migration, (d) decay and down-drift migration, and (e) pure decay of the feature. Thereby, it is essential to analyze the effect integrated on the whole domain of the different terms in equations (8) or (10) in order to evaluate their influence on growth, decay or migration of the features. As a first step, this can be done in a qualitative way, i.e., by visual observation of the erosion/deposition patterns created by each of the terms (and comparing with the patterns in Figure 9). For instance, in the case of the first term on the RHS of equation (8), and consistently with the local analysis presented in section 3.2, if the regions with $h > 0$ and the current opposing the gradients in DASC (or $h < 0$ and the current running with the gradients in DASC) dominate over the regions where the contrary occurs, this term will contribute to the growth of the feature. Alternatively, a quantitative global analysis of the equations can be performed by taking a specific average over the horizontal domain of the different terms in equations (8) or (10). The global effect of each term on the development of the morphological patterns can then be studied quantitatively. The technical details of how such a quantitative global analysis is performed are given in Appendix C.

In the next sections it will be demonstrated that, for a wide range of alongshore rhythmic morphological patterns, the global effect of the first RHS term of equation (10) essentially contributes to the initial growth of the features, the second RHS term essentially contributes to their alongshore migration (in the presence of an alongshore current), and the last two terms produce decay of the features. This is a powerful result: the 'spontaneous' breaking of alongshore uniformity of the nearshore bathymetry and the emergence of alongshore rhythmic morphological patterns can be understood by knowing only the cross-shore gradient of the equilibrium DASC, $d\mathcal{C}_0/dx$ and the cross-shore perturbation of the induced horizontal currents, u (first RHS term of equation (10)).

3.5. Methodology to use the DASC to explain pattern development

The development of four different alongshore rhythmic morphodynamic patterns are explained in the next sections: two surf zone patterns (crescentic bars and transverse bars), one at the continental shelf (shoreface-connected ridges) and one at the swash zone (beach cusps). The following three steps are taken to use the DASC to understand the formation of these morphological patterns.

First, it is essential to have information on the gradients in DASC. This quantity is difficult to measure in the surf zone due to the highly complex dynamics of sediment transport under breaking waves [*Soulsby*, 1997] and it is also highly unknown in the swash zone. Thereby, very often the formulations are inferred from laboratory data and theoretical reasoning. Different parameterizations found in the literature (like those in Table 2) lead to different results for $\mathcal{C}$, which can strongly affect the morphological changes. Here, physical reasons will be presented as to what $\mathcal{C}$ profiles are expected in the areas where features develop. Also, one of the formulas in Table 2 (which has been extensively calibrated against data) will be applied to substantiate the reasoning. Since the bed evolution depends on the gradients of the concentration (section 3.2), it is crucial that the parameterizations of sediment transport adequately represent not only the magnitude of DASC, but especially the gradients of DASC.

Second, some information on the hydrodynamics induced by the growing feature is needed. This information can be obtained by measurements and/or with the hydrodynamic module of the morphodynamic models. The latter is usually quite robust, i.e., there is little difference between the different models, even though different parameterizations are used for the bed shear stresses, the turbulence-induced effects, wave energy dissipation through breaking, etc. Here, the focus will be on describing the horizontal currents (and especially the cross-shore component u) associated with each feature, discussing in a qualitative way the essential physical processes that create these currents.

Third, a global analysis (either qualitative or quantitative) of the linearized BEE (10) must be performed in order to understand the erosion/deposition patterns, created by the joint action of the horizontal currents and the gradients in DASC, that causes the initial formation of the features. This allows understanding the initial shape of the pattern, its initial growth and migration rates, and under which climate conditions the feature develops.

Finally, a global analysis (either qualitative or quantitative) of the nonlinear BEE (8) is performed to understand the finite amplitude behavior of the features: *saturation of the growth* and changes in shape and migration rate. In some cases, this analysis also allows explaining the destruction of the features by certain climate conditions.

4. CRESCENTIC BARS

4.1. Characteristics of observed crescentic bars (and rip channels)

Crescentic bars are located in the surf zone of micro to meso-tidal sandy beaches [*Lippmann and Holman*, 1990; *van Enckevort et al.*, 2004; *Lafon et al.*, 2004] (Figures 1a and 2g). The alongshore spacing between crescentic bar horns is relatively constant for a specific system. They have been reported at different scales with a mean spacing ranging from tens of m up to 2-3 km. Crescentic bars are sometimes also called rip channel systems because the rip channels are a striking and well known characteristic of them [*van Enckevort and Ruessink*, 2003]. Note, however, that rip channels, i.e., bed depressions or cross-shore oriented channels in the surf zone where rip currents concentrate, can also be observed without the presence of crescentic bars (see, e.g., *MacMahan et al.* [2005] and also section 5).

Crescentic bars are linked to shore-parallel bars, which are alongshore uniform sand bars parallel to the coast. The latter form in medium sand beaches during high-energy wave events. Crescentic bars develop out of the shore-parallel bar during decreasing wave energy (Figure 10), i.e., during post-storm conditions. In the widely accepted beach state classification [*Wright and Short*, 1984; *Lippmann and Holman*, 1990], such process is classified as the down state transition from the Longshore Bar and Trough state to the *Rhythmic Bar and Beach (RBB) state.* Crescentic bars can become shore-parallel again in the reverse (up state) transition if wave energy increases again (Figure 10). The latter process is called bar straightening or morphologic reset. Recent studies have stressed the effect of wave obliquity in the transitions between shore-parallel and crescentic bars, revisiting the traditional classification of *Wright and Short* [1984]. They found that crescentic bars seem to develop preferably for normal wave incidence and bar straightening occurs for highly oblique waves [*Holman et al.*, 2006; *Thornton et al.*, 2007; *Splinter et al.*, 2011; *Price and Ruessink*, 2011].

Along beaches with crescentic bars the shoreline often features undulations with a similar alongshore spacing. Since this spacing is typically significantly larger than the one of ordinary beach cusps, these undulations are called megacusps [*Thornton et al.*, 2007]. The horns of the crescentic bars can connect to the shoreline and to the megacusp system during long-lasting conditions of low wave energy (down state transition from the RBB state to the *Transverse Bar and Rip (TBR) state* [*Wright and Short*, 1984; *Ranasinghe et al.*, 2004]). The resulting transverse bar system is a particular case of the four different types of transverse bar systems that will be discussed in section 5.

4.2. Existing theories for their formation

The origin of crescentic bars was first explained with the so-called hydrodynamic template theory, in which the morphologic pattern is the result of a pre-existing similar pattern in the hydrodynamics [see the review by *Coco and Murray*, 2007]. More specifically, their formation was attributed to the pattern of near-bed velocities associated with *edge waves* [*Bowen and Inman*, 1971; *Holman and Bowen*, 1982], which are alongshore propagating trapped waves. Edge waves with alongshore spacings at the crescentic bar scale can be generated by infragravity oscillations associated with the incident wind or swell waves. However, more recent studies have shown that the edge wave hypothesis is only partially consistent with available field data [*Coco and Murray*, 2007].

The second theory, which was first suggested by *Hino* [1974], is that crescentic bars emerge as a *morphodynamic instability* of the system with a shore-parallel bar. That is, they emerge from a positive feedback between wave-driven currents and morphology, starting from any perturbation of the featureless state. The first study modeling the formation of a crescentic bar from a shore-parallel bar by *self-organization* was that of *Deigaard et al.* [1999]. *Falqués et al.* [2000] described in more detail the physical mechanisms involved, emphasizing the role of the depth-averaged sediment concentration (called potential stirring in that paper). The instability mechanism was called 'bed-surf instability' (term introduced by *Falqués et al.* [1996]) because it is essentially due to the positive feedback between the sea bed perturbations and the distribution of wave breaking. Later on, *Calvete et al.* [2005] used a more realistic model that reproduced many of the observed characteristics of crescentic bars and confirmed the important role of the DASC in crescentic bar formation. The self-organized origin of crescentic bars has been supported by numerous other modeling studies [*Caballeria et al.*, 2002; *Damgaard et al.*, 2002; *Ranas-*

inghe et al., 2004; *Reniers et al.*, 2004; *Klein and Schuttelaars*, 2006; *Garnier et al.*, 2008; *Smit et al.*, 2008] making this theory currently more widely accepted than the hydrodynamic template theory. In the next section, the role of the DASC in the transformation of shore-parallel bars into crescentic bars will be discussed based on the studies of *Falqués et al.* [2000], *Calvete et al.* [2005] and *Garnier et al.* [2008].

4.3. Role of DASC in the formation mechanism

For the sake of simplicity, and since crescentic bars mainly develop for relatively small wave incidence angles, the focus of this section is on the case of normally incident waves (i.e., no alongshore current, $V_0 = 0$). The case of oblique waves will be discussed later in section 4.4. As explained in section 3, the joint effect of the gradients in DASC and the horizontal circulation induced by the growing feature creates the erosion/deposition patterns that explain why the feature grows. The three steps of the methodology (section 3.5) to explain crescentic bar formation when $V_0 = 0$ are: 1) describing the cross-shore distribution of the DASC (i.e., $d\mathcal{C}_0/dx$), 2) understanding the horizontal circulation induced by the growing feature (i.e., u), and 3) analyzing the erosion/deposition patterns with the linearized BEE (10) and the knowledge of $d\mathcal{C}_0/dx$ and u. These steps are done in the three following subsections.

4.3.1. Depth-averaged sediment concentration profile

As stated before, measuring the sediment concentration in the surf zone is difficult, hence available data are scarce. However, the theory presented here is based on a simple and robust property of the sediment concentration in the surf zone of barred beaches. For moderate wave conditions, waves break predominantly over the shore-parallel bar inducing a strong sediment concentration over it. This intuitive property is confirmed by most of the sediment transport formula applied for the surf zone. More precisely, in surf zones that are characterized by a shore-parallel bar waves can break on the bar (somewhat seaward of it) if they have a sufficient height (Figure 11). This causes an intense sediment resuspension in that area (by wave orbital velocities and turbulent vortices, if included), i.e., the sediment load α (equation 3) is maximum at a certain point on the seaward flank of the bar. Furthermore, the water depth has a local minimum at the top of the bar and increases onshore and offshore of the crest. Therefore, the depth-averaged concentration (DASC, $\mathcal{C} = \alpha/D$) is maximum at a location $x = x_m$ slightly seaward from the crest. Thus, there is an offshore-directed gradient in $\mathcal{C}$ for $x < x_m$ and an onshore-directed gradient for $x > x_m$. This qualitative behavior is reproduced by all the formulations for nearshore sediment transport included in Table 2. As an example, the middle panel of Figure 11 shows the DASC profile obtained with the Soulsby-van Rijn formula [*Soulsby*, 1997], extended to include an extra sediment stirring produced by turbulent vortices [*Reniers et al.*, 2004; *Ribas et al.*, 2011].

4.3.2. Rip current circulation

The horizontal circulation that is produced over an incipient crescentic bar (i.e., a shore-parallel bar with small-amplitude channels) is the well known rip current circulation. For normally or nearly normal wave incidence, breaking waves over the small-amplitude crescentic bar induce a circulation cell with offshore flow at the channels and onshore flow at the *shoals* (Figure 12a). This is a robust characteristic that has been observed in the field [*MacMahan et al.*, 2006; *Moulton et al.*, 2013] and in wave-basin experiments [*Haller et al.*, 2002; *Castelle et al.*, 2010a], and that is also commonly reproduced by models [*Garnier et al.*, 2008; *Dalrymple et al.*, 2011]. Thereby, the cross-shore flow perturbation

u (equation 10) can be assumed to have its maximum seaward-directed value ($u > 0$) in the channels (i.e., where $h < 0$) and its maximum shoreward-directed value ($u < 0$) over the shoals (i.e., where $h > 0$). The basic physics underlying this circulation is explained in Appendix D.

4.3.3. Formation mechanism

Now, the joint morphodynamic effect of the gradients in DASC ($\mathcal{C}$) and the horizontal circulation can be inferred from the linearized BEE (10). Since we focus on the case of normally incident waves, there is no alongshore current in the equilibrium state ($V_0 = 0$) and the second RHS term of equation (10) drops out. The gradient in $\mathcal{C}$ is offshore-directed over the bar crest, where the current flows onshore (negative u, see Figure 12a). Thereby, $u\, d\mathcal{C}_0/dx < 0$ in equation (10), which means that the current carries sediment from offshore, where $\mathcal{C}$ is largest, to the shoal (see section 3.2 and Figure 8). In the channels, it is the other way around: the current flows offshore and it carries sediment from the channel to offshore. In this way, the circulation will further erode the channels and deposit the sand on the shoals. Thus a positive feedback will occur that will enhance both the circulation and the bed undulation and the initially shore-parallel bar will develop rip channels flanked by shoals (Figure 12b). In addition to that, and given that the position of the maximum in DASC, $x = x_m$, is close to the crest, the rip currents extend offshore of this location and cause deposition of sediment seaward of it because the gradient in $\mathcal{C}$ has an opposite sign there. Similarly, the onshore flowing part of the circulation will cause erosion seaward of the shoals. Thus, the combination of the DASC and the circulation creates not only channels and shoals on the bar but a mirrored pattern offshore of the bar (Figure 12b). The addition of the initial shore-parallel bar and the double rows of alternating shoals and channels produces an undulation of the bar in plan-view, with onshore protruding sections coinciding with the shoals over the bar and offshore protruding sections at the rip channels. This is the typical crescentic bar morphology (Figure 10).

4.4. Finite amplitude behavior

The self-organization models cited in section 4.2 are able to reproduce the initial formation of the crescentic bars with the appropriate shape, but they are unable to explain the saturation of growth of crescentic bars. The latter process was first simulated by *Garnier et al.* [2008] (Figure 13). The specific mechanisms for the growth saturation were explained by *Garnier et al.* [2010] with the use of the global analysis (methodology described in Appendix C). The saturation of bar height, preventing the accreting shoals to reach the sea surface, occurs mainly due to a weakening of the positive feedback (term $-D\vec{v} \cdot \nabla \mathcal{C}$ in equation (8)) rather than to an increase of the damping caused by the diffusive transport. The positive feedback weakens but does not vanish: it balances with the diffusive term (which remains constant), and therefore the latter is also essential to the saturation process. The weakening of the positive feedback is related to changes in bar shape rather than to the growth in amplitude. It turns out that the most important change in shape is that the shoals widen and the channels narrow. More details of the global analysis applied to the full saturation of crescentic bars are given in Appendix E. Furthermore, the shoals shift shoreward and the channels seaward with the result that the bars move overall onshore. This last result shows that the current circulation associated with well developed crescentic bars system contributes to the attachment of the crescentic bars to the shore observed in the field [*Ranasinghe et al.*, 2004; *Garnier et al.*, 2008].

Another important finite amplitude behavior of the crescentic bar systems is the bar straightening. Using the global analysis, *Garnier et al.* [2013] explained why a developed crescentic bar straightens due to wave obliquity. Oblique waves inhibit the formation of rip channels and straighten crescentic bars because they weaken the rip current intensity and cause a down-wave shift of the rips with respect to the channels (i.e., a phase lag between the rips and the channels). This weakens the positive feedback between flow and morphology given by the term $-D\vec{v} \cdot \nabla\mathcal{C}$ in equation (8). A more detailed explanation is included in Appendix E.

4.5. Discussion

All the analysis presented so far in this section concerns a single crescentic bar system. In nature, two crescentic bars can coexist in the same beach at different cross-shore positions [*van Enckevort et al.*, 2004; *Castelle et al.*, 2007; *Price and Ruessink*, 2011]. In general, such double bars do not behave independently. The outer crescentic bar may emerge from self-organization (independently of the inner bar), it then induces alongshore variability in the onshore hydrodynamics, which in turn forces the morphologic response of the inner bar. This behavior is called morphologic coupling [*Castelle et al.*, 2010b]. It is important to notice that even in the case of morphologic coupling, the self-organization feedbacks between flow and morphology described in section 4.3 still affect the evolution of both bars [*Coco and Calvete*, 2009; *Thiebot et al.*, 2012]. Particularly, for a double crescentic bar system the DASC profile exhibits a local maximum over each bar system.

Although the present contribution is dedicated to rhythmic patterns observed in open beaches, it should be stated that crescentic bars are also observed in embayed beaches [*Short*, 1999; *Holman et al.*, 2006] that are beaches laterally bounded by headlands or coastal structures. The presence and characteristics of those bars are then conditioned by the length of the beach (i.e., distance between headlands) but they still seem to emerge from the basic positive feedback described in section 4.3 [*Castelle and Coco*, 2012].

The results presented in this section are taken from previous studies that consider idealized simplified conditions. Particularly these studies consider an initial bathymetry that is alongshore uniform [*Falqués et al.*, 2000; *Garnier et al.*, 2008, 2010] or a bathymetry with a very specific variability [*Garnier et al.*, 2013]. Furthermore, the incoming wave field is assumed to be time invariant and alongshore uniform. Other modeling studies have discussed the variability in the wave forcing [*Reniers et al.*, 2004; *Castelle and Ruessink*, 2011] or in the initial bathymetry [*Tiessen et al.*, 2011; *Smit et al.*, 2012]. They show that this affects the characteristics (e.g., spacing between rip channels) and the dynamics (e.g., growth times) of the crescentic bars. However, the feedbacks between flow and morphology associated with the advection of DASC by the rip currents described in section 4.3 still play a key role.

5. TRANSVERSE BARS

5.1. Characteristics of observed transverse bars

Apart from the crescentic bars discussed in section 4, the surf zone can also display another kind of morphodynamic feature consisting of several transverse bars separated by an approximately constant alongshore distance (Figures 1b,c and 2f). The alongshore spacing is defined as the distance between successive bar crests. They are typically attached to the shoreline and extend into the seaward direction, either approximately perpendicular to the coastline or with a certain oblique orientation if an alongshore current is present. If the crests are shifted in (against) the direction of the alongshore current we use the term *down-current* (*up-current*) *oriented bars* (Figure 14). However, we use the general term transverse bars to refer to all of them, a term introduced by *Shepard* [1952] to distinguish them from the shore-parallel bars. In the presence of an alongshore current, they migrate downdrift with migration rates up to 40 m/day [*Hunter et al.*, 1979; *Konicki and Holman*, 2000; *Ribas and Kroon*, 2007; *Pellón et al.*, 2014]. Amplitudes (from a point in the bar crest to a point in the trough) can range from 0.3 to 2 m [*Konicki and Holman*, 2000; *De Melo Apoluceno et al.*, 2002; *Pellón et al.*, 2014; *Gelfenbaum and Brooks*, 2003]. In some cases, the bars have been observed to show an asymmetry of the alongshore shape (the down-current flank being steeper than the up-current flank [*Pellón et al.*, 2014]). Various types of transverse bars (in their characteristics and origin) have been reported in the literature (Table 3). In order to distinguish between them, we first follow the classification made by *Pellón et al.* [2014], based on the differences in bar length scales and in the environment where they are observed.

Type (1): TBR bars. The most common type is that conforming the transverse bar and rip (TBR) state in the standard beach state classifications [*Wright and Short*, 1984; *Lippmann and Holman*, 1990; *Castelle et al.*, 2007]. The TBR bars are commonly observed in open beaches under medium-energy conditions. They are typically wide and short-crested (Figure 1b) and their origin is the merging of a crescentic bar into the beach [*Sonu*, 1973; *Wright and Short*, 1984] (they have been mentioned in section 4.1), so that their spacing is strongly related to that of the pre-existing crescentic bar. They can be approximately perpendicular to the shore [*Hunter et al.*, 1979; *Wright and Short*, 1984] or down-current oriented (Figure 14b) when incoming waves arrive with a predominant obliquity [*Lafon et al.*, 2004; *Castelle et al.*, 2006]. As in the case of crescentic bars, TBR bars also show strong and narrow rip currents flowing seaward in the troughs and wider and weaker onshore flows over the crests [*Short*, 1999].

Type (2): Medium energy finger bars. These transverse bars (Figure 14d) have been observed in open microtidal beaches under medium-energy conditions [*Konicki and Holman*, 2000; *Ribas and Kroon*, 2007; *Ribas et al.*, 2014] and they always coexist with shore-parallel (or crescentic) bars. The term finger bars refers to their thin and elongated nature, and distinguishes them from the wider and shorter TBR bars. These bars are ephemeral (residence time from one day to one month), attached to the low-tide shoreline or, occasionally, to the shore-parallel bar [*Konicki and Holman*, 2000; *Price and Ruessink*, 2011]. *Ribas and Kroon* [2007] and *Ribas et al.* [2014] have shown that they are linked to the presence of obliquely incident waves that create a significant alongshore current and that they are up-current oriented.

Type (3): Low energy finger bars. These transverse bars (Figure 14c) are persistent features in fetch-limited beaches without a shore-parallel bar [*Falqués*, 1989; *Bruner and Smosna*, 1989; *Eliot et al.*, 2006; *Pellón et al.*, 2014]. Only *Bruner and Smosna* [1989] and *Pellón et al.* [2014] gave information concerning both their orientation and the forcing direction. At the two sites, the bars were down-current oriented with respect to the alongshore current generated by the wind-waves.

Type (4): Large scale finger bars. These transverse bars (Figure 14a) are characterized by long cross-shore spans of O(1 km) and develop across both the surf and the *shoaling zone*. They are generally observed to be persistent features in low-energy microtidal environments [*Niederoda and Tanner*, 1970; *Gelfenbaum and Brooks*, 2003], typically oriented almost perpendicular to the shore. Although their dynamics is less understood, the wave focusing caused by refraction of normal incident waves by the bars seems to be essential [*Niederoda and Tanner*, 1970]. The recent study of *Levoy et al.* [2013] describes bars with similar cross-shore spans, but in a macrotidal medium-energy environment. Consequently, such bars can be governed by different drivers and will not be dealt specifically in the present study.

Table 4 shows an alternative classification of transverse bars based on their orientation, an important property that will turn out to depend critically on the DASC profile. The orientation down-current or up-current is sometimes difficult to differentiate in the field as this require the identification of the main forcing, so only the sites where the latter has been identified are included in Table 4. For this, a forcing analysis must be performed if the incoming waves have two dominant directions or in the presence of tidal currents [*Pellón et al.*, 2014]. The slope of the part of the beach where the bars appear is also indicated in Table 4. The shore-normal large-scale finger bars appear on flat terraces (e.g., slope of 0.003). The beach profiles below the shore-normal TBR bars and the down-current bars are similar: gentle-sloping upper (or low-tide) terraces. Up-current bars appear for larger beach slopes (0.02-0.04) in the subtidal zone [*Ribas et al.*, 2014].

5.2. Existing theories for their formation

As occurred for the case of crescentic bars (section 4.2), during the 80's and the 90's the formation of rhythmic patches of transverse bars was commonly conceived to be caused by hydrodynamic template models, in which rhythmic morphologic patterns are forced solely by edge waves [e.g., *Holman and Bowen*, 1982]. However, as discussed by *Coco and Murray* [2007], such theory is hardly consistent with observations by a number of reasons, the most outstanding being that the template theory neglect the (strong) interactions between the hydrodynamics and the evolving bed level. In addition, in case of oblique wave incidence, the edge waves are progressive and they would cause a nonstationary flow pattern that moves much faster than the transverse bars migrating downdrift.

During the last two decades other hypotheses have been preferentially adopted. A first distinction has to be made between the TBR bars, which form from the welding to the shore of a previous crescentic bar [*Ranasinghe et al.*, 2004; *Garnier et al.*, 2008], and the finger bars, which grow from alongshore uniform conditions. The hypothesis that will be here adopted for the formation of transverse finger bars is that the feedback between components of the fluid/topography system can lead to their development (self-organization hypothesis, first proposed by *Sonu* [1968]). Some of the initial studies in this line of thought [*Barcilon and Lau*, 1973; *Hino*, 1974; *Christensen et al.*, 1994; *Falqués et al.*, 1996] had important shortcomings but were certainly pioneering and distinguished between the bed-flow instability (term introduced by *Falqués et al.* [1996] to refer to the positive feedback between the sea bed and an alongshore current) and the bed-surf instability (positive feedback between the bed and the breaking waves, already described in section 4.3). The subsequent studies [*Caballeria et al.*, 2002; *Ribas et al.*, 2003; *Klein and Schuttelaars*, 2005; *van Leeuwen et al.*, 2006; *Garnier et al.*, 2006; *Ribas et al.*, 2012] have been more satisfactory: shore-normal, up-current and down-current oriented bars with realistic spacings have been obtained and the self-organization mechanisms underlying transverse bar formation and the role of DASC have been explained in more detail. The knowledge gained in these studies is discussed in the next section.

5.3. Role of DASC in the formation mechanism

As explained in section 3, the joint effect of the gradients in DASC and the horizontal circulation induced by the growing feature creates the erosion/deposition patterns that explain why the feature grows. The case of transverse bars is more complicated than that of crescentic bars (section 4.3) for two reasons. Firstly, there are different types of transverse bars with distinct orientations and growing under different beach conditions (Table 4). Secondly, some of them develop with the presence of an alongshore current, V_0. The three steps of the methodology (section 3.5) to explain pattern formation from the first RHS term of equation (10) are taken in the three following subsections. At the end, the role of the second RHS term of that equation (important if $V_0 \neq 0$) is discussed.

5.3.1. Depth-averaged sediment concentration profile

The sediment concentration profiles, corresponding to the beach conditions in the different types of transverse bars, are here described based on simple physical arguments, similar as in section 4.3.1. Shore-normal and down-current oriented bars typically emerge in terraced profiles with gentle slopes under normal and oblique waves (section 5.1). Waves dissipate their energy slowly across a wide saturated surf zone (Figure 15a), with the wave orbital velocity amplitude decreasing onshore across the surf zone. In the case of oblique wave incidence, an alongshore current is also generated, which typically has a maximum somewhere in the middle of the surf zone. Under such conditions, the combined action of the wave orbital velocities, the depth-averaged current (and the turbulent vortices, if included) will produce a DASC profile, $\mathcal{C}(x)$, that has a maximum somewhere in the outer part of the surf zone. Thereby, across the terrace there is an offshore-directed gradient of $\mathcal{C}$. This behavior is reproduced by all the formulas given in Table 2. As an example, the third panel of Figure 15a shows the DASC profile obtained with the Soulsby-van

Rijn formula [*Soulsby*, 1997], extended to include an extra sediment stirring produced by turbulent vortices [*Reniers et al.*, 2004; *Ribas et al.*, 2011].

On the other hand, up-current oriented bars occur in the steepest parts of profiles with shore-parallel bars (section 5.1), either in the inner surf zone or in the seaward side of the bar. In such situation, incident waves shoal before the crest of the shore-parallel bar (thereby increasing the orbital velocity amplitude), break over the bar, then reform over the trough and finally break again in the inner surf zone (Figure 15b). The $\mathcal{C}$ profile across the shore-parallel bar, with a local maximum slightly seaward of the crest, has already been discussed in section 4.3.1. Somewhere in the inner surf zone, a second local maximum in $\mathcal{C}(x)$ is also obtained, related with the second breaker zone. The type of breaking occurring there and the fact that waves dissipate their remaining energy in a relatively narrow area, with strong breaking-induced turbulent vortices, can make that the latter contribute significantly to the sediment resuspension (third panel of Figure 15b). Such process can increase significantly the DASC across the inner surf zone. Also, the second local maximum in the alongshore current profile in such relatively steep inner surf zones can be quite close to the shoreline. For all these reasons, the second local maximum in $\mathcal{C}(x)$ is found very close to the shoreline and there is an onshore-directed gradient of $\mathcal{C}$ across the inner surf zone (Figure 15b). No experimental validation of the DASC profile in such complex natural surf zones is presently available.

5.3.2. Horizontal flow pattern over transverse bars

The horizontal circulation that occurs over incipient transverse bars depends critically on the orientation of the bars (blue streamlines in Figure 16). Such circulation is well established for the TBR bars and it is the same type of rip current circulation occurring over crescentic bars (discussed in section 4.3.2). Rip current flow seaward in the troughs between bars (either shore-normal or down-current oriented) and onshore currents are observed over the bars [*Wright and Short*, 1984; *MacMahan et al.*, 2006; *Dalrymple et al.*, 2011] (Figure 16a). For the case of large-scale finger bars and low-energy finger bars, observations of the induced currents are scarce but they indicate the same type of circulation as for the TBR bars. An interesting experiment in a laboratory wave basin was made by *Niederoda and Tanner* [1970]. On a shore-normal (short-crested) finger bar, an onshore current was measured over the bar crest, which diverged close to the beach to flow in the seaward direction through the troughs. An onshore-directed current over the crest of a low-energy finger bar (with a shore-oblique orientation) was also observed in the field by *Falqués* [1989].

The physical processes driving the hydrodynamic circulation over approximately shore-normal transverse bars can be qualitatively explained from wave-induced forces. Focusing of wave energy due to refraction and wave breaking is enhanced over transverse bars and this creates onshore directed currents (model studies that support this explanation are *Caballeria et al.* [2002] and *van Leeuwen et al.* [2006]). Such currents are forced to diverge near the shoreline into two alongshore parallel feeder currents that converge in the trough and flow seaward as a rip current (similar to the case of crescentic bars, see Appendix D).

In the case of shore-oblique finger bars, which always coexist with a significant alongshore current (Table 4), other hydrodynamic processes that induce a meandering of the alongshore current can be more important. Due to frictional forces and mass conservation, the current experiences a seaward deflection over up-current oriented bars and a shoreward deflection over the up-current troughs (Figure 16c), as explained in more detail in

Appendix F. No observations of such current circulation induced by up-current oriented finger bars in open beaches are available but model confirmation was given by *Ribas et al.* [2003], *Garnier et al.* [2006], and *Ribas et al.* [2012]. Such circulation (current deflection over up-current bars) opposes the one due to wave-induced forces and is only dominant for obliquely incident waves. In the case of down-current oriented bars, the alongshore current experiences the opposite deflection, veering towards the shore over the crests and towards the sea over the troughs (Figure 16b), so that the corresponding current perturbations are reinforced by those created by wave-induced forces.

5.3.3. Formation mechanism and transverse bar orientation

The cross-shore profile of the DASC plays a crucial role in explaining the orientation of the growing transverse bars. Indeed, according to the first RHS term of the linearized BEE (10), for seaward increasing $\mathcal{C}$ ($d\mathcal{C}_0/dx > 0$) a shoreward current perturbation ($u < 0$) causes sediment deposition and a seaward current perturbation ($u > 0$) causes erosion. Since this is the type of flow occurring on the crests and troughs, respectively, of shore-normal or down-current oriented bars, (Figure 16a,b), a positive feedback between flow and morphology occurs making the bar system grow. Note that shore-normal or down-current oriented bars are observed on terraced planar beaches, where $d\mathcal{C}_0/dx > 0$ across the terrace (Figure 15a). In other words, shore-normal/down-current bars are formed because the onshore-directed flows over their crests carry sediment from offshore, where $\mathcal{C}$ is largest, to the crests (see also Figure 8). This formation mechanism is similar to that of crescentic bars (discussed in section 4.3.3). Such a growth mechanism can be dominant for shore-normal waves and oblique waves because both the meandering of the alongshore current over down-current bars and the wave-induced forces create an onshore current perturbation over the crests. Notice that the origin of TBR bars is the merging of a pre-existing crescentic bar into the beach, i.e., they do not grow from an alongshore uniform planar beach. However, the mechanism described in this paragraph, based on the DASC profile, explains why such TBR bars can maintain their shape without being destroyed, being the most frequently occurring beach state in some beaches (e.g., 55% in Palm beach, Australia, with a residence time of some 20 days [*Ranasinghe et al.*, 2004]).

In contrast, for shoreward increasing $\mathcal{C}$ ($d\mathcal{C}_0/dx < 0$) a seaward ($u > 0$) current perturbation causes sediment deposition and a shoreward current perturbation ($u < 0$) causes erosion. This is the type of flow occurring on the crests and troughs, respectively, of up-current oriented bars (Figure 16c). A positive feedback therefore takes place and the bars grow. Note that up-current oriented bars are observed in steep inner surf zones and seaward slopes of shore-parallel bars, where $d\mathcal{C}_0/dx < 0$ (Figure 15b). This mechanism only works if the angle of wave incidence is large. If waves are less oblique, the meandering of the alongshore current that creates a positive u over the up-current oriented crests become less effective whilst the wave-induced forces (onshore-directed over the crests) become more effective, inhibiting bar growth.

Whilst the role of the first RHS term of equation (10) is mainly related to the growth or decay of the bars, the second RHS term of that equation turns out to be mainly related to the migration of the bars [*Garnier et al.*, 2006; *Ribas et al.*, 2012]. Thereby, analyzing transverse bar migration is more complicated because it depends on the alongshore gradients of the perturbations of the DASC. The migration direction depends on the alongshore phase shift between the bathymetry and the perturbation of the depth-averaged concentration, c. If the maximum of c is located around the crests of the bars this term will produce pure downdrift migration (like in Figure 9c). The picture is even more complicated because, often, the first RHS term of equation (10) not only explains the growth but also adds to the migration (in case of an alongshore phase shift between the maximum in u and the maximum in h).

5.4. Finite amplitude behavior

Garnier et al. [2006] reproduced, for the first time, the saturation of growth of transverse bars (with all possible orientations, see Figure 17). The overall characteristics of finite-amplitude bars were similar to those of the initially growing bars, only differences up to a factor of 2 occurred in spacings and migration rates. The shape of finite amplitude bars included typical nonlinear characteristics like the asymmetry of the alongshore shape, as observed in the field [*Pellón et al.*, 2014], and the asymmetry between offshore flow (rip current) and onshore flow, in accordance to observed rip current systems [*Short*, 1999]. Other nonlinear phenomena like merging of individual bars, and oscillatory behavior (dynamic equilibrium) was also reproduced. *Garnier et al.* [2006] also made for the first time a quantitative global analysis (see Appendix C) to understand the physical reasons for the saturation of transverse bar growth. Essentially, two possible different scenarios were found for the saturation: (i) the damping term, related with the downslope gravitational transport (the second RHS term in equation (8)), strengthens so that it eventually balances the instability source or (ii) the production term, related with the instability due to the gradients in DASC (the first RHS term in equation (8)), weakens so that it becomes balanced by the damping term. This means that saturation can occur, depending on the type of transverse bars, either because the finite-amplitude shape of the bars enhances downslope transport (i) or because it weakens the instability mechanism (ii).

5.5. Discussion

An important aspect that deserves discussion is that in the modeling studies on transverse bar formation that included the sediment stirring by turbulent vortices [e.g., *Ribas et al.*, 2012], the perturbations of the sediment load α (equation 3) were neglected. Numerical experiments in which these perturbations were maintained resulted in an output that was highly sensitive to numerical parameters (number of grid points and their distribution over the computational domain). This model behavior was in line with that of models for the initial formation of shoreface-connected sand ridges (section 6.5) when perturbations in sediment stirring by waves were included [e.g., *Vis-Star et al.*, 2007]. Given that these numerical instabilities were not standard (e.g., due to a too large timestep), this suggests that the presently available sediment transport formulations are not yet sufficiently accurate to correctly describe spatial variations in α due to the bars. As a consequence, the role of the perturbations of α into the second RHS term of equation (10) is unknown to a great extent. Some insight has been provided by *Thiebot et al.* [2012], who modeled the nonlinear development of rhythmic surf zone bars, including the perturbations of α, in a beach with two shore-parallel bars. In the case of oblique waves with a large angle of incidence, they reproduced the formation of down-current oriented bars at the inner surf zone (where $d\mathcal{C}_0/dx > 0$, so in agreement with the theory presented here). However, they showed that the second RHS term of equation (10) also contributed significantly to bar growth.

6. SHOREFACE-CONNECTED SAND RIDGES

6.1. Characteristics of observed shoreface-connected sand ridges

These large-scale bed forms (horizontal extents of several km) are observed on inner continental shelves (depths of 5-80 m) with a sandy bottom and where storms frequently occur (Figure 18). Inner shelves are characterized by a transverse bottom slope of about 1 m/km, i.e., substantially smaller than that in the surf zone, but much larger than that on the outer shelf. Shoreface-connected sand ridges, hereafter called 'ridges', occur on both meso-tidal and micro-tidal shelves and manifest themselves in patches. They are for example present on shelves along the east coast of the United States [*Duane et al.*, 1972; *Swift et al.*, 1985], Argentina [*Parker et al.*, 1982], Germany [*Antia*, 1996] and the Netherlands [*van de Meene and van Rijn*, 2000].

The ridges have an along-shelf spacing between successive crests that varies from 1 km to 8 km. They have asymmetrical profiles, with their steepest slope on the landward sides, where their sediment is relatively coarse. Heights of the ridges are in the range 1-12 m and they migrate in the direction of the storm-driven currents with velocities of 1-10 m yr^{-1}. Interestingly, their crests are persistently up-current oriented with respect to the wind-driven alongshore current that occurs during storms. *Swift et al.* [1978] already pointed out that these facts suggests that the ridges evolve during storms, when high waves and intense storm-driven currents cause abundant erosion and transport of sand. In contrast, during fair weather conditions the ridges would be inactive, because bottom shear-stresses do not exceed the critical stress for erosion of sand. Some ridges turn out to be moribund features, i.e., they are no longer active under present-day hydrodynamic conditions [*Goff et al.*, 1999].

Other large-scale bed forms that occur on continental shelves are tidal sand ridges. Although their dimensions are similar to those of shoreface-connected sand ridges, they appear on outer shelves and when tidal currents are stronger than 0.5 m s^{-1}. Furthermore, the orientation of tidal sand ridges is related to tidal currents, in the sense that they are rotated cyclonically with respect to the direction of the dominant tidal current [see *Dyer and Huntley*, 1999, and references herein]. The focus of this section is on shoreface-connected sand ridges, as their formation is related to gradients in the DASC.

6.2. Existing theories for their formation

A number of theories have been suggested to explain the origin of shoreface-connected sand ridges. In early studies it was argued that they could be relict features from before the Holocene transgression [e.g., *Swift et al.*, 1972], or that they evolved from relict features [e.g., *McBride and Moslow*, 1991], such as former dunes and ebb-tidal deltas, which were flooded due to the rising sea level and subsequently being reworked by waves and currents. Indeed, observations have shown that sediment transport during storm conditions is significant in ridge areas [*Swift et al.*, 1978]. For example, the ridges along the east coast of the US and on Dutch inner shelf started to form several thousands years ago and they are active under the present hydrodynamic conditions [*Swift et al.*, 1978; *Duane et al.*, 1972; *van de Meene and van Rijn*, 2000].

Although there is nowadays ample evidence that many ridges are not relict features, there is less consensus about the dominant physical processes that control their evolution. *Swift et al.* [1978] suggested that helical circulation cells in the vertical plane might transport sand from troughs to crests, thereby resulting in a positive feedback. In this study it was also stated that tides would not be a primary forcing agent of the ridges, as the latter occur on both micro-tidal and meso-tidal inners shelves. *Niedoroda et al.* [1985] argued that during storms the ridges receive sand from the nearshore zone, because the wind creates downwelling conditions leading to an offshore-directed (Ekman) flow near the bottom. This sand would be subsequently reworked by waves and currents.

A limitation of the studies cited above is that they did not demonstrate how ridges would form and what mechanism explains their characteristics. In this regard, a major step forward was made by *Trowbridge* [1995], who demonstrated, by means of a linear stability analysis, that formation of bed forms resembling ridges can be simulated with a model that governs interactions between storm-driven currents and the sandy bed on an idealized inner shelf with a sloping bottom (Figure 4). His model assumed bed load sediment transport to be a constant times the current velocity. The constant reflects the spatially uniform stirring of sediment by waves. Subsequent investigations, based on linear stability analyses, have shown that the growth of the ridges is mainly caused by suspended load transport [*Calvete et al.*, 2001] and that the effect of wave shoaling and refraction, resulting in spatially non-uniform stirring of sediment, is to enhance their growth [*Vis-Star et al.*, 2007]. The effect of tides on the initial formation of the ridges, subject to both bed load and suspended load transport, was examined by *Walgreen et al.* [2002]. They showed that tidal currents only mildly affected the shoreface-connected sand ridges and merely resulted in tidal sand ridges on the outer shelf. These findings supported the earlier hypothesis of *Swift et al.* [1978]. When accounting for different grain sizes [*Walgreen et al.*, 2003], the model was capable of explaining the observed distribution of mean grain size over the sand ridges (coarser sediment on the landward side of the crests). Here, the concepts of *Trowbridge* [1995] and follow-up studies will be discussed in more detail, because they highlight again the importance of gradients in the DASC for the dynamics of these bed forms, whilst at the same time explaining many aspects of observed ridges.

6.3. Role of DASC in the formation mechanism

The role of the DASC in the physical mechanism underlying the initial growth and orientation of shoreface-connected sand ridges can be understood following the three steps of the methodology (section 3.5). This is done in the next subsections, emphasizing the details required to understand ridge formation. Migration is also discussed at the end.

6.3.1. Depth-averaged sediment concentration profile

Consider the situation during storms, as shown in Figure 19, when the sediment is stirred by the waves and a storm-driven current (typically of order 0.5 m s^{-1}) flows along the coast. Under these conditions, the sediment transport is proportional to the sediment load α and the current as described by equation (3). The sediment load will decrease in the offshore direction, because waves will be less efficient in stirring sand from the bottom, and the DASC ($\mathcal{C} = \alpha/D$) will decrease in the offshore direction as well.

6.3.2. Horizontal flow pattern over ridges

When the storm-driven current encounters an up-current oriented ridge, conservation of water mass will force the flow component perpendicular to the ridge to increase, causing an offshore deflection of the current over the ridges. Likewise, the current will have an onshore component in the troughs. The result is a meandering storm-driven flow. This mechanism also acts in the case of up-current transverse finger bars and it was described in section 5.3.2 and, in more detail, in Appendix F.

6.3.3. Formation mechanism

From the considerations above, it immediately follows that in the ridge areas the gradient of the DASC has a negative projection on the current $\vec{v}$ (i.e., $\vec{v} \cdot \vec{\nabla}\mathcal{C} < 0$, Figure 19). Likewise, $\vec{v} \cdot \vec{\nabla}\mathcal{C} > 0$ in the trough areas. Thus, according to the first RHS term of the BEE (8), a positive feedback mechanism occurs, leading to growth of the ridges.

Note that the formation mechanism of the ridges resembles that of up-current oriented bars in the surf zone (section 5.3). The differences between the two features, besides their geomorphological characteristics (size, location and time-scales), concern the sediment stirring process and the mechanisms causing the offshore deflection of the current over the crests (see also Appendix F).

In the models that describe the dynamics of sand ridges, bed load transport and suspended load transport play a different role in the formation of bottom patterns [*Calvete et al.*, 2001]. Suspended load transport is linked to a DASC that is proportional to u_b^3, where u_b is the amplitude of near-bed wave orbital motion. This is because the models assume settling lag effects to be small, so the mass balance of suspended sediment reduces to an approximate balance between erosion of sediment (modeled as being proportional to u_b^3) and deposition of sediment (assumed proportional to DASC). This term is primarily responsible for the growth of the ridges and its divergence produces maximum deposition approximately at the crest of the ridges. Thereby it essentially leads to growth of the ridges without migration (like in Figure 9a). On the other hand, bed load transport is modeled as in equation (3), with depth-integrated sediment concentration α (i.e., DASC times depth) being proportional to u_b^2. Its divergence produces maximum deposition between the crest and the subsequent trough, thus produces essentially pure downdrift migration of the feature (like in Figure 9c). Although bed load transport is considerably weaker than suspended load transport, it is this component that controls the downstream migration of the ridges. The largest deposition of the total sediment transport takes place slightly downstream of the crests, which produces their growth and downstream migration (like in Figure 9b).

6.4. Finite amplitude behavior

Following the general theory of section 3, saturation of bed forms towards finite heights must be due to either changes in the distribution of DASC, or from changes in the flow over the bottom pattern, or from an increase of the diffusive term. Regarding the finite amplitude behavior of ridges, this problem was studied by several authors [*Calvete et al.*, 2002; *Calvete and de Swart*, 2003; *Vis-Star et al.*, 2008; *de Swart et al.*, 2008]. They derived a nonlinear model from projection of the equations of motion onto the adjoint eigenmodes of the linearized system. The result are differential equations that govern the time evolution amplitudes of the different bottom modes. Amplitudes of flow modes follow from algebraic equations, as it is assumed that the flow adjusts instantaneously to a new bed level. The results showed that, after an initial phase in which ridges grow exponentially, they saturate and reach a finite height on timescales of several thousands of years (Figure 20). The resulting profiles of the ridges are highly asymmetrical, with steep stoss sides and mild lee sides, consisting with what is observed in the field. Moreover, smaller-scale bed forms, with length scales of a few hundred meters, are superimposed on the ridges. Note that these small scale bed forms have the size of sand waves. A detailed analysis revealed that both the small-scale bed forms and the diffusive sediment transport induced by bed slopes are responsible for the saturation of the ridges to a constant height.

Using a more sophisticated wave model, *Vis-Star et al.* [2008] was able to demonstrate patch behavior of the ridges.

One of the limitations of nonlinear spectral models is that they do not allow for variations of mean sea level, because that would affect the spatial structure of the eigenfunctions. On the other hand, field data clearly suggest that ridges are affected by sea-level changes [*Swift et al.*, 1978]. These considerations have motivated the development of an alternative nonlinear model for shoreface-connected sand ridges, which is based on finite-difference techniques. A recent study by *Nnafie et al.* [2014a] shows that changes in mean sea level can have a profound impact on the long-term evolution of the ridges. In particular, when sea level rise is too fast compared to typical deposition rates, the ridges drown and become moribund features.

In a separate study, *Nnafie et al.* [2014b] investigated the impact of extraction of sand from fully developed ridges. Their main findings are that the intervened ridge partly restores, on a time scale of centuries, albeit that its final volume of sand is smaller than its volume prior to the intervention. The sand needed for filling the extraction pit originates from different sources, such as the downstream trough, the part of the ridge upstream of the pit and the outer shelf and nearshore zone.

6.5. Discussion

There are a number of open issues with regard to further understanding of the dynamics of shoreface-connected sand ridges. The first is that nonlinear spectral models had problems to simulate the ridges for a realistic value of the shelf slope (typically 10^{-3} m/m). Nevertheless, output of these models could be used to make educated estimates of expected heights and saturation time scales (i.e., the time at which finite heights are reached) for realistic shelf slopes. This is because the models showed that, for the range of shelf slopes that finite amplitude ridges were simulated, the height and saturation time scale depended linearly on the shelf slope and the inverse of the shelf slope, respectively. Assuming these relationships to hold for larger shelf slopes as well, modeled heights and saturation time scales were extrapolated to realistic shelf slopes. It turned out [*Calvete and de Swart*, 2003; *Vis-Star et al.*, 2008] that the results thus obtained agreed fairly well with field data. An important breakthrough in this respect was achieved with a recently developed nonlinear finite difference code [*Nnafie et al.*, 2014b], which is capable of simulating ridges for realistic shelf slopes. Moreover, this model confirmed that the earlier applied extrapolation method, as discussed above, was indeed correct.

A second discussion point concerns the feedback between wind waves and ridges (as occurs for transverse bars, see section 5.5). Their effect on the initial formation of ridges was examined by *Lane and Restrepo* [2007] and *Vis-Star et al.* [2007]. Outcomes were different: the former study revealed no growth of bed forms, whereas the latter study showed that the growth of the ridges was significantly enhanced by perturbations in wave stirring. The latter study already provided a physical reason for this enhanced growth, and this finding was confirmed in a later study [*Nnafie et al.*, 2011], in which an independent, numerical morphodynamic model was used. These studies reveal that allowing for directional spreading of waves seems a necessary condition to properly account for these feedbacks in nonlinear models.

A third interesting extension would be to study the potential interactions between storm-driven sand ridges and other bed forms, such as tidal sand waves and megaripples. As a first step, this could be done by improving formulations for bottom roughness that are related to smaller scale bed forms. Ultimately, such interactions should be studied with (at least quasi) three-dimensional models, as tidal sand waves and megaripples are the result of flow circulations that act in the vertical plane. This approach is quite challenging, as since tidal sand wave/megaripples evolve on much shorter time scales than the ridges. Thus simulations would require small grid sizes and small time steps.

7. BEACH CUSPS

7.1. Characteristics of observed beach cusps

Beach cusps are alongshore rhythmic features of the swash zone (Figures 1d and 2e), the region that is quasi-periodically covered and uncovered by successive waves. Beach cusps consist of lunate embayments separated by relatively narrow shoals or horns, the apices of which point seaward, see Figure 21. These horns and embayments, which are ostensibly areas of deposition and erosion respectively, have sometimes been observed to be accompanied by corresponding areas of, respectively, erosion and deposition further seaward. Beach cusps typically have horn-to-horn distances, or spacings of $1 - 50$ m, and the spacing is proportional to incoming wave period and beach slope. The reader is referred to *Coco et al.* [1999] for a comprehensive review of the main features of cusps, their development and occurrence, in laboratory and field conditions. An excellent set of images of cusp development is provided by *Almar et al.* [2008], in which their morphology can clearly be seen.

As described by *Coco et al.* [1999, 2000], cusps can occur on different beach slopes, with different sediment sizes, and under different wave conditions. However, they are predominantly features of steeper beaches, and most observations are on beach slopes of between 0.08 to 0.16 [*Coco et al.*, 1999]. Also, typically sediments are relatively coarse and well-sorted, almost all observed cuspate beach grain sizes are > 0.2 mm, with modal values being about 0.5 mm (medium to coarse sand [see, e.g., *Soulsby*, 1997]), but with sometimes considerably larger sediment sizes [e.g., gravel, *Coco et al.*, 1999]. Frequently, there is also evidence of sorting of grain sizes, with coarser sediments typically accumulating on the horns, and finer ones in bays [*Coco et al.*, 1999]. Cusps are observed under partially reflective wave conditions (i.e., where a significant proportion of the wave energy is reflected back out to sea), for normal or near-normal wave incidence. Consistent with the partially reflective nature of waves in cusp systems, it is most commonly observed that for cusp formation waves break either by plunging or collapsing, in other words by expending a lot of their energy in a narrow region near to the shore (the shorebreak), and then running up (and back down) the beachface. They are rarely observed where spilling breakers occur (which is consistent with the steeper slopes on which they are observed), and also less commonly where there is no breaking.

Field data is equivocal regarding whether beach cusps are erosive or accretionary features, although more recent literature seems to point toward their being a combination of the two [*Coco et al.*, 2004a; *van Gaalen et al.*, 2011]. What does seem clear now is that individual cusps can merge [*Almar et al.*, 2008], forming larger local spacings. Further, once formed, cusp systems can be removed both by erosion (i.e., storms) or by continued accretionary (i.e., low energy) conditions. This implies that cusps are by their nature ephemeral features, which are likely to persist longest on a falling tide [*Coco et al.*, 2004a].

7.2. Existing theories for their formation

More controversy surrounds the mechanism of beach cusp formation. The theory that pertained predominantly, prior to about 1993, was that of edge waves scouring out the observed beach patterns [*Guza and Inman*, 1975; *Guza and Bowen*, 1975]. The amplitude of the zero-mode edge waves achieves a maximum at the shore, decays exponentially offshore and varies sinusoidally alongshore. In the edge wave theory for beach cusps, the pattern is "carved" into the beach by the hydrodynamics. The hydrodynamic motion is therefore often viewed as a *template*, which then imposes that pattern on the beach, which is in contrast to all the earlier explanations of morphodynamic pattern formation mentioned herein. *Coco et al.* [1999] have compared these edge wave theories (in the form of observed cusp spacings and wave periods) to numerous historical data-sets and found that there is reasonable agreement. On the other hand, *Coco et al.* [1999] also conclude that observed wave breaking is predominantly plunging in character, and too dissipative to account for the edge wave model being operative in at least 50% of data-sets. Indeed, in some field studies edge waves were not present during the initiation of beach cusps [*Masselink et al.*, 2004].

The main other explanation for beach cusps has its origins in morphodynamics, and relies on a positive feedback between bed and water motions. *Werner and Fink* [1993] and *Coco et al.* [2000] presented compelling arguments, based on simple models that utilize Newtonian dynamics to simplify swash flow as a series of balls moving up and down a beach that erode or accrete [see also *Coco et al.*, 2001]. From an initial alongshore uniform beach, cusps emerge as a larger-scale organized pattern of water motions and bathymetry. The resulting cusp spacing showed a correlation with the swash excursion (the distance measured along the beach from the base of the swash to the position at which maximum run-up is achieved), in line with data [*Werner and Fink*, 1993; *Coco et al.*, 2000]. Significantly, this type of model was shown generally to agree with observations made within an experiment designed specifically to monitor beach cusp development from an initially plane beach [*Coco et al.*, 2003].

To date, the only other attempt to understand and describe cusp development has been by *Dodd et al.* [2008], who formulated a fully coupled morphodynamic model in which equations describing the fluid flow are coupled to bed change, thus (in theory) allowing feedback processes, but also allowing true hydrodynamic motions. In other words, this description allowed both edge wave and self-organization processes to be operational. The model reproduced the formation of beach cusps with spacings consistent with field observations. Notably, the introduction of infiltration, consistent with steeper beaches with coarser sediments, promoted cusp development. It should be noted, however, that the model of *Dodd et al.* [2008] did not include sediment settling lags (as explained in Appendix A), an effect shown to be important in promoting deposition of suspended sediment in the upper swash [*Pritchard and Hogg*, 2005]. This deposition occurs because sediment that was entrained in the inner surf zone or lower swash soon begins to settle out because the flow is decelerating for most of the uprush, but only finally comes out of suspension in the upper swash. This sediment is not all re-entrained in the backwash because of the smaller velocities in this region and the corresponding lag in entrainment. The absence of this process probably overemphasizes the importance of infiltration in the model.

The edge wave theory was examined by conducting purely hydrodynamic experiments. Significantly, cusp-like circulations did develop, but were more ephemeral, often evolving to larger scales, but with some evidence that edge waves were indeed being excited. Overall, it was concluded that edge waves might play a part in initiating cusp development, but that (a) these were part of an instability mechanism, and (b) an erodible bed significantly enhanced this mechanism. In the next section, the role of the depth-averaged concentration (DASC) in beach cusp formation through self-organization will be described.

7.3. Role of DASC in the formation mechanism

As mentioned in sections 2 and 3, beach cusps have unique characteristics (compared to the other three morphodynamic features studied here), related to the fact that they occur in the swash, where it is essential to retain the back and forth water movement driven by successive waves (i.e., non-steady hydrodynamic conditions). This is because there is no obvious wave average to be calculated in this region [see *Brocchini and Peregrine*, 1996]. Further, waves in the swash are highly nonlinear, even when non-breaking, so parameterizing their effect in a satisfactory way in a time-averaged description is difficult. Furthermore, and more fundamentally, because of the high Froude number flows that can occur in the swash, the hydro- and morphodynamic time scales are no longer necessarily distinct from each other, so the quasi-steady approximation cannot formally be applied. So, the equations and variables are not wave-averaged and the quasi-steady hypothesis does not hold. Furthermore, the BEE must be solved during the wave cycle, because of the aforementioned non-separation in time scales, and because the differences in the sediment transport during *uprush* and *backwash* processes are what lead to gradients, over a wave cycle, in the depth-averaged sediment concentration. Note also that this does not mean that a wave-averaged picture of the morphodynamics is not useful, just that the wave-averaging is best done after the modeling in order to reveal the dynamics [see *Dodd et al.*, 2008].

7.3.1. Depth-averaged sediment concentration during a wave cycle

In the non-steady swash conditions, it is instructive to first see how the DASC, $\mathcal{C}$, varies during a swash cycle on an alongshore uniform beach (Figure 22). At the shore-break the wave collapses (or plunges) onto the beach and the water rushes up the beachface (the *uprush*). The uprush is initially of very high velocity (O(2 m/s)) and sometimes initially supercritical. Thus, at the tip of the uprush, where depths are very small, $\mathcal{C}$ achieves a maximum (recall that $\mathcal{C}$ responds immediately to the flow) and (at the same instant in time) decays, but is still significant, seaward (Figure 22a). Thus sediment is set in motion at the start of the uprush, thus eroding the beach in the lower swash. As the uprush diminishes so does $\mathcal{C}$. Therefore, deposition pertains over the rest of the uprush. The flow reverses first in the lower swash, and the *backwash* develops, which soon encompasses the whole swash region as gravity accelerates the flow seaward, thus increasing $\mathcal{C}$, which can then achieve values comparable with those in the uprush late in the backwash (Figure 22b). Therefore, sediment is once more mobilized and this time transported offshore. The backwash therefore erodes the upper and mid-swash, eventually depositing sediment in the lower swash. The net sediment transport depends on the balance of these two processes (see *Masselink and Kroon* [2006], and also *Dodd et al.* [2008] for simulation of this process).

7.3.2. Non-steady flow on a cusp system

In an incipient cuspate system, the horns (slightly elevated areas of beach level) are separated by embayments (slightly lowered areas of beach level), along with the corresponding regions of lowered and elevated level further offshore. If we now consider such a morphology on a non-erodible beach we can see the effect on the circulation. The purely one-dimensional motion described in section 7.3.1 becomes two dimensional. At horns, uprush is diverted to either side of the horn (because of the shape of the horn), into the adjacent embayments. The backwash then occurs, with significantly more water at the embayments. Additionally, there is a phase lag that accompanies this circulation. As a normally incident and initially plane wave front approaches the beach it is first affected by the seaward regions of lowered (just seaward of horns) and elevated (just seaward of embayments) level, with the result that just offshore of the horns waves propagate faster (because the bed level is lower and the wave speed is proportional to $\sqrt{gD}$ [*Svendsen*, 2006]), and so encounter the shoreline (and break) a little ahead of the wave front at embayment locations. At the horn location the uprush therefore occurs slightly ahead of that at embayments, exacerbating the effect of the flow divergence at the horn because of the absence of water at the embayments in the early uprush. Also, the relatively weak backwash at horns finishes ahead of that at embayments, because of the earlier uprush and the larger beach slope at horn locations, which also means that the next wave is relatively unaffected by the preceding backwash there. However, as the embayment backwash ends, it frequently interacts with (and therefore further delays) the next incident wave at that location. The result is that the horn locations are uprush dominated while the embayments are backwash dominated. What emerges is an overall (wave-averaged) circulation pattern as depicted in Figure 21.

7.3.3. Formation mechanism

In order to understand the role of DASC in creating the erosion/deposition patterns that explain cusp formation, the bed evolution equation (BEE) during a wave cycle must be analyzed. As pointed out in section 3.1, in swash zone morphodynamics the BEE takes the form of equation (7) because of its second RHS term can no longer be assumed negligible as the quasi-steady hypothesis does not hold [*Dodd et al.*, 2008]. Here, we rewrite equation (7) [following *Dodd et al.*, 2008] to include a (positive) vertical infiltration velocity w (which also requires an alteration to equation (4), as mentioned in section 2.2),

$$(1-p)\,\frac{\partial h}{\partial t} = -D\vec{v}\cdot\vec{\nabla}\mathcal{C} - \mathcal{C}\,\vec{\nabla}\cdot(D\vec{v}) + \mathcal{C}w + \vec{\nabla}\cdot(\gamma\vec{\nabla}h)\ . \qquad (11)$$

Note also that, although $\mathcal{C}$ is still a depth-averaged sediment concentration, α is now more appropriately seen as a bed mobility parameter rather than as a wave stirring function. The depositional effect of infiltration can clearly be seen in equation (11) (i.e., the third RHS term is always positive).

The contribution to erosion or deposition of the first and second RHS terms during the uprush and backwash in the case of alongshore uniform conditions are depicted in Figure 23a. In the upper plot we see $-\overline{\mathcal{C}\,\vec{\nabla}\cdot(D\vec{v})}$ and $-\overline{D\vec{v}\cdot\vec{\nabla}\mathcal{C}}$ for uprush and backwash (note that the overbars here denote time averages over only those phases of the swash), and their net contribution during the whole wave cycle. The pattern of erosion/deposition produced by the sum of the net contributions of these two terms is shown in the middle plot, and the corresponding change in bed level is shown in the lower plot. During the uprush, the flow divergence term is positive, $-\overline{\mathcal{C}\,\vec{\nabla}\cdot(D\vec{v})} > 0$, because the flow is converging ($\vec{\nabla}\cdot(D\vec{v}) < 0$), and therefore this term leads to deposition. Conversely, during the uprush the concentration gradient term is negative, $-D\vec{v}\cdot\vec{\nabla}\mathcal{C} < 0$, because the flow is moving toward a region of high DASC, the tip of the swash. However, this erosive effect is mainly limited to the lower swash, where the stronger gradients in $\mathcal{C}$ induce a removal of sediment just seaward of the horns. In the backwash these effects reverse, with the flow divergence term removing sediment in the upper swash (as $\vec{\nabla}\cdot(D\vec{v}) > 0$), and the concentration gradient term depositing in the lower swash. The latter occurs because the fast (often supercritical) offshore flow meets relatively static water thus creating a very large DASC gradient effect such that offshore flow moves down this gradient, and thus deposits rapidly. Note that on an alongshore uniform beach these effects will often, to a first order of approximation, be in balance, i.e., the two effects cancel each other out (solid lines in Figure 23a, top panel). In such a situation, infiltration (or lack thereof) can tip the balance in favor of deposition (erosion).

In the presence of incipient cusps, the balance described in the paragraph above is broken. The flow during the uprush remains relatively unchanged but, during the backwash, it is diminished in the horns and enlarged at the embayments (see section 7.3.2). Thereby, in the horns, the net erosion/deposition is dominated by the uprush processes whilst in the embayments the net change is dominated by the backwash processes (see Figure 23b,c). On the horns, the balance is shifted to deposition in the mid- and upper swash via flow convergence ($-\overline{\mathcal{C}\,\vec{\nabla}\cdot(D\vec{v})} > 0$), and erosion in the lower swash via DASC gradient ($-\overline{D\vec{v}\cdot\vec{\nabla}\mathcal{C}} < 0$). Therefore, an incipient horn grows further, accompanied by eroded areas just seaward, and thus there is positive feedback. At incipient embayments, conversely, the erosive effect of the increased divergent flow ($-\overline{\mathcal{C}\,\vec{\nabla}\cdot(D\vec{v})}$) in the upper and mid swash, and the accompanying depositional effect of the DASC gradient ($-\overline{D\vec{v}\cdot\vec{\nabla}\mathcal{C}}$) in the lower swash predominate. Thereby, the embayments are further eroded, accompanied by regions of deposition just seaward, again leading to positive feedback. Moreover, any infiltration effects will mean that some uprush does not return as surface flow, thus further enhancing this effect.

7.4. Finite amplitude behavior

The formation mechanism described in the previous section is operational when the cusps are of small amplitude. Later, limiting effects come into play. Eventually, the horns may no longer experience run-up, and therefore become static, which in turn will tend to equalize uprush and backwash at embayments, thus reducing differences in erosion and deposition there. Similarly, exaggerated alongshore beach gradients (on the sides of horns) may lead to local accelerations and erosion, and therefore the erosion of the flanks of the horns. A model result showing the development of a large-amplitude cusp system can be seen in Figure 24, in which we can see the bathymetry and the current in different simulation times [*Dodd et al.*, 2008]. *Sriariyawat* [2009] undertook long-term simulations, and applied the global analysis to the cusp system, and in doing so obtained a variety of finite amplitude states, some apparently physical and some not. This points to the difficulty of describing dynamic equilibria in a highly energetic moving boundary problem (because small effects can tip the balance one way or another). There is therefore a need for further work in this area.

7.5. Discussion

From a combination of field and laboratory work, and numerical studies, a reasonable understanding of beach cusp formation has emerged. Nonetheless, some issues remain unresolved as yet. The most obvious is what dictates the alongshore spacing of the cusps. It is often difficult to pinpoint a clear physical reason for a length scale selection, even if it can be shown mathematically or numerically that a certain length scale has the fastest growth rate. As discussed by *Coco et al.* [1999], the field and laboratory data correlate reasonably well with both edge wave length scales (both subharmonic and synchronous) and swash excursion, and that the latter is to be expected even if edge waves play a part in the cusp development. This leads to the possibility that the self-organization mechanism and the edge wave hypothesis are not mutually exclusive, even if they perhaps they do not both pertain simultaneously. Interestingly, the work of *Dodd et al.* [2008] gives some support for this, because, as was mentioned above, in their numerical experiments they observed weak, cusp-like circulations develop on non-erodible beaches. It was clear, however, that beach erodibility significantly enhances this mechanism.

Note also that, as explained in section 7.3, the case of beach cusps is different from those presented earlier. A wave-resolving approach is best taken here to represent the dynamics of the feature. Thus, the current represented by $\vec{v}$ simultaneously mobilizes and transports the sediment. This is in contrast to the wave-averaged studies presented heretofore, in which entrainment is produced by waves and current and the mobilized sediment is transported by the current. Therefore, splitting sediment transport divergence into depth-averaged concentration divergence and current divergence (as done in section 3.1), makes less sense, because there is no separate mechanism (wave stirring) for creating gradients in $\mathcal{C}$. Nonetheless, the interpretation embodied in equation (11) can successfully be used to understand the feedback mechanisms. Finally, using equation (11) implies that the sediment transport responds (effectively) immediately to flow changes, which is reasonable for transport by bedload or by suspension of coarse grains (see Appendix A). However, if smaller grain sizes are suspended then a modified form of equation (11) is necessary because sediment is not immediately deposited as flow decelerates (settling lag). This can be an important effect in the swash, leading to deposition in the upper swash [*Pritchard and Hogg*, 2005].

8. CONCLUDING REMARKS

In this contribution a general formulation and methodology are presented to infer the erosion and deposition patterns of sediment transport only from the gradients in the depth-averaged sediment concentration (DASC) and the spatial structure of the current. This can be applied whenever the sediment transport is equal to a sediment load times the current, which means assuming that waves essentially stir the sediment and the current augments this stirring and advects the sediment. Note that, in the application to the swash zone, the stirring is due only to the current. The DASC is then defined as the total sediment load divided by water depth. In this formulation the current is the depth-averaged current and its dynamics must be described within the context of a time- and depth-averaged shallow water model. The key point of the formulation is a bed evolution equation (BEE) that describes the bed changes solely in terms of the advection of the DASC by the current (section 3). This applies when the time scale on which the bed evolves is much larger than the hydrodynamic time scales (i.e., when the quasi-steady approximation is applicable). When these time scales are comparable, the bed level changes depend also on the DASC itself and the convergence/divergence of the water volume flux, but the methodology can still be generalized. In the former, most common case, deposition (erosion) occurs where the current flows from areas of high to low (low to high) values of DASC (section 3.2). Thus, analyzing the resulting erosion/deposition patterns leads to an understanding of why different features with a specific pattern grow in different coastal zones. In addition, the DASC, in combination with knowledge of the currents associated with emerging patterns, and the BEE, provides insight into some important aspects of the finite-amplitude behavior, such as the saturation of the growth of the features. In particular, the BEE can be integrated over a region of the coastal zone, and then provides quantitative information about the mechanisms behind growth, saturation and migration of morphologic features (global analysis). Note that this methodology is not a modeling technique since it is not closed, the currents must be externally provided from models (either hydrodynamic or morphodynamic), from observations or from physical reasoning. Rather, it is a way of gaining physical understanding of why alongshore rhythmic patterns of a certain shape grow and sometimes migrate or a way of making predictions of what type of pattern will emerge.

This methodology has proven to be a powerful tool with which to gain insight into the feedback mechanisms between the morphology and the hydrodynamics, and so to explain the formation of four morphologic features in the coastal zone that display alongshore rhythmic patterns: crescentic and transverse surf zone bars, shoreface-connected ridges and beach cusps. The key mechanism for the growth of crescentic bars can be understood from a seaward increase of the DASC at the bar zone: above shoals (channels) the DASC decreases (increases) along the onshore (offshore) directed current, causing deposition (erosion) (section 4.3). Similarly, down-current or shore-normal transverse bars, with their onshore current perturbations on the crests, create a positive feedback in the case of seaward increasing DASC (section 5.3). On the other hand, in the case of shoreward increasing DASC the positive feedback occurs if transverse bars are up-current oriented because this enhances the convergence of sediment transport in the seaward current perturbations that occur over the up-current crests. Similarly, on the inner continental shelf, the combination of the DASC increasing onshore and the offshore (onshore) directed currents over the up-current oriented ridges (troughs) causes deposition (erosion) (section 6.3). The application to cusps in the swash zone is more complicated because the bed evolves at the same time scale as the free surface and the convergence/divergence of the flow caused by free surface changes cannot be ignored in the BEE (section 7.3). However, we can still apply these ideas to analyze these features. At an area of raised bed level (incipient horn) there is reduced backwash, because return flow is channeled into adjacent regions. There is therefore net deposition in the mid and upper swash (flow convergence), and net erosion in the lower swash (onshore directed DASC gradient during the uprush), both because the reduced backwash fails now to counteract these effects in the uprush. Related to this, in regions of relatively reduced bed level (incipient embayments) there is an excess of backwash, which leads to net erosion in the upper and mid swash (flow divergence), and deposition in the lower swash (onshore directed DASC gradient in the backwash).

For nearly normal wave incidence there is no significant alongshore current and the alongshore gradients in DASC do not affect the development of the features (as discussed in section 3.3). As a result, the formation of crescentic bars and shore-normal transverse bars (which grow for normal wave conditions) can be fully understood because their dynamics are controlled just by the cross-shore DASC profile and the cross-shore current perturbations (first RHS term in the linearized BEE (10)). For the features that develop when a significant alongshore current is present (e.g., shore-oblique transverse bars and shoreface-connected ridges), the second RHS term in the linearized BEE (10)), related to the alongshore current and the alongshore gradients in DASC, also affects bed changes. Often, it causes only alongshore migration of the features and the growth/decay is still fully described by the first RHS term. However, for highly oblique waves in the surf zone, the second RHS term can contribute to the changes in amplitude and the first RHS term can contribute to the migration [*Ribas et al.*, 2012; *Thiebot et al.*, 2012]. All this makes the analysis more complicated as the second RHS term, which is related to the perturbations produced in DASC by the growing features, is difficult to model given our limited knowledge of the sediment transport processes.

The feedback mechanisms involved in the formation and subsequent dynamics of the morphodynamic patterns addressed here have been confirmed with a number of morphodynamic models [*Garnier et al.*, 2008; *Dodd et al.*, 2008; *Ribas et al.*, 2012; *Nnafie et al.*, 2014a, and references therein]. Some of these models have been calibrated against field data and shown to give reliable predictions for other situations in beach morphodynamics [e.g., *Reniers et al.*, 2004; *Smit et al.*, 2008; *Castelle et al.*, 2010b]. This gives ample support for the results from the DASC formulation presented here. However, the models are often quite sensitive to the parameterization used for sediment transport in case of oblique wave incidence in the surf zone [e.g., *Klein and Schuttelaars*, 2005]. The results of our contribution reveal the following reasons for such modeling problems. Firstly, differences in DASC profiles can produce completely different patterns. This is especially clear in the case of transverse bars: if the DASC decreases (increases) offshore inside the surf zone, the bars will grow with an up-current (down-current) orientation. Secondly, the migration of the surf zone features can be very sensitive to the sediment transport parameterization because it depends on the alongshore phase lags between the bathymetry and the perturbations in the depth-averaged concentration and the latter has unknown functional dependences on the perturbations in the water depth, wave orbital velocity, current and turbulent eddies. This might explain why migration of the surf zone features is generally not well modeled at present [*Garnier et al.*, 2006, 2008; *Ribas et al.*, 2012].

The formulation presented here can also be used in the opposite sense: knowing the characteristics of the observed bars, the distribution of the DASC can be inferred in a qualitative manner. This may be particularly useful in determining the validity of different sediment transport parameterizations depending on weather and wave conditions, morphology and beach conditions. The results presented here are also of interest for coastal engineering because they can be used to improve numerical models and existing integrated transport formulas (e.g., CERC formula for total alongshore transport rate or cross-shore transport formulas), which, at present, neglect the effect of alongshore rhythmic morphologies. For instance, *Splinter et al.* [2011] modeled the cross-shore migration of shore-parallel bars using a parameterization to describe the effect of possible alongshore rhythmicities. These results can aid in designing beach nourishments or coastal structures, or to understand the complex morphodynamic pattern evolution under time-varying forcing conditions. They can also be a guide for the design of field experiments: by measuring the currents and the cross-shore distribution of the DASC, the nature of the underlying morphodynamic rhythmic pattern can be assessed. Finally, the formulation and methodology that we have presented here could also be applied to other natural sand features whose dynamics can be described by depth-averaged shallow water models, such as sand bars in rivers [*Zolezzi et al.*, 2012], sand bars or shoals in tidal embayments (inlets or estuaries) [*de Swart and Zimmerman*, 2009] and tidal sand banks [*Blondeaux*, 2001].

9. FUTURE RESEARCH

9.1. Field observations

During the last two decades much theoretical research has been done on the development of alongshore rhythmic patterns based on the self-organization hypothesis. While the model studies have gone from very idealized to quite realistic, in some circumstances, including many of the possibly relevant processes, there is a lack of the necessary quantitative validation of those studies with field observations. Comparisons of the characteristics of the modeled features with field observations that have been made so far are mostly qualitative and more quantitative model-data comparison should be a guide to improve the models so that they can better reproduce the observations. One reason is that field observations that are adequate to test the proposed feedback mechanisms are limited. Also, a detailed analysis of such existing observations during the events of formation and evolution of the morphologic features is often missing. Therefore an important issue in future research is provision of high quality measurements of the variables involved in the dynamics of the morphologic features during the events of pattern development.

Measurement of the characteristics of the patterns (alongshore spacing, orientation, migration rate, amplitude, shape) is important, together with the ambient bathymetry (i.e., that without bed-forms). In the swash and surf zones, some of these bathymetric variables are nowadays measured with remote sensing techniques and thereby they are available with a good time and space resolution (e.g., *Konicki and Holman* [2000]; *van Enckevort et al.* [2004]; *Holman et al.* [2006]; *Ribas and Kroon* [2007]). Others (such as the amplitude of the features and the ambient bathymetry) must be measured in situ, and such data are expensive and thereby scarce. In particular, the lack of large scale bathymetric surveys near in time to an event of pattern development is very often the most important limitation for successfully applying the models and comparing their results with the observations. Important climate (wave and atmospheric) conditions that are needed to verify the mechanisms vary from feature to feature. For surf zone bars, offshore wave height, period and direction (and also tide and wind properties, if significant at the site) are typically available. In the case of shoreface-connected ridges, obtaining estimations of wind and wave conditions and coastal currents during storms is a challenge. For beach cusps, wave conditions at the beachface (i.e., type of breaking, as well as height, period and direction) are important quantities and they are hardly measured. Measurements of in/exfiltration would also aid in determining cusps dynamics.

Measurements of DASC and the horizontal circulation would provide a direct experimental validation of the formulation and the methodology presented here. Note that, although the sediment transport formulas used in models are widely used formulas, they are largely based on laboratory calibrations and it is often unclear how appropriate they are for field conditions [*Soulsby*, 1997; *Amoudry and Souza*, 2011]. The cross-shore distribution of DASC is important to know, ideally both when features are present and absent. Measuring the alongshore profile of the perturbation of DASC over the growing features would be particularly difficult, but it would help in understanding its potential role in the growth and migration of the features. Measurements of the horizontal circulation induced by the growing features would then reveal a detailed picture of the mechanisms discussed in this contribution. In particular, measurements of the DASC profile in the inner surf zone of natural beaches (i.e., beneath broken waves, with the resuspension produced by breaking-induced turbulent velocities), and of current deflections over shore-oblique transverse bars and shoreface-connected ridges would be unique. Sediment concentration profiles can be measured with acoustic backscatter systems (ABS) and acoustic Doppler current profilers (ADCP), which provide reliable data when waves are not breaking. However, measuring sediment concentration under breaking waves (i.e., inside the surf zone) remains a challenge due to the interference of air bubbles and strong turbulent vortices, in addition to the difficulty to maintain the tripods well anchored in such high energy environment. Also, errors in estimating the water depth (i.e., when no bathymetric surveys are available) lead to critical inaccuracies in the DASC profile ($C = \alpha/D$).

9.2. Laboratory experiments

Wave basin experiments are also likely to reveal important dynamics and confirm (or otherwise) hypotheses. Experiments like these would have to be at large scale, because of scaling difficulties with sediment grain sizes, and careful control would have to be exerted over extraneous effects (e.g., the re-reflection of waves, and the generation of seiching modes). If these issues are carefully addressed such experiments are likely to be useful in examining DASC and circulation patterns in great detail, as well as providing very high resolution bathymetric data-sets. Note that, compared to the natural variability in the field, in a wave basin the forcing conditions are controlled, so that features and mechanisms to be studied could be isolated. Beach cusp generation would seem the most auspicious case to examine, because of the relatively small spatial scales (such an experiment could be at prototype scale). Edge wave activity could be carefully monitored, along with monitoring of sediment sorting (although water levels within the beach would have to be carefully considered to ensure that they were consistent with field values).

9.3. Modeling

Necessary future modeling research again depends on the features considered, but, generically, should focus on testing the effect of heretofore neglected processes, improving representation of some of those included (not that this is not necessarily just incremental, but may require wholly different approaches), and developing better numerical techniques so that modeling can be carried out in circumstances that were previously prohibitively difficult. Note that models have been very useful to isolate and study processes and mechanisms but, at a certain point, the effect of including the neglected processes must be checked.

The cross-shore sediment transport processes have so far been assumed to play a passive role (see section 2.1). The essential mechanisms behind the development of the features are unraveled with this assumption but including a more accurate cross-shore transport description would be an important step forward because the latter explains beach profile dynamics (e.g., the formation and migration of the shore-parallel bars). To study this issue, (quasi) three-dimensional models should be developed because including a description of the vertical structure of the flow and the intra-wave oscillatory motion [*Putrevu and Svendsen*, 1999] is mandatory to successfully describe cross-shore sediment transport processes. This should be a priority to gain more understanding on the development of crescentic bars since the transformation of a shore-parallel bar into a crescentic bar often occurs whilst the bar migrates onshore [*Short*, 1999]. The intra-wave approach is, as has been mentioned earlier (section 7), intrinsic to the modeling of beach cusps, but a better description of the boundary layer in the swash zone would also be highly desirable because it is unsteady and reverses during the swash event, and its impact on sediment movement is still not fully understood [see *Barnes and Baldock*, 2010; *Briganti et al.*, 2011]. Including cross-shore sediment transport processes would be also desirable to model shoreface-connected ridges because they could be affected by the net exchange of sediment between the inner shelf and the nearshore zone. The present-day models consider only a weak exchange, but that assumption is controversial [*Kana et al.*, 2011; *Schwab et al.*, 2013]. *Niedoroda et al.* [1985] already pointed out that during storms the offshore Ekman flow near the bottom might bring large amounts of sediment to the inner shelf, thereby feeding the ridges.

There is one aspect of the current-driven sediment transport considered in the present contribution (i.e., the sediment transport occurring in the presence of depth-averaged currents) that deserve attention in future research. As has been mentioned, in some applications it has thus far been assumed that the sediment load in equation (3) is unaffected by perturbations [*Ribas et al.*, 2012] (for numerical reasons). However, inclusion of this effect can be important in the case of oblique wave incidence and understanding their role on transverse bar formation should be a priority in future research. Moreover, a more realistic description of suspended load transport would include considering the time and space dynamics of the suspended sediment concentration, rather than assuming that the concentration is always in equilibrium with local hydrodynamics as done in most of the present models. This would allow for time and space lags in the sediment exchange with the bed. This was already included by *Reniers et al.* [2004] for crescentic bar dynamics and the effect was minor. However, *Murray* [2004] described the formation of transverse bars and rip-channels in the surf zone, in which the lags in the sediment exchange with the bed were crucial for the growth. Also, we know that these lags are important for beach cusp formation (section 7.5). So future surf zone models for transverse bar formation should take these lags into account.

Studying the evolution of alongshore rhythmic patterns with the sand being composed of multiple grain sizes is also a challenge for the future (notice that describing the dynamics of the smaller grain sizes in suspension would require taking settling lags into account). Field data [e.g., *Baptist et al.*, 2006] reveal a positive correlation between density and diversity of benthos communities on one hand and fining of sediment on the other hand. Modeling and understanding the distribution of mean sediment grain size and sorting over finite-amplitude shoreface-connected sand ridges, that are important in the context of modeling ecology of coastal, remain a challenge. So far studies have considered such problems only during the initial formation of the bed forms [e.g., *Walgreen et al.*, 2003], when vertical sorting can be ignored.

Some aspects of wave climate also require study. Spreading of wave incidence angle and period has been considered in modeling crescentic bars [*Reniers et al.*, 2004; *Smit et al.*, 2008; *Castelle et al.*, 2010b] but not for transverse bars. These effects could affect the sediment stirring process (and hence the DASC) and might alter the formation mechanisms of the features. The effect of including a wave spectrum on cusps has been considered by *Coco et al.* [2001], but has not yet been taken into account in fluid dynamical modeling [*Dodd et al.*, 2008]. Dealing with storms that have different durations and intensities, and with different ocean swell conditions is another challenge. This would require the application and statistical analysis of Monte Carlo simulations. Also, modeling the interaction between transverse bars and low frequency hydrodynamic oscillations is another issue that deserves further exploration.

Including tides is important for surf zone bars because tidal variability moves the shoreline and the surf zone back and forth at a time scale comparable to the characteristic time scale of bar morphodynamics. This can have an important effect on transverse bar formation, especially in the intertidal features. Also, the tides may cause a significant variability on the water depth over the crescentic bars. In spite of this, the effect of tides has been generally ignored in the modeling because of the mathematical complexity of the problem, wherein we have a moving boundary (the shoreline), which renders both analytical and numerical description difficult. This is in fact the same problem encountered in modeling beach cusps, where the swash variability must be taken into account. Therefore, the development of numerical techniques suited to obtaining high accuracy solutions in this type of non-steady boundary problem would be desirable. These improvements should be a priority in describing the long-term evolution of beach cusps to a dynamic equilibrium (see section 7.5).

Modeling the potential interaction between different features is another challenge. *Castelle et al.* [2010b] and *Tiessen et al.* [2011] examined the effect of pre-existing bedforms (of the same type) on subsequent development, but studying the interaction of different types of features would be also interesting. For instance, up-current finger bars in open beaches tend to occur when an outer crescentic bar is present [*Ribas et al.*, 2014]. In this sense, future modeling studies of open-beach finger bars should use a non-linear model and start with a realistic initial bathymetry, incorporating pre-existing larger-scale variability. In the same way, a system of shoreface-connected ridges in the inner shelf can affect the dynamics of the smaller scale surf zone bars.

Finally, a big challenge for the future is to incorporate biologic variables to the morphodynamic models in order to study the interaction between the morphologic features, hydrodynamics and vegetation or benthic life and fish. Study of how the transport of pollutants is modified in the presence of morphodynamic patterns (due, e.g, to rip current circulation) is also relevant.

APPENDIX A: DERIVATION OF THE BED EVOLUTION EQUATION (2) AND THE SEDIMENT TRANSPORT EQUATION (3)

The dynamics of the depth-integrated volume concentration of sediment in suspension, α_s (different from α in equation (3) that includes both the suspended and the bedload contributions) can be described with the following simple advection equation

$$\frac{\partial \alpha_s}{\partial t} + \vec{\nabla} \cdot (\alpha_s \vec{v}) = (E - D) \ , \tag{A1}$$

stating that the total suspended load in the water column changes due to both the advection by the current and the exchange with the bed [*Murray*, 2004]. The latter is described by the entrainment function E (the upwards flux due to stirring by waves, currents and turbulence) and the deposition function D (the downwards flux due to the settling of the grains towards the bed due to gravity). Other terms can be added to equation (A1), such as a slope term and a horizontal diffusive term [*Amoudry and Souza*, 2011], but the objective here is keeping it as simple as possible. The bed evolution equation then becomes

$$(1-p)\frac{\partial z_b}{\partial t} + \vec{\nabla} \cdot \vec{q}_b = -(E - D) \ , \tag{A2}$$

stating that the total exchange of sediment with the bed results in changes in bed level [*Amoudry and Souza*, 2011], and that the total exchange is due to both divergence of bedload transport, where $\vec{q}_b \propto \alpha_b \vec{v}$ (and α_b is the sediment load as bedload), and exchange with suspended load. Substituting $E - D$ from equation (A1) into equation (A2), and defining $\vec{q}$ as in equation (3) with $\alpha = \alpha_s + \alpha_b$, yields

$$(1-p)\frac{\partial z_b}{\partial t} + \frac{\partial \alpha_s}{\partial t} + \vec{\nabla} \cdot \vec{q} = 0 \ , \tag{A3}$$

Since the dynamics of suspended sediment grains (described by equation (A1)) occurs at hydrodynamic time scales, when the quasi-steady approximation is applied, $\partial \alpha_s / \partial t = 0$, and this term drops out from equation (A3). This means that temporal lags between flow and suspended load are disregarded. Another assumption is that α_s depends only on the local hydrodynamics, i.e., the spatial lags are not considered because the length scale of sediment settling or picking-up processes is much smaller than that of the morphodynamic features. As a result, α_s is considered as a known function of the flow, which shortcuts solving equation (A1). After applying all these assumptions, equation (A3) leads to equation (1), with the sediment transport described by equation (3) and α being a local quantity (meaning that sediment load is in equilibrium with the local hydrodynamics).

Three additional assumptions are implicit in our sediment transport formulation (3). First of all, sediment sorting is not accounted for and a single grain diameter is considered. Although systematic gradients in grain size can be observed on the studied features (e.g., across shoreface connected ridges), the hypothesis here is that this is not essential for explaining their formation. Second, as a result of the joint action of waves and currents acting in different directions, $\vec{q}$ may not be parallel to $\vec{v}$ in some cases. In other words, the proportionality factor α may be a second order tensor rather than a scalar. Again, this is not considered because we assume that these effects are not essential for the formation of our morphological patterns. Finally, in addition to the sediment transport driven by the depth-averaged currents (first term on the RHS of equation (3)), in the coastal zone there are also cross-shore sediment transport processes driven by, e.g., the waves alone (due to nonlinearities and streaming), the vertical structure of the currents (e.g., undertow [*Svendsen*, 2006]) and the gravity-driven transport. The joint action of these three latter components controls the long-term dynamics of the cross-shore profile (i.e., time scales of weeks-months, see *Ruessink et al.* [2007]) and is typically at least one order of magnitude smaller than the transport driven by the alongshore current or the rip current circulation. Since the working hypothesis here is that those latter currents, in combination with the DASC distribution, control the dynamics of the morphological features of interest, we assume that the cross-shore transport processes build an alongshore uniform equilibrium profile which is stable, so that the deviations from it just cause a net diffusive transport (second term of the RHS of equation (3)).

APPENDIX B: WAVE EQUATIONS

As it has been stated in section 2.2, the knowledge of wave radiation stresses, wave orbital velocity and wave energy dissipation is necessary to solve the hydrodynamic equations for the currents. Although the description of the incoming surface gravity waves is generally complicated, it is sufficient for our purpose to assume waves have random heights with a Rayleigh distribution characterized by the root-mean-square height, H, but a narrow spectrum in frequency and direction. The simplest set of equations describing their transformation from deep water to shore includes the dispersion relation, the wavenumber irrotationality relation and the wave energy balance. The dispersion relation (with Doppler shift) reads

$$\omega = \sqrt{gk \tanh{(kD)}} + \vec{v} \cdot \vec{k} \ . \tag{B1}$$

where g is gravity, $\vec{k} = (k_x, k_y)$ is the wavenumber vector and k its modulus. The absolute frequency (frequency with respect an observer at rest on Earth) is ω and is assumed constant. The wavenumber irrotationality (conservation of wave crests) reads

$$\frac{\partial k_x}{\partial y} = \frac{\partial k_y}{\partial x} \ . \tag{B2}$$

The depth-integrated wave energy balance reads

$$\frac{\partial E}{\partial t} + \vec{\nabla} \cdot ((\vec{v} + \vec{c}_g)E) + \mathbf{S} : \vec{\nabla}\vec{v} = -\mathcal{D} \ , \tag{B3}$$

where $E = \rho g H^2/8$ is the wave energy density (energy for horizontal area unit), ρ is water density, $\vec{c}_g$ is the group velocity vector, and $\mathcal{D}$ is the wave energy dissipation rate, which must be parameterized. In the surf zone, the main source of energy dissipation is wave breaking [parameterized following, e.g., *Thornton and Guza*, 1983], which is much larger than dissipation by bed friction so that the latter is neglected. In the shoaling zone, however, wave energy dissipation by bed friction must be accounted for. According to the notation in tensor algebra,

$$\mathbf{S} : \vec{\nabla}\vec{v} = S_{xx}\frac{\partial v_x}{\partial x} + 2S_{xy}\frac{\partial v_x}{\partial y} + S_{yy}\frac{\partial v_y}{\partial y} \ . \tag{B4}$$

The wave transformation equations described above can be solved to find the wavenumber k, the wave angle (angle between the direction of propagation of the wave and the shore normal direction, see Figure 4) θ ($k_x = -k\cos\theta, k_y = k\sin\theta$), and the wave energy E as a function of x, y and t. Expressions for the wave radiation stresses, group velocity and orbital velocity amplitude at the bed, as function of E, k and θ, are obtained from linear wave theory [*Mei et al.*, 2005]. In some applications, it is also necessary to describe the dynamics of the *roller*, i.e., the aerated mass of water located on the shoreward face of breaking waves. This is achieved with an extra equation for the balance of the roller energy density. The set of equations above describe wave refraction (by topography and currents), shoaling and breaking, the wave processes that are essential for the creation of the morphodynamic features of interest. More complex wave characteristics, like a spectral dispersion of wave frequency and direction, and other processes in wave propagation, such as wave diffraction and reflection, are not accounted for. The potential role of these neglected wave processes and properties on morphodynamic pattern formation is discussed in section 9. The specific wave equations used to describe the different features can be found in *Ribas et al.* [2012] (surf zone bars) and *Vis-Star et al.* [2007] (shoreface connected ridges). A detailed description of the depth-integrated momentum balance and the wave equations is given in *Phillips* [1977] and *Svendsen* [2006].

APPENDIX C: QUANTITATIVE GLOBAL ANALYSIS

In order to perform a quantitative global analysis of the BEE, as described in section 3.4, the starting point is to multiply the nonlinear BEE, equation (8), by the bed level perturbation associated to the feature, $h(x, y, t)$, and to integrate this equation over the domain. By defining the average of $f(x, y)$ over the computational domain (with the alongshore distance of the domain, L_y, being a multiple of the alongshore spacing of the feature)

$$\overline{f} = \frac{1}{L_x L_y} \int_0^{L_y} \int_0^{L_x} f(x, y)\, dxdy \tag{C1}$$

the integrated nonlinear BEE multiplied by h reads

$$(1-p)\overline{h\frac{\partial h}{\partial t}} = -\overline{h\, D\vec{v} \cdot \nabla \mathcal{C}} - \overline{\gamma |\nabla h|^2}. \tag{C2}$$

The second RHS term has been obtained by integrating by parts and using the alongshore periodicity of $h(x, y, t)$. Importantly, the LHS term can be written as

$$\overline{h\frac{\partial h}{\partial t}} = \frac{1}{2}\frac{d}{dt}\left(\overline{h^2}\right) \tag{C3}$$

because the computational domain is constant in time. Therefore, the LHS term is proportional to the time derivative of the potential energy of the pattern, that is, the gravitational potential energy of bed sediment grains (like the potential energy of water surface gravity waves). If such derivative is positive (negative), the morphologic pattern will grow (decay). Accordingly, we define the global growth rate of an alongshore rhythmic morphologic pattern as

$$\Omega = \frac{1}{\overline{h^2}}\overline{h\frac{\partial h}{\partial t}} \ . \tag{C4}$$

The meaning of the global growth rate becomes clearer if we consider an idealized morphological pattern consisting of a sinusoidal bed wave with growth/decay given by Ω_s and alongshore propagation celerity c_s,

$$h(x, y, t) = \exp(\Omega_s t)\hat{h}(x)\cos(\kappa(y - c_s t) + \psi(x))\} \ . \tag{C5}$$

Here, $\hat{h}(x)$ is a function that stands for the cross-shore structure of the bed wave, κ is its alongshore wavenumber and $\psi(x)$ accounts for the possible differences in spatial lags at each cross-shore position (i.e., yielding an obliquely oriented feature). For such morphologic pattern, it can be proved that

$$\overline{h\frac{\partial h}{\partial t}} = \Omega_s\overline{h^2} \ , \tag{C6}$$

so that its growth rate coincides with the global growth rate as defined in equation (C4), $\Omega_s = \Omega$.

Returning to the general case, by inserting the global growth rate, equation (C4), into the integrated BEE, equation (C2), the master equation governing the growth/decay of the pattern follows as

$$\Omega = \frac{1}{\overline{h^2}}(\mathcal{P} - \Delta) \; . \tag{C7}$$

where

$$\mathcal{P} = -\frac{1}{1-p}\overline{hD\vec{v}\cdot\nabla\mathcal{C}} \; , \quad \text{and} \qquad \Delta = \frac{1}{1-p}\overline{\gamma|\nabla h|^2} \; . \tag{C8}$$

Notice that $\Delta > 0$ so that it always causes decay of the pattern and it is called the damping term. Thus, any growth of the pattern must be described by $\mathcal{P}$, which is called the production term. Notice that the production term measures the cross-correlation between $h(x, y, t)$ and the quantity $D\vec{v} \cdot \nabla\mathcal{C}$ that has been discussed in section 3.2 as being responsible of the erosion/deposition processes driven by the joint action of the gradients in DASC and the currents. Consistently with the local analysis presented in that section, if the regions where $h > 0$ and the current opposes the gradients in DASC (or $h < 0$ and the current runs with the gradients in DASC) dominate over the regions where the contrary occurs, $\mathcal{P} > 0$. Then, if the production term is positive and larger than the damping term, the pattern will grow. If the opposite is true, the pattern will decay. If $\mathcal{P} = \Delta$ the pattern can change its shape or migrate but its global amplitude will remain constant.

Regarding the alongshore migration, for the case of a sinusoidal wave, it is seen that its propagation celerity fulfills

$$\overline{\frac{\partial h}{\partial y}\frac{\partial h}{\partial t}} = -c_s\overline{\Big(\frac{\partial h}{\partial y}\Big)^2} \; . \tag{C9}$$

Therefore, this brings us to define the global migration celerity of any alongshore rhythmic morphologic pattern as

$$c = -\frac{1}{\overline{\left(\frac{\partial h}{\partial y}\right)^2}} \overline{\frac{\partial h}{\partial y}\frac{\partial h}{\partial t}} \ . \tag{C10}$$

As far as we know, this quantitative global analysis of pattern growth/decay and migration in the nearshore was first presented and applied in *Garnier et al.* [2006]. The methodology was extended and further interpreted by *Vis-Star et al.* [2008].

APPENDIX D: PHYSICS OF BATHYMETRICALLY INDUCED RIP CURRENT CIRCULATION

To understand the physics behind rip current circulation (blue streamlines in Figure 12), we first consider the hydrodynamics originated by a shoal on an otherwise alongshore uniform topography in an area of breaking waves. The momentum carried by the waves is described by the *radiation stress tensor*, $S_{xx}, S_{yy}, S_{xy} = S_{yx}$ (see section 2.2 and Appendix B). This momentum is released at breaking originating a hydrodynamic force in the wave-averaged momentum equation through the divergence of the wave radiation stresses (equation 5). It is important to notice that in case of normal wave incidence S_{xx} is larger than S_{yy} because of the anisotropy caused by wave propagation direction [*Mei*, 1989; *Svendsen*, 2006]. In general, the wave height reduction at breaking produces an onshore directed hydrodynamic force on the water motions and hence a set-up of the mean sea level $z_s = z_s(x)$. Since breaking is induced by a reduction in water depth, there is more energy dissipation over the shoal than at its deeper sides. Therefore, there is more set-up, i.e., a higher water level, shoreward of the shoal than shoreward of its sides. This difference in water level can not be balanced by the alongshore gradients in S_{yy} because they are smaller. Therefore, the water flows alongshore from behind the shoal down to the deeper area and produces a higher level there. Again, this is not balanced by the cross-shore gradients in S_{xx} and the water flows offshore. In this way, a circulation cell is created with onshore current over the shoal and offshore current at the sides (Figure 12). Apart from this simple physical explanation, the conclusion that there is no possible steady solution balancing gradients in radiation stresses with pressure gradients without a circulation is readily seen by working out the momentum balance equations. When there are a number of shoals separated by channels, seaward flowing currents or rip currents are originated at the channels in this manner.

APPENDIX E: GLOBAL ANALYSIS FOR FINITE AMPLITUDE BEHAVIOR OF CRESCENTIC BARS

Following the analysis by *Garnier et al.* [2010], the first step is a careful analysis of the production ($\mathcal{P}$) and the damping (Δ) terms introduced in Appendix C (equation C8) when the bed level deviations h (difference in bed level with respect to straight bar situation) of the shoals and channels increases. Since $\mathcal{P}$ and Δ describe the tendency to grow or to decay (respectively) of the shoals and channels, their competition determines the instantaneous growth rate Ω (equation C7). Initially, $\Omega > 0$ so that the crescentic shape of the bar grows but, as the amplitude increases, Ω decreases and it eventually becomes 0. At this stage the pattern does not grow anymore, i.e., saturation occurs. Although there is a slight increase of Δ that contributes to the decrease of Ω, the latter is mainly due to a weakening of the production term, that is, a weakening of the positive feedback between morphology and circulation (Figure 25a). Then, it can be shown that the cross-shore flow component together with the cross-shore gradients in DASC dominate the production term,

$$\mathcal{P} = -\frac{1}{1-p}\overline{hD\vec{v}\cdot\nabla\mathcal{C}} \simeq -\frac{1}{1-p}\overline{uhD\frac{\partial\mathcal{C}}{\partial x}}\ . \tag{E1}$$

Finally, it is found that the decrease of the production term when the amplitude increases is controlled by the cross-correlation between cross-shore flow and bed level perturbation, $\mathcal{S} = \overline{uh}/\|u\|\|h\|$. To elucidate which of the characteristics of the finite-amplitude crescentic bars causes the decrease in the latter quantity, numerical experiments of the hydrodynamics over a fixed bathymetry with a crescentic bar are done. Increasing the amplitude of the shoals and channels but keeping the shape, $\mathcal{S}$ hardly decreases. In contrast, widening the shoals and narrowing the channels, $\mathcal{S}$ significantly decreases because the onshore current u over the shoals strongly weakens with the result that the whole circulation cell weakens. A similar effect (but less significant) is obtained with the shoreward (seaward) shift of the shoals (channels) and the overall seaward shift of the bar.

A similar analysis of the production and damping terms is carried out to investigate the influence of the wave incidence angle on the transitions between shore-parallel bars and crescentic bars [*Garnier et al.*, 2013]. Again, the damping term does not play an important role as it hardly depends on the wave angle. Both the inhibition of crescentic bar formation for oblique wave incidence and the bar straightening for increasing wave angle are caused by a weakening of the production term (see Figure 25b). And, again, this is in turn controlled by a decrease of the cross-correlation between cross-shore flow and bed level perturbation, $\mathcal{S}$. It is shown that, by increasing the wave angle, this term decreases due to both a weakening of the rip current intensity and a down-wave shift of the rips (i.e., a phase lag between the rips and the channels). This decrease of $\mathcal{S}$ explains the weakening of the positive feedback between flow and morphology.

APPENDIX F: PHYSICS OF CURRENT MEANDERING OVER SHORE-OBLIQUE BARS OR RIDGES

There are two potential hydrodynamic mechanisms that can create a meandering of the alongshore current over the crests of shore-attached oblique bars or ridges (blue streamlines in Figures 16b,c and 19). The first one is water mass conservation in the cross-bar direction. Consider first the case where the bar is up-current oriented. When the alongshore current flows over an up-current oriented bar, the cross-bar component of the current becomes larger due to water mass conservation (because depth decreases, the mechanism is sketched in Figure 5b). Since bar length is much larger than bar width, the along-bar component hardly changes. This gives an offshore current deflection (positive u) over up-current bar crests. *Trowbridge* [1995] showed quantitatively that, in the potential flow approximation of his idealized model, this was the mechanism responsible for the offshore deflection over the shoreface connected sand ridges. The second mechanism is related to the frictional torques created by depth changes as the alongshore current flows over the bar. When the current runs from the trough to the crest of an up-current oriented bar, it experiences a clockwise rotation because friction is larger over the crest that it is at the trough. This again gives an offshore current deflection (positive u) over up-current bar crests. This effect was described by *Zimmerman* [1981] and was recognized as crucial in the context of tidal currents over tidal sand banks. *Ribas et al.* [2012] showed that frictional torques were the essential mechanism to produce the offshore current deflection over the up-current oriented transverse bars in their model. If the bars are down-current oriented, both mechanisms create an onshore deflection of the current (negative u) over bar crests.

GLOSSARY

Advection: Forward carrying by a current.

Alongshore current: Current along the coast. In case of the surf zone it refers to the current driven by the breaking waves with oblique incidence.

Backwash: Flow of water down the swash zone during the backward motion of a wave incoming at the beach face.

Bedload transport: Sediment transport corresponding to particles that are in frequent contact with the sea bed (sliding, rolling or bouncing).

Bed shear stresses: Tangential forces per unit area exerted on the sea bed by a flow (and vice versa).

Cross-shore sediment transport: Sediment transport in the cross-shore direction driven by the combination of the waves (asymmetry, skewness and streaming), the undertow and the gravity.

Depth-averaged current (or current): Time-averaged water volume flux per unit width, after filtering out the fast oscillatory motions, divided by the time-averaged water depth (also called mass-transport current in the literature).

Depth-averaged sediment concentration (DASC): The total volume of mobilized sediment in a water column (including bedload and suspended load) per water volume unit in case of sediment transport by a current.

Down-current orientation: Orientation of a transverse bar or ridge so that its offshore end is shifted downstream.

Edge wave: Surface gravity wave that propagates along the coast and is trapped against it in such a way that its amplitude decays roughly exponentially in the seaward direction with an e-folding distance of the order of the alongshore wavelength.

Feedback mechanism: Loop wherein the hydrodynamics affects the morphology via the sediment transport and the morphology affects in turn the hydrodynamics setting the solid boundaries of the water body. Starting in a perturbed equilibrium situation, the changes in hydrodynamics cause changes in morphology and these may in turn reinforce (damp) the changes in hydrodynamics. In such case the feedback is called positive (negative).

Infragravity wave: Surface gravity waves of lower frequency than the incident wind or swell waves, with wave periods ranging from about 20 s to a few minutes.

Inner shelf: Region in the nearshore spanning from water depths of a few meters to tens of meters, between the surf zone and the middle continental shelf (where the along-shelf circulation is usually in geostrophic balance).

Linear wave theory: A simplified (linearized) description of surface gravity waves, applicable to waves of small height to depth ratio and steepness.

Low frequency eddies: Horizontal eddies in the surf zone generated by incident wave groups that evolve at time scales of O(30 min) and have length scales of O(100 m).

Morphodynamic instability: A perturbation growing out of a morphodynamic equilibrium due to a positive feedback between flow and morphology so that a new morphologic pattern showing higher complexity level than the equilibrium emerges.

Morphodynamic pattern: Spatial pattern in the morphology and the water motions due to their mutual coupling.

Net: Adjective applied to variables that result from a time averaging over a time scale shorter than that of interest.

Quasi-steady approximation: Approximation in coastal morphodynamics where the flow is assumed to be steady at each time over the morphology at that time, even though the morphology is changing slowly with time. Mathematically this means dropping out all the partial time-derivatives from the hydrodynamic equations.

Reynolds stress tensor: Stress tensor in the depth and time-averaged momentum balance equations that accounts for the momentum flux from the turbulent flow fluctuations into the mean motions.

Rhythmic Bar and Beach (RBB) state: Beach state characterized by a rhythmic shoreline and one or more crescentic bars in the beach state classification of *Wright and Short* [1984].

Rip channel: Elongated bed depression or channel trending shore-normal (or nearly) in the surf zone where commonly a rip current occurs.

Rip-channel system: Patch of several rip channels along the coast.

Rip current: Jet-like seaward flowing current that can easily reach O(1 m s^{-1}) and can be very dangerous for beach users. Rip currents may be due to many causes, one of them are breaking waves in a surf zone with one or more rip channels.

Root-mean-square wave height: Square root of the mean squared wave height, taking all the waves in a wave record.

Saturation of the growth: The process whereby an instability mode growing out of an unstable equilibrium stops its growth and a new equilibrium displaying certain pattern is reached.

Sediment load: The total volume of mobilized sediment per horizontal area unit in case of sediment transport by a current (also called transport capacity, stirring function or depth-integrated sediment concentration).

Sediment porosity: Measure of the void (i.e., ”empty”) spaces in bed sediment and is the fraction of the volume of voids over the total volume, between 0 and 1.

Sediment transport: Movement of sediment particles driven by the forces exerted by water motion.

Self-organization (process): Process where some form of global order (pattern) emerges out of the local interactions between the components of an initially disordered system. This process is spontaneous: the spatial characteristics of the emergent patterns do not require spatial variations in the forcing. It is often triggered by random fluctuations that are amplified by positive feedback.

Shear wave: Oscillatory water motion in the surf zone in case of oblique wave incidence originated by a shear instability of the alongshore current. It consists of a meandering of the current that propagates downstream with a celerity of the order of the current magnitude and with a period similar to infragravity waves but with significantly smaller wavelengths.

Shoal: Sand deposit with higher bed levels than the surrounding area.

Shoaling zone: Nearshore zone offshore the surf zone where the waves feel the sea bed and thereby change propagation direction (refraction), wave amplitude and shape.

Shore-parallel bar: Elongated shoal parallel to the shore (also called linear bar, alongshore-uniform bar or straight bar).

Surf zone: Nearshore zone spanning from the beach face to the breaker line, where waves break and propagate onshore as bores.

Suspended load transport: Sediment transport corresponding to particles that are advected by the current in suspension within the water flow.

Swash zone: Zone of the beach face that is covered and uncovered by water as the water front moves up and down following the incoming waves.

Transverse Bar and Rip (TBR) state: Beach state characterized by transverse bars associated to the horns of a crescentic bar that have been attached to the shoreline in the beach state classification of *Wright and Short* [1984].

Turbulence: Random and fast motion of water as small eddies, characterized by small length and time scales.

Undertow: A nearshore seaward-directed near-bed current that is feeded by the return flow from broken waves and is caused by the unbalance between the vertical distribution of wave radiation stresses and pressure gradients (also called bed return current in the literature).

Up-current orientation: Orientation of a transverse bar or ridge so that its offshore end is shifted upstream.

Uprush: Flow of water up the swash zone during the forward motion of a wave incoming at the beach face.

Wave basin: Laboratory basin with width and length of comparable magnitude and a wave maker on one side and a beach or wave-absorbing surface on the opposite side to observe the 3D behavior of waves and related processes.

Wave energy density: Total mechanical energy of the wave water motion per horizontal area unit.

Wave flume: Long and narrow wave-basin of a width much smaller than length to observe the 2D behavior of waves and related processes.

Wave orbital velocity: Velocity of the water parcels associated with a wave.

Wave radiation stresses: Time-averaged and depth-integrated flux of momentum caused by the wave oscillatory motion only, i.e., excluding the contribution of hydrostatic pressure related to the mean-surface elevation.

Wave refraction: Change in wave direction due to a change in phase celerity. It can occur because of bathymetric changes or due to the action of a current and it causes a reduction of the angle between wave crests and the coastline when waves approach the shore.

Wave shoaling: Change in wave height due to the reduction in water depth when waves approach the shore. For small angles of wave incidence wave heights first slightly decrease and then increase significantly before breaking.

NOTATION

x	spatial coordinate in the cross-shore direction
y	spatial coordinate in the along-shore direction
z	spatial coordinate in the vertical direction
t	time
$\vec{v}$	Depth-averaged current

z_b sea bed level

z_s time-averaged sea level

D time-averaged water depth

H root-mean-square wave height

E wave energy density

ρ sea water density

g gravitational acceleration

$\vec{\tau}_b$ bed shear stress

$\vec{\tau}_s$ wind surface shear stress

$\mathbf{R}$ Reynolds turbulent stress tensor

$\mathbf{S}$ wave radiation stress tensor

u_b root-mean-square amplitude of the wave orbital velocity near the bed

k wavenumber of the incident waves

θ wave propagation angle with respect to the shore normal ($-x$ axis)

$\vec{q}$ sediment transport (volume of sediment crossing a vertical surface per width unit and time unit)

α sediment load (total sediment volume in a water column per horizontal area unit)

γ sediment diffusivity coefficient

h	bed level deviation with respect to alongshore uniform long-term equilibrium
z_{b0}	bed level corresponding to the alongshore uniform long-term equilibrium
p	bed sediment porosity
$\mathcal{C} = \alpha/D$	depth-averaged sediment concentration (DASC)
$\mathcal{C}_0(x)$	depth-averaged sediment concentration for the alongshore uniform long-term equilibrium
$D_0(x)$	water depth for the alongshore uniform long-term equilibrium
$V_0(x)$	alongshore current for the alongshore uniform long-term equilibrium
c	small perturbation in DASC
d	small perturbation in water depth
u	small perturbation in the cross-shore component of $\vec{v}$
v	small perturbation in the alongshore component of $\vec{v}$
x_m	cross-shore position of a local maximum in DASC
w	vertical infiltration velocity in the swash zone

ACKNOWLEDGMENTS. Data supporting Figures 11, 15a and 15b are available as Data sets S1, S2 and S3, respectively (more details in Supporting Information file).

This research has been funded by the Spanish government through the research project CTM2012-35398 and by NWO research grant 820.01.003. We thank Dr. David Pino for reading a preliminary version of the paper and making useful suggestions. We thank the associate editor Prof. Gregory Okin, the reviewer Prof. Brad Murray and three other anonymous reviewers for their fruitful comments during the revision process, which resulted in an improved version of the manuscript.

REFERENCES

Ackers, P., and W. R. White (1973), Sediment transport: a new approach and analysis, in *Proc. ASCE*, vol. 99(HY11), pp. 2041–60.

Almar, R., G. Coco, K. Bryan, D. Huntley, A. Short, and N. Senechal (2008), Video observations of beach cusp morphodynamics, *Mar. Geol.*, doi:10.1016/j.margeo.2008.05.008, in press.

Amoudry, L. O., and A. J. Souza (2011), Deterministic coastal morphological and sediment transport modeling: A review and discussion, *Rev. Geophys.*, *49*(RG2002), doi:10.1029/2010RG000341.

Antia, E. E. (1996), Rates and patterns of migration of shoreface–connected sandy ridges along the southern North Sea coast, *J. Coastal Res.*, *12*, 38–46.

Bailard, J. A., and D. L. Inman (1981), An energetics bedload model for a plane sloping beach: local transport, *J. Geophys. Res.*, *86*(C3), 2035–2043.

Baptist, M., J. Van Dalfsen, A. Weber, S. Passchier, and S. Van Heteren (2006), The distribution of macrozoobenthos in the southern North Sea in relation to meso-scale bedforms, *Estuar. Coast. Shelf Sci.*, *68*, 538 – 54.

Barcilon, A. I., and J. P. Lau (1973), A model for formation of transverse bars, *J. Geophys. Res*, *78*(15), 2656–2664.

Barnes, M. P., and T. E. Baldock (2010), A Lagrangian model for boundary layer growth and bed shear stress in the swash zone, *Coast Eng.*, *57*, 385–396.

Benedet, L., C. W. Finkl, and W. N. Hartog (2007), Processes controlling development of erosional hot spots on a beach nourishment project, *J. Coast. Res.*, *23*(1), 33–48.

Bijker, E. W. (1968), Littoral drift as function of waves and current, in *Coastal Eng. 1968*, pp. 415–435, Am. Soc. of Civ. Eng.

Blondeaux, P. (2001), Mechanics of coastal forms, *Annu. Rev. Fluid Mech.*, *33*, 339–370.

Bowen, A. J., and D. L. Inman (1971), Edge waves and crescentic bars, *J. Geophys. Res.*, *76*, 8662–8671.

Briganti, R., N. Dodd, D. Pokrajac, and T. O'Donoghue (2011), Nonlinear shallow water modelling of bore-driven swash: description of the bottom boundary layer, *Coast Eng.*, *58*(6), 463–477.

Brocchini, M., and D. H. Peregrine (1996), Integral flow properties of the swash zone and averaging, *J. Fluid Mech.*, *317*, 241–273.

Bruner, K. R., and R. A. Smosna (1989), The movement and stabilization of beach sand on transverse bars, Assateague Island, Virginia, *J. Coastal Res.*, *5*(3), 593–601.

Butt, T., P. Russel, J. Puleo, J. Miles, and G. Masselink (2004), The influence of bore turbulence on sediment transport in the swash and inner surf zones, *Cont. Shelf Res.*, *24*, 757–771.

Caballeria, M., G. Coco, A. Falqués, and D. A. Huntley (2002), Self-organization mechanisms for the formation of nearshore crescentic and transverse sand bars, *J. Fluid Mech.*, *465*, 379–410.

Calvete, D., and H. E. de Swart (2003), A nonlinear model study on the long-term behavior of shoreface-connected sand ridges, *J. Geophys. Res.*, *108*(C53169), doi:10.1029/2001JC001091.

Calvete, D., A. Falqués, H. E. de Swart, and M. Walgreen (2001), Modelling the formation of shoreface-connected sand ridges on storm-dominated inner shelves, *J. Fluid Mech.*, *441*, 169–193.

Calvete, D., H. E. de Swart, and A. Falqués (2002), Effect of depth-dependent stirring on the final amplitude of the shoreface-connected sand ridges, *Cont. Shelf Res.*, *22*, 2763–2776.

Calvete, D., N. Dodd, A. Falqués, and S. M. van Leeuwen (2005), Morphological development of rip channel systems: Normal and near normal wave incidence, *J. Geophys. Res.*, *110*(C10006), doi:10.1029/2004JC002803.

Camenen, B., and P. Larroudé (2003), Comparison of sediment transport formulae for a coastal environment, *Coastal Eng.*, *48*, 111–132.

Castelle, B., and G. Coco (2012), The morphodynamics of rip channels on embayed beaches, *Cont. Shelf Res.*, *43*, 10–23.

Castelle, B., and G. Coco (2013), Surf zone flushing on embayed beaches, *Geophys. Res. Lett.*, *40*(10), 2206–2210, doi:10.1002/grl.50485.

Castelle, B., and B. G. Ruessink (2011), Modeling formation and subsequent nonlinear evolution of rip channels: time-varying versus time-invariant wave forcing, *J. Geophys. Res.*, *116*(F04008), doi:10.1029/2011JF001997.

Castelle, B., P. Bonneton, N. Senechal, H. Dupuis, R. Butel, and D. Michel (2006), Dynamics of wave-induced currents over an alongshore non-uniform multiple-barred sandy beach on the aquitanian coast, france, *Cont. Shelf Res.*, *26*(1), 113–131.

Castelle, B., P. Bonneton, H. Dupuis, and N. Senechal (2007), Double bar beach dynamics on the high-energy meso-macrotidal French Aquitanian coast: A review, *Mar. Geol.*, *245*, 141–159.

Castelle, B., H. Michallet, V. Marieu, F. Leckler, H. Dubarbier, A. Lambert, C. Berni, P. Bonneton, E. Barthlemy, and F. Bouchette (2010a), Laboratory experiment on rip current circulations over a movable bed: Drifter measurements, *J. Geophys. Res.*, *115*(C12008), doi:10.1029/2010JC006343.

Castelle, B., B. G. Ruessink, P. Bonneton, V. Marieu, N. Bruneau, and T. D. Price (2010b), Coupling mechanisms in double sandbar systems. part 1: Patterns and physical explanation, *Earth Surf. Process. Landforms*, *35*(doi:10.1002/esp.1929), 476–486.

Christensen, E., R. Deigaard, and J. Fredsoe (1994), Sea bed stability on a long straight coast, in *Coastal Eng. 1994,* vol. 4, pp. 1865–1879, Am. Soc. of Civ. Eng.

Coco, G., and D. Calvete (2009), The use of linear stability analysis to characterize the variability of multiple sandbars systems, in *Proceedings of the Coastal Dynamics 2009, Impacts of Human Activities on Dynamic Coastal Processes*, World Scientific.

Coco, G., and A. B. Murray (2007), Patterns in the sand: From forcing templates to self-organization, *Geomorphology*, *91*(271-290).

Coco, G., T. J. O'Hare, and D. A. Huntley (1999), Beach cusps: a comparison of data and theories for their formation, *J. Coastal Res.*, *15*(3), 741–749.

Coco, G., D. A. Huntley, and T. J. O'Hare (2000), Investigation of a self-organization model for beach cusp formation and development, *J. Geophys. Res.*, *105*(C9), 21,991–22,002.

Coco, G., D. A. Huntley, and T. J. O'Hare (2001), Regularity and randomness in the formation of beach cusps, *Mar. Geol.*, *178*, 1–9.

Coco, G., T. K. Burnet, B. T. Werner, and S.Elgar (2003), Test of self-organization in beach cusp formation, *J. Geophys. Res.*, *108*(C33101), doi:10.1029/2002JC001496.

Coco, G., T. K. Burnet, B. T. Werner, and S. Elgar (2004a), The role of tides in beach cusp development, *J. Geophys. Res.*, *109*(C04011), doi:10.1029/2003JC002154.

Coco, G., B. G. Ruessink, I. M. J. van Enckevort, M. Caballeria, A. Falqués, R. A. Holman, N. G. Plant, and I. L. Turner (2004b), Video observations of crescentic sandbar formation and modelling implications, in *Coastal Eng. 2004,* vol. 3, pp. 2767–2775, Am. Soc. of Civ. Eng.

Dalrymple, R. A., J. H. MacMahan, A. J. H. M. Reniers, and V. Nelko (2011), Rip currents, *Ann. Rev. Fluid Mech.*, *43*, 551–581.

Damgaard, J., N. Dodd, L. Hall, and T. Chesher (2002), Morphodynamic modelling of rip channel growth, *Coastal Eng.*, *45*, 199–221.

De Melo Apoluceno, D., H. Howa, H. Dupuis, and G. Oggian (2002), Morphodynamics of ridge and runnel systems during summer, *J. Coastal Res.,* Special Issue, *36*, 222–230.

de Swart, H., M. Walgreen, D. Calvete, and N. Vis-Star (2008), Nonlinear modelling of shoreface-connected ridges; impact of grain sorting and interventions, *Coastal Eng.*, *55*(78), 642 – 656, doi:10.1016/j.coastaleng.2007.11.007.

de Swart, H. E., and J. T. F. Zimmerman (2009), Morphodynamics of tidal inlet systems, *Annu. Rev. Fluid Mech.*, *41*, 203–229.

Deigaard, R., N. Drønen, J. Fredsoe, J. H. Jensen, and M. P. Jørgensen (1999), A morphological stability analysis for a long straight barred coast, *Coastal Eng.*, *36*(3), 171–195.

Dodd, N., P. Blondeaux, D. Calvete, H. E. de Swart, A. Falqués, S. J. M. H. Hulscher, G. Różyński, and G. Vittori (2003), The use of stability methods in understanding the morphodynamical behavior of coastal systems, *J. Coastal Res.*, *19*(4), 849–865.

Dodd, N., A. Stoker, D. Calvete, and A. Sriariyawat (2008), On beach cusp formation, *J. Fluid Mech.*, *597*, 145–169.

Duane, D. B., M. E. Field, E. P. Miesberger, D. J. P. Swift, and S. Williams (1972), Linear shoals on the Atlantic continental shelf, Florida to Long Island, in *Shelf sediment transport: process and patterns*, edited by D. J. P. Swift, D. B. Duane, and O. H. Pilkey, Van Nostrand Reinhold, New York, U.S.A.

Dyer, K. R., and D. A. Huntley (1999), The origin, classification and modelling of sand banks and ridges, *Cont. Shelf Res.*, *19*(10), 1285–1330.

Eliot, M. J., A. Travers, and I. Eliot (2006), Morphology of a low-energy beach, Como Beach, Western Australia, *J. Coastal Res.*, *22*(1), 63–77.

Engelund, F., and E. Hansen (1972), A monograph on sediment transport in alluvial streams, *Tech. Rep. 3rd edn. Technical Press*, Copenhagen, Denmark.

Falqués, A. (1989), Formación de topografía rítmica en el Delta del Ebro, *Revista de Geofísica*, *45*(2), 143–156.

Falqués, A., A. Montoto, and V. Iranzo (1996), Bed-flow instability of the longshore current, *Cont. Shelf Res.*, *16*(15), 1927–1964.

Falqués, A., G. Coco, and D. A. Huntley (2000), A mechanism for the generation of wave-driven rhythmic patterns in the surf zone, *J. Geophys. Res.*, *105*(C10), 24,071–24,088.

Feddersen, F., R. T. Guza, S. Elgar, and T. H. C. Herbers (2000), Velocity moments in alongshore bottom stress parameterizations, *J. Geophys. Res.*, *105*(C4), 8673–8686.

Fredsoe, J., and R. Deigaard (1992), *Mechanics of Coastal Sediment Transport*, *Advanced Series on Ocean Engineering*, vol. 3, World Scientific, Singapore.

Gallagher, E. L. (2011), Computer simulations of self-organized megaripples in the nearshore, *J. Geophys. Res.*, *116*(F01004), doi:10.1029/2009JF001473.

Garnier, R., D. Calvete, A. Falqués, and M. Caballeria (2006), Generation and nonlinear evolution of shore-oblique/transverse sand bars, *J. Fluid Mech.*, *567*, 327–360.

Garnier, R., D. Calvete, A. Falqués, and N. Dodd (2008), Modelling the formation and the long-term behavior of rip channel systems from the deformation of a longshore bar, *J. Geophys. Res.*, *113*(C07053), doi:10.1029/2007JC004632.

Garnier, R., N. Dodd, A. Falqués, and D. Calvete (2010), Mechanisms controlling crescentic bar amplitude, *J. Geophys. Res.*, *115*(F02007), doi:10.1029/2009JF001407.

Garnier, R., Falqués, D. Calvete, J. Thiébot, and F. Ribas (2013), A mechanism for sandbar straightening by oblique wave incidence, *Geophys. Res. Lett.*, *40*, doi:10.1002/grl.50464.

Gelfenbaum, G., and G. R. Brooks (2003), The morphology and migration of transverse bars off the west-central Florida coast, *Mar. Geol.*, *200*, 273–289.

Goff, J. A., D. J. P. Swift, C. S. Duncan, L. A. Mayer, and J. Hughes-Clarke (1999), High-resolution swath sonar investigation of sand ridge, dune and ribbon morphology in the offshore environment of the New Jersey margin, *Mar. Geol.*, *161*, 307–337.

Grass, A. J. (1981), Sediment transport by waves and currents, *Tech. Rep. FL29*, SERC London Cent. Mar. Technol., London, UK.

Guza, R. T., and A. Bowen (1975), On the amplitude of beach cusps, *J. Geophys. Res.*, *86*, 4125–4131.

Guza, R. T., and D. Inman (1975), Edge waves and beach cusps, *J. Geophys. Res.*, *80*(21), 2997–3012.

Haller, M. C., R. A. Dalrymple, and I. A. Svendsen (2002), Experimental study of nearshore dynamics on a barred beach with rip channels, *J. Geophys. Res.*, *107*(C6), 10.1029/2001JC000,955.

Hino, M. (1974), Theory on formation of rip-current and cuspidal coast, in *Coastal Eng. 1974*, pp. 901–919, Am. Soc. of Civ. Eng.

Holman, R. A., and A. J. Bowen (1982), Bars, bumps, and holes: models for the generation of complex beach topography, *J. Geophys. Res.*, *87*(C1), 457–468.

Holman, R. A., G. Symonds, E. B. Thornton, and R. Ranasinghe (2006), Rip spacing and persistence on an embayed beach, *J. Geophys. Res.*, *111*(C01006), doi:10.1029/2005JC002965.

Hunter, R. E., H. E. Clifton, and R. L. Phillips (1979), Depositional processes, sedimentary structures, and predicted vertical sequences in barred nearshore systems, Southern Oregon coast, *J. Sediment. Petrol.*, *49*(3), 711–726.

Kana, T. W., J. D. Rosati, and S. B. Traynum (2011), Lack of evidence for onshore sediment transport from deep water at decadal time scales: Fire Island, New York, *J. Coastal Res.*, *SI*(59), 61–75, doi:10.2112/SI59-007.

Klein, M. D., and H. M. Schuttelaars (2005), Morphodynamic instabilities of planar beaches: sensitivity to parameter values and process formulations, *J. Geophys. Res.*, *110*(F04S18), doi:10.1029/2004JF000213.

Klein, M. D., and H. M. Schuttelaars (2006), Morphodynamic evolution of double-barred beaches, *J. Geophys. Res.*, *110*(C06017), doi:10.1029/2005JC003155.

Komar, P. D. (1998), *Beach Processes and Sedimentation*, second ed., Prentice Hall, Englewood Cliffs, N.J.

Konicki, K. M., and R. A. Holman (2000), The statistics and kinematics of transverse bars on an open coast, *Mar. Geol.*, *169*, 69–101.

Lafon, V., D. D. M. Apoluceno, H. Dupuis, D. Michel, H. Howa, and J. M. Froidefond (2004), Morphodynamics of nearshore rhythmic sandbars in a mixed-energy environment (SW France): I. Mapping beach changes using visible satellite imagery, *Estuar. Coast. Shelf Sci.*, *61*, 289–299.

Lane, E. M., and J. M. Restrepo (2007), Shoreface-connected ridges under the action of waves and currents, *J. Fluid Mech.*, *582*, 23–52.

Levoy, F., E. J. Anthony, O. Monfort, N. Robin, and P. Bretel (2013), Formation and migration of transverse bars along a tidal sandy coast deduced from multi-temporal lidar datasets, *Mar. Geol.*, *342*, 39–52.

Lippmann, T. C., and R. A. Holman (1990), The spatial and temporal variability of sand bar morphology, *J. Geophys. Res.*, *95*(C7), 11,575–11,590.

Longuet-Higgins, M. S., and R. W. Stewart (1964), Radiation stresses in water waves: a physical discussion with applications, *Deep Sea Res.*, *11*, 529–562.

MacMahan, J. H., E. B. Thornton, T. P. Stanton, and A. J. H. M. Reniers (2005), RIPEX: Observations of a rip current system, *Mar. Geol.*, *218*, 113–134.

MacMahan, J. H., E. B. Thornton, and A. J. H. M. Reniers (2006), Rip current review, *Coastal Eng.*, *53*, 191–208.

Masselink, G., and A. Kroon (2006), Morphodynamics of intertidal bars in wave-dominated coastal settings – a review, *Geomorphology*, *73*, 33–49.

Masselink, G., P. Russell, G. Coco, and D. A. Huntley (2004), Test of edge wave forcing during formation of rhythmic beach morphology, *J. Geophys. Res.*, *109*(C06003), doi:10.1029/2004JC002339.

McBride, R. A., and T. F. Moslow (1991), Origin, evolution and distribution of shoreface sand ridges, Atlantic inner shelf, USA, *Mar. Geol.*, *97*, 57–85.

Mei, C. C. (1989), *The Applied Dynamics of Ocean Surface Waves*, *Advanced Series on Ocean Engineering*, vol. 1, World Scientific, Singapore.

Mei, C. C., M. Stiassnie, and D. K. P. Yue (2005), *Theory and Applications of Ocean Surface Waves: Part I, Linear Aspects*, *Advanced Series on Ocean Engineering*, vol. 23, World Scientific, Singapore.

Moulton, M., S. Elgar, and B. Raubenheimer (2013), Structure and evolution of dredged rip-channels, in *Extended Abstracts of Coastal Dynamics 2013*, edited by P. Bonneton and T. Garlan, pp. 1263–1274.

Murray, A. B. (2004), Rip channel development on nonbarred beaches: The importance of a lag in suspended-sediment transport, *J. Geophys. Res.*, *109*(C04026), doi:10.1029/2002JC001581.

Niederoda, A. W., and W. F. Tanner (1970), Preliminary study on transverse bars, *Mar. Geol.*, *9*, 41–62.

Niedoroda, A. W., D. J. P. Swift, A. G. F. Jr., and G. L. Freeland (1985), Barrier island evolution, Middle Atlantic shelf, U.S.A., part ii: evidence from the shelf floor, *Mar. Geol.*, *63*, 363–396.

Nnafie, A., H. E. de Swart, D. Calvete, and R. Garnier (2011), Formation of shoreface connected sand ridges: effects of rigid-lid approach, quasi-steady approach and wave-topography feedbacks, in *Proceeding of the 7th IAHR Symposium on River, Coastal and Estuarine Morphodynamics*, pp. 2114–2123, Tsinghua University Press, Beijing.

Nnafie, A., H. E. de Swart, D. Calvete, and R. Garnier (2014a), Effects of sea level rise on the formation and drowning of shoreface-connected sand ridges, a model study, *Continental Shelf Res.*, *80*, 32–48, doi:10.1016/j.csr.2014.02.017.

Nnafie, A., H. E. de Swart, D. Calvete, and R. Garnier (2014b), Modeling the response of shoreface-connected sand ridges to sand extraction on an inner shelf, *Ocean Dyn.*, pp. 1–18, doi:10.1007/s10236-014-0714-9.

Parker, G., N. W. Lanfredi, and D. J. P. Swift (1982), Seafloor response to flow in a Southern Hemisphere sand-ridge field: Argentina inner shelf, *Sediment. Geol.*, *33*, 195–216.

Pellón, E., R. Garnier, and R. Medina (2014), Intertidal finger bars at El Puntal, Bay of Santander, Spain: observation and forcing analysis, *Earth Surface Dynamics*, under revision.

Phillips, O. M. (1977), *The Dynamics of the Upper Ocean*, Cambridge University Press, Cambridge, U.K.

Price, T. D., and B. G. Ruessink (2011), State dynamics of a double sandbar system, *Cont. Shelf Res.*, *31*, 659–674.

Pritchard, D., and A. J. Hogg (2005), On the transport of suspended sediment by a swash event on a plane beach, *Coast. Eng.*, *52*, 1–23.

Putrevu, U., and I. A. Svendsen (1999), Three-dimensional dispersion of momentum in wave-induced nearshore currents, *Eur. J. Mech. B/Fluids*, pp. 83–101.

Ranasinghe, R., G. Symonds, K. Black, and R. Holman (2004), Morphodynamics of intermediate beaches: A video imaging and numerical modelling study, *Coastal Eng.*, *51*, 629–655.

Reniers, A. J. H. M., J. A. Roelvink, and E. B. Thornton (2004), Morphodynamic modeling of an embayed beach under wave group forcing, *J. Geophys. Res.*, *109*(C01030), doi:10.1029/2002JC001586.

Ribas, F., and A. Kroon (2007), Characteristics and dynamics of surfzone transverse finger bars, *J. Geophys. Res.*, *112*(F03028), doi:10.1029/2006JF000685.

Ribas, F., A. Falqués, and A. Montoto (2003), Nearshore oblique sand bars, *J. Geophys. Res.*, *108*(C43119), doi:10.1029/2001JC000985.

Ribas, F., H. E. de Swart, D. Calvete, and A. Falqués (2011), Modelling waves, currents and sandbars on natural beaches: the effect of surface rollers, *J. Marine Syst.*, *88*, 90–101, doi:10.1016/j.jmarsys.2011.02.016.

Ribas, F., H. E. de Swart, D. Calvete, and A. Falqués (2012), Modeling and analyzing observed transverse sand bars in the surf zone, *J. Geophys. Res.*, *117*(F02013), doi:10.1029/2011JF002158.

Ribas, F., A. ten Doeschate, H. E. de Swart, G. Ruessink, and D. Calvete (2014), Observations and modelling of surf-zone transverse finger bars, *Ocean Dynamics*, in press.

Ruessink, B. G., G. Coco, R. Ranasinghe, and I. L. Turner (2007), Coupled and noncoupled behavior of three-dimensional morphological patterns in a double sandbar system, *J. Geophys. Res.*, *112*(C07002), doi:10.1029/2006JC003799.

Schwab, W. C., W. E. Baldwin, C. J. Hapke, E. E. Lentz, P. T. Gayes, J. F. Denny, J. H. List, and J. C. Warner (2013), Geologic evidence for onshore sediment transport from the inner continental shelf: Fire Island, New York, *J. Coastal Res.*, *29*(3), 526544, doi:10.2112/JCOASTRES-D-12-00160.1.

Shepard, F. P. (1952), Revised nomenclature for depositional coastal features, *Bull. Am. Assoc. Petrol. Geol.*, *36*(10), 1902–1912.

Short, A. D. (1999), *Handbook of Beach and Shoreface Morphodynamics*, Wiley, Chichester.

Slacum, H. W., W. H. Burton, E. T. Mehtratta, E. D. Weber, R. L. Llansó, and J. De-Baxter (2010), Assemblage structure in shoal and flat-bottom habitats on the inner continental shelf of the Middle Atlantic Bight, USA, *Marine and Coastal Fisheries*, *2*, 277–298, doi: 10.1577/C09-012.1.

Smit, M., A. Reniers, B. Ruessink, and J. Roelvink (2008), The morphological response of a nearshore double sandbar system to constant wave forcing, *Coastal Eng.*, *55*, 761–770.

Smit, M., A. Reniers, and M. Stive (2012), Role of morphological variability in the evolution of nearshore sandbars, *Coastal Eng.*, *69*, 19–28.

Sonu, C. J. (1968), Collective movement of sediment in littoral environment, in *Coastal Eng. 1968*, pp. 373–400, Am. Soc. of Civ. Eng.

Sonu, C. J. (1973), Three-dimensional beach changes, *J. Geology*, *81*, 42–64.

Soulsby, R. L. (1997), *Dynamics of Marine Sands*, Thomas Telford, London, U.K.

Splinter, K. D., R. A. Holman, and N. G. Plant (2011), A behavior oriented dynamic model for sandbar migration and 2dh evolution, *J. Geophys. Res.*, *116*(C01020), doi:10.1029/2010JC006382.

Sriariyawat, A. (2009), Formation and evolution of beach cusps, Ph.D. thesis, School of Civil Engineering, University of Nottingham, Nottingham, UK.

Svendsen, I. A. (2006), *Introduction to Nearshore Hydrodynamics*, *Advanced Series on Ocean Engineering*, vol. 24, World Scientific, Singapore.

Swift, D. J. P., B. Holliday, N. Avignone, and G. Shideler (1972), Anatomy of a shoreface ridge system, False Cape, Virginia, *Mar. Geol.*, *12*, 59–84.

Swift, D. J. P., G. Parker, N. W. Lanfredi, G. Perillo, and K. Figge (1978), Shoreface-connected sand ridges on American and European shelves: a comparison, *Estuarine and Coastal Mar. Sci.*, *7*, 257–273.

Swift, D. J. P., A. W. Niedoroda, C. E. Vincent, and T. S. Hopkins (1985), Barrier island evolution, Middle Atlantic Shelf, U.S.A., part 1: shoreface dynamics, *Mar. Geol.*, *63*, 331–361.

Thiebot, J., D. Idier, R. Garnier, A. Falqués, and B. G. Ruessink (2012), The influence of wave direction on the morphological response of a double sandbar system, *Cont. Shelf Res.*, *32*, 71–85, doi:10.1016/j.csr.2011.10.014.

Thornton, B., and R. T. Guza (1983), Transformation of wave height distribution, *J. Geophys. Res.*, *88*(10), 5925–5938.

Thornton, E. B., J. MacMahan, and A. S. Jr. (2007), Rip currents, mega-cusps, and eroding dunes., *Mar. Geol.*, *240*, 151–167.

Tiessen, M., N. Dodd, and R. Garnier (2011), Development of crescentic bars for a periodically perturbed initial bathymetry, *J. Geophys. Res.*, *116*(F04016), doi:10.1029/2011JF002069.

Trowbridge, J. H. (1995), A mechanism for the formation and maintenance of shore-oblique sand ridges on storm-dominated shelves, *J. Geophys. Res.*, *100*(C8), 16,071–16,086.

van de Meene, J. W. H., and L. C. van Rijn (2000), The shoreface-connected ridges along the central Dutch coast - part 1: field observations, *Cont. Shelf Res.*, *20*(17), 2295–2323.

van den Berg, N., A. Falqués, and F. Ribas (2012), Modelling large scale shoreline sand waves under oblique wave incidence, *J. Geophys. Res.*, *117*(F03019), doi:10.1029/2011JF002177.

van Enckevort, I. M. J., and B. G. Ruessink (2003), Video observations of nearshore bar behaviour. Part 1: alongshore uniform variability, *Cont. Shelf Res.*, *23*, 501–512.

van Enckevort, I. M. J., B. G. Ruessink, G. Coco, K. Suzuki, I. L. Turner, N. G. Plant, and R. A. Holman (2004), Observations of nearshore crescentic sandbars, *J. Geophys. Res.*, *109*(C06028), doi:10.1029/2003JC002214.

van Gaalen, J. F., S. E. Kruse, G. Coco, L. Collins, and T. Doering (2011), Observations of beach cusp evolution at Melbourne Beach, Florida, USA, *Geomorphology*, *129*, 131–140.

van Leeuwen, S. M., N. Dodd, D. Calvete, and A. Falqués (2006), Physics of nearshore bed pattern formation under regular or random waves, *J. Geophys. Res.*, *111*(F01023), doi:10.1029/2005JF000360.

Vis-Star, N., H. de Swart, and D. Calvete (2008), Patch behaviour and predictability properties of modelled finite-amplitude sand ridges on the inner shelf, *Nonlinear Proc. Geophys.*, *15*, 943–955.

Vis-Star, N. C., H. E. de Swart, and D. Calvete (2007), Effect of wave-topography interactions on the formation of sand ridges on the shelf, *J. Geophys. Res.*, *112*(C06012), doi:10.1029/2006JC003844.

Voulgaris, G., and M. B. Collins (2000), Sediment resuspension on beaches: response to breaking waves, *Mar. Geol.*, *167*, 167–187.

Walgreen, M., D. Calvete, and H. E. de Swart (2002), Growth of large–scale bed forms due to storm–driven and tidal currents: a model approach, *Cont. Shelf Res.*, *22*, 2777–2793.

Walgreen, M., H. E. de Swart, and D. Calvete (2003), Effect of grain size sorting on the formation of shoreface-connected ridges, *J. Geophys. Res.*, *108*(C3), doi:10.1029/2002JC001435.

Werner, B. T., and T. M. Fink (1993), Beach cusps as self-organized patterns, *Science*, *260*, 968–971.

Wright, L. D., and A. D. Short (1984), Morphodynamic variability of surf zones and beaches: A synthesis, *Mar. Geol.*, *56*, 93–118.

Wright, L. D., and B. G. Thom (1977), Coastal depositional landforms, a morphodynamic approach, *Prog. Phys. Geog.*, *1*, 412–459.

Wright, L. D., J. Chappell, B. G. Thom, M. P. Bradshaw, and P. J. Cowell (1979), Morphodynamics of reflective and dissipative beach and inshore systems, Southeastern Australia, *Mar. Geol.*, *32*, 105–140.

Zimmerman, J. T. F. (1981), Dynamics, diffusion and geomorphological significance of tidal residual eddies, *Nature*, *290*, 549–555.

Zolezzi, G., R. Luchi, and M. Tubino (2012), Modeling morphodynamic processes in meandering rivers with spatial width variations, *Rev. Geophys.*, *50*(RG4005), doi:10.1029/2012RG000392.

Figure 1. Pictures of (a) a crescentic bar at the Truc Vert beach, France (spacing order of hundreds of m; source: Google Earth, image from NASA), (b) transverse bars at Byron Bay beach, Australia (spacing order of a few hundreds of m), (c) transverse bars at the Ebro delta, Spain (spacing order of a few tens of m), and (d) beach cusps at an Australian beach (spacing order of a few tens of m). The three latter photographs were taken by the authors.

TABLE 1. Examples of the coastal sandy features with alongshore rhythmic patterns described in the different sections of the manuscript

Coastal feature	Coastal part	Spatial scale	Temporal scale	Section[a]
Crescentic bars/ rip-channel systems	Surf zone	0.1-3 km	hours-days	4
Transverse bars	Surf zone	10-750 m	hours-days	5
Shoreface-connected ridges	Inner shelf	1-8 km	centuries-millenia	6
Beach cusps	Swash zone	1-50 m	minutes-hours	7

[a] In each section, a list of references with feature observations is included that substantiate the length and time scales.

Figure 2. Illustration of the incoming waves (panel a), depth-averaged sediment concentration profile (DASC, panel b), and bed level (panel c) on the coastal zone. Satellite image (panel d) of the coastal zone in front of Duck, North Carolina, USA (panel d, source: Google Earth, image from Terrametrics and DigitalGlobe). Superimposed to the satellite image, examples of coastal features described in the manuscript: beach cusps (panel e, with a bathymetry from a nearby island; adapted from *Coco et al.* [2004b]), surf zone transverse and crescentic bars (panels f and g, respectively, with time-averaged video images from the same Duck beach; source: Dr. N. Plant, from U. S. Geological Survey), and shoreface-connected sand ridges (panel h, with a bathymetry in front of Long Island, New York; source: NOAA National Geophysical Data Center, USA). Each feature figure has its own scale. The transverse bars and the ridges are up-current oriented.

Figure 3. Sketch of the general framework of coastal morphodynamic models.

Figure 4. Schematic drawing of the coastal system and its four different zones (these zones are defined in the Glossary). The coordinate system and some important variables used in this contribution are also plotted (the meaning of the different symbols is described in the Notation).

Figure 5. Sketch of two example processes that can be explained with the mass conservation equation: (a) case where a convergence of water flux leads to an increase in water depth, and (b) case where the quasi-steady hypothesis is assumed and a decrease in water depth leads to an acceleration of the flow.

TABLE 2. The Sediment Load α in Standard Sediment Transport Formulas.

Formula name [a]	Stirring processes	Reference	Sediment load α [b]
Bijker bedload	Waves/currents	*Bijker* [1968]	$\frac{A_B 0.40\, d_{50}}{\ln(12D/\Delta_r)} \exp\left(\frac{-0.27 g\,(s-1)\, d_{50}}{\mu_B (u_*^2 + 0.016\, u_o^2)}\right)$
Engelund-Hansen	Currents	*Engelund and Hansen* [1972]	$\frac{0.04\, c_D^{3/2} \lvert\vec{v}\rvert^4}{g^2 (s-1)^2\, d_{50}}$
Ackers-White	Currents	*Ackers and White* [1973]	$C_{AW} d_{35} \left(\frac{\lvert\vec{v}\rvert}{u_*}\right)^n \left(\frac{F_{AW} - A_{AW}}{A_{AW}}\right)^m$
Bailard bedload	Waves [c]	*Bailard and Inman* [1981]	$\frac{\epsilon_B c_f u_b^2}{g(s-1)\tan\phi_i}$
Bailard suspended load	Waves [c]	*Bailard and Inman* [1981]	$\frac{\epsilon_S c_f u_b^3}{g(s-1) w_s}$
Grass	Waves/currents	*Grass* [1981]	$A_G \left(\lvert\vec{v}\rvert^2 + \frac{0.08}{c_D} u_b^2\right)^{(n_G-1)/2}$
Soulsby-van Rijn	Waves/currents	*Soulsby* [1997]	$A_s \left(\left(\lvert\vec{v}\rvert^2 + \frac{0.018}{c_D} u_b^2\right)^{1/2} - u_c\right)^{2.4}$

[a] If not mentioned in the name of the formula, it describes total load transport (bedload plus suspended load).

[b] In the formulas, d_n is the grain diameter for which n% of the grains are finer, s is the density ratio of grain and water, u_* is the total friction velocity due to current alone, c_D is the drag coefficient applicable to depth-averaged current and c_f is the drag coefficient applicable to wave orbital velocities at the bed. More details and the meaning of the other variables and parameters can be found in *Soulsby* [1997].

[c] In the two Bailard formulas, wave orbital velocity amplitude is assumed to be much larger than depth-averaged currents, which is only valid for weak currents.

Figure 6. Sources of sediment stirring: wave orbital velocity at the bed (blue circles), depth-averaged current (blue wide arrow) and turbulent vortices (red swirls).

Figure 7. Sketches to interpret the sediment conservation equation in case of (a) bed accretion due to convergence of sediment transport, and (b) bed erosion due to divergence of sediment transport.

Figure 8. Sketch to interpret the erosion/deposition processes from the nonlinear BEE (8) in case of (a) bed accretion produced by a current with a component that opposes the gradient in $\mathcal{C}$ and (b) bed erosion produced by a current with a component in the direction of the gradient in $\mathcal{C}$. The lower panels show a plan-view of the water column, with a bump on the bed plotted in yellow and brown/grey colors representing accretion/erosion of the bump.

Figure 9. Erosion/deposition patterns producing (a) pure growth, (b) growth and down-drift migration, (c) pure down-drift migration, (d) decay and down-drift migration, and (e) pure decay of a morphologic feature consisting of an alongshore rhythmic system of bars and troughs. The bars are plotted in yellow and the brown (grey) colors represent the areas with accretion (erosion).

Figure 10. Time exposure images of a straight bar configuration (top) and a crescentic bar configuration (bottom), Duck, North Carolina, USA. The coast is at the top of the images. Courtesy of Prof. R. Holman, Oregon State University. Figure adapted from *Garnier et al.* [2013].

Figure 11. Modeled wave height H_0 (upper panel), depth-averaged sediment concentration $\mathcal{C}_0$ (middle panel), and bed level z_{b0} (lower panel). The variables have been computed with the model by *Ribas et al.* [2011] using normal wave incidence with an offshore wave height of 1.5 m and a wave period of 8 s. The $\mathcal{C}_0$ has been calculated with the Soulsby-van Rijn formula (Table 2), extended to include the stirring by turbulent vortices. In the middle panel, the dashed-blue line is the $\mathcal{C}_0$ due to the stirring by wave orbital velocities alone (the only stirring process in the original Soulsby-van Rijn formula), the red line is the $\mathcal{C}_0$ obtained due only to the turbulent vortices and the black line is the total $\mathcal{C}_0$ obtained when both stirring processes are accounted for.

Figure 12. Sketch of the formation mechanism of crescentic bars from a shore-parallel bar for normal wave incidence. Left: Gradients in DASC in surf zones with a shore-parallel bar (as shown in Figure 11) and rip current circulation induced by an incipient crescentic bar. Right: Morphologic effect of the joint action of the gradients of DASC and the rip current circulation (brown are accretion areas and grey are erosion areas).

Figure 13. Modeled formation and finite-amplitude behavior of a crescentic bar system. Modeled bathymetry at (a) $t = 0$, (b) $t = 20$ d and (c) $t = 100$ d, and (d) time evolution of bar amplitude $\|h\| = \overline{h^2}^{1/2}$. Figure adapted from *Garnier et al.* [2008].

Figure 14. Examples of observed transverse bars with different orientations: (a) shore-normal large-scale finger bars at Anna Maria Island, USA (source: Google Earth, image from U.S. Geological Survey and USDA Farm Service Agency) [details in *Gelfenbaum and Brooks*, 2003], (b) down-current oriented TBR bars at the French Atlantic coast, France (source: Google Earth) [details in *Castelle et al.*, 2006], (c) down-current oriented low-energy finger bars at El Puntal, Santander, Spain (source: Google Earth) [details in *Pellón et al.*, 2014] and (d) up-current oriented medium-energy finger bars at Noordwijk, the Netherlands (time exposure video image) [details in *Ribas and Kroon*, 2007].

TABLE 3. Classification of observed transverse bars, following *Pellón et al.* [2014], depending on the wave energy environment, their length scales (wavelength and cross-shore span) and their aspect ratio (wavelength divided by cross-shore span).

Type	Wave energy	Wavelength	Cross-shore span	Aspect ratio	References
(1) TBR bars	Medium-High	75–750 m	< 150 m	< 0.5	*Hunter et al.* [1979] *Wright et al.* [1979] *Lafon et al.* [2004] *MacMahan et al.* [2005] *Holman et al.* [2006] *Castelle et al.* [2006]
(2) Medium-energy finger bars	Medium	15–200 m	< 100 m	~ 1	*Konicki and Holman* [2000] *Ribas and Kroon* [2007] *Ribas et al.* [2014]
(3) Low-energy finger bars	Low	15–80 m	40–250 m	2–3	*Falqués* [1989] *Bruner and Smosna* [1989] *Eliot et al.* [2006] *Pellón et al.* [2014]
(4) Large-scale finger bars	Low-Medium	50–500 m	~ 1000 m	2–4	*Niederoda and Tanner* [1970] *Gelfenbaum and Brooks* [2003] *Levoy et al.* [2013]

TABLE 4. Classification of observed transverse bars depending on their orientation, when the main driving processes (and the bar orientation) have been identified. The mean beach slope below the bars is also indicated.

Orientation	Type	Beach slope	Main driving processes	References
Shore-normal	(1)	0.01	Wave breaking	*MacMahan et al.* [2005]
	(4)	0.003	Wave refraction	*Niederoda and Tanner* [1970]
Down-current	(1)	0.01	Wave breaking Wave-driven alongshore current	*Castelle et al.* [2006]
	(3)	0.015	Wind-waves incoming obliquely	*Bruner and Smosna* [1989] *Pellón et al.* [2014]
Up-current	(2)	0.02–0.04	Wave breaking Wave-driven alongshore current	*Ribas and Kroon* [2007] *Ribas et al.* [2014]

Figure 15. Modeled wave height H_0 (upper panel), alongshore current, V_0, depth-averaged sediment concentration $\mathcal{C}_0$ (middle panel), and bed level z_{b0} (lower panel) in the case of (a) terraced profile and (b) profile with a shore-parallel bar. The variables have been computed with the model by *Ribas et al.* [2011] using oblique wave incidence with an offshore wave height of 1 m, an offshore wave angle of (a) 20° and (b) 50° (at 28 m depth), and a wave period of 8 s. The $\mathcal{C}_0$ has been calculated with the Soulsby-van Rijn formula (Table 2), extended to include the stirring by turbulent vortices. In the middle panels, the solid-blue line is the $\mathcal{C}_0$ due to the stirring by depth-averaged current alone, the dashed-blue line is the $\mathcal{C}_0$ due to the stirring by wave orbital velocities alone, the red line is the $\mathcal{C}_0$ obtained due only to the turbulent vortices and the black line is the total $\mathcal{C}_0$ with the three processes included.

Figure 16. Sketch of the formation mechanism (gradients of DASC, horizontal circulation induced by the growing pattern in blue streamlines and accretion areas in brown) of transverse bars with (a) shore-normal, (b) down-current and (c) up-current orientations.

Figure 17. Simulations of (a) shore-normal (b) down-current (c) up-current oriented transverse bars obtained with a nonlinear model. Results of the bathymetry after several day of simulations, all the simulations have started with an alongshore uniform planar beach. Figures adapted from *Garnier et al.* [2006].

Figure 18. Bathymetric map of the Long Island continental shelf. Figure from *Nnafie et al.* [2014a].

Figure 19. Sketch of the formation mechanism of shoreface-connected sand ridges with the gradients of DASC, the horizontal circulation induced by the growing pattern (blue streamlines), and the accretion areas (in brown).

Figure 20. Contour plots of perturbations in bed level at different times (dimensional times $T = 0$, 300, 600, 900, 1200, 1500 yr) during a model simulation of shoreface-connected sand ridges. Figure adapted from *Calvete et al.* [2002]. The shoreline is located on the left of the panels.

Figure 21. Schematic diagram of a cuspate bathymetry, showing cusp horns and bays, together with the wave-averaged current circulation.

Figure 22. Schematic diagram showing cross-shore current (top), DASC (middle) and free surface (bottom) versus the cross-shore distance at different stages of the uprush (a) and backwash (b) in a swash excursion.

Figure 23. Schematic diagram showing the pattern of erosion and deposition in the swash zone in case of (a) alongshore uniform conditions, (b) horn location in presence of cusps and (c) bay location in presence of cusps. In b) and c), the dynamics is illustrated by altering backwash only: diminished at horns and enhanced at embayments. The upper plots show $\overline{-\mathcal{C}\nabla \cdot (D\vec{v})}$ and $\overline{-D\vec{v} \cdot \vec{\nabla}\mathcal{C}}$, terms of equation (11), for uprush and backwash (overbars here denote time averages over only those phases of the swash), and their net contribution during the whole wave cycle, versus the cross-shore distance. The pattern of erosion / deposition produced by the sum of the net contributions of these two terms is shown in the middle plots, and the corresponding change in bed level is shown in the lower plots.

Figure 24. Model simulation showing bed level change in colors (m), relative to a planar beach, and wave-averaged current vectors at $t = 0$ (upper panel), $t = 20$ wave periods (middle panel) and $t = 100$ wave periods (lower panel). Figure adapted from *Dodd et al.* [2008]. The shoreline is located on the top of the panels.

Figure 25. Global analysis for finite amplitude behavior of crescentic bars. (a) Normal wave incidence, saturation mechanism. Production $\mathcal{P}/\overline{h^2}$ and damping $\Delta/\overline{h^2}$ as a function of $\|h\| = \overline{h^2}^{1/2}$. Figure adapted from *Garnier et al.* [2010]. (b) Inhibition of rip channel formation for oblique waves. Maximum production and maximum damping as a function of the wave incidence angle (θ, at 4.5 m depth). Figure adapted from *Garnier et al.* [2013]. Note that the growth rate $\Omega = \mathcal{P}/\overline{h^2} - \Delta/\overline{h^2}$.

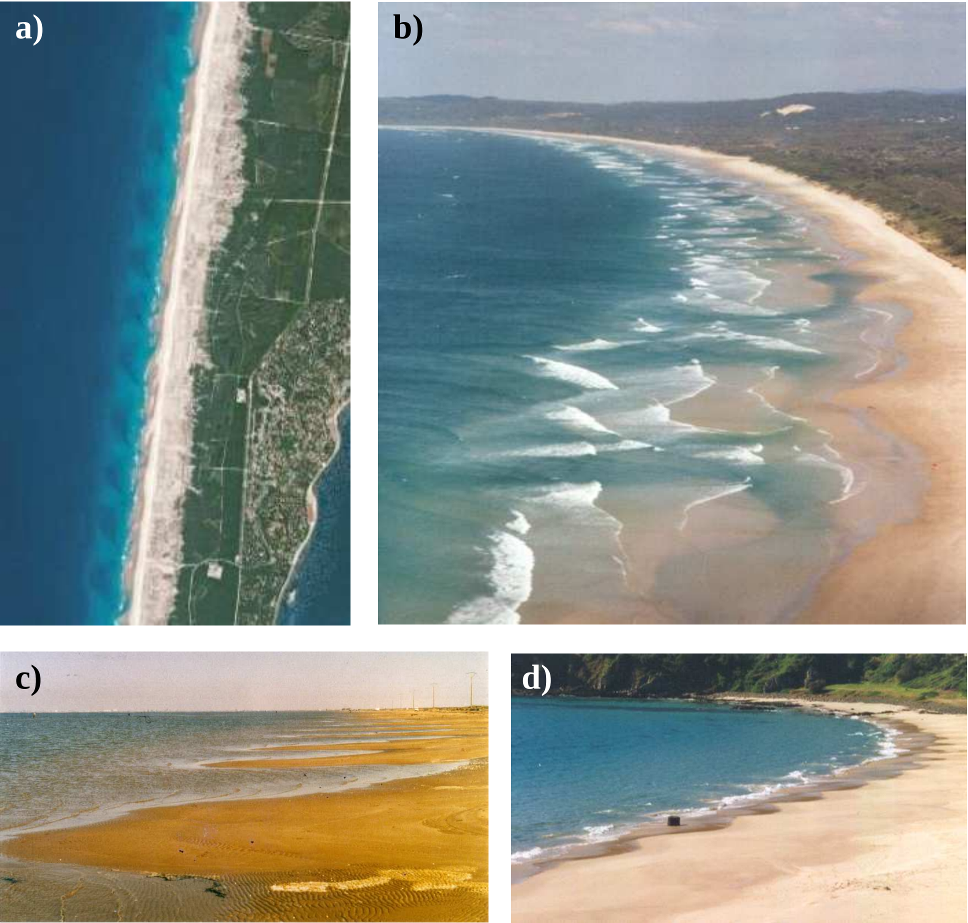
a)
b)
c)
d)

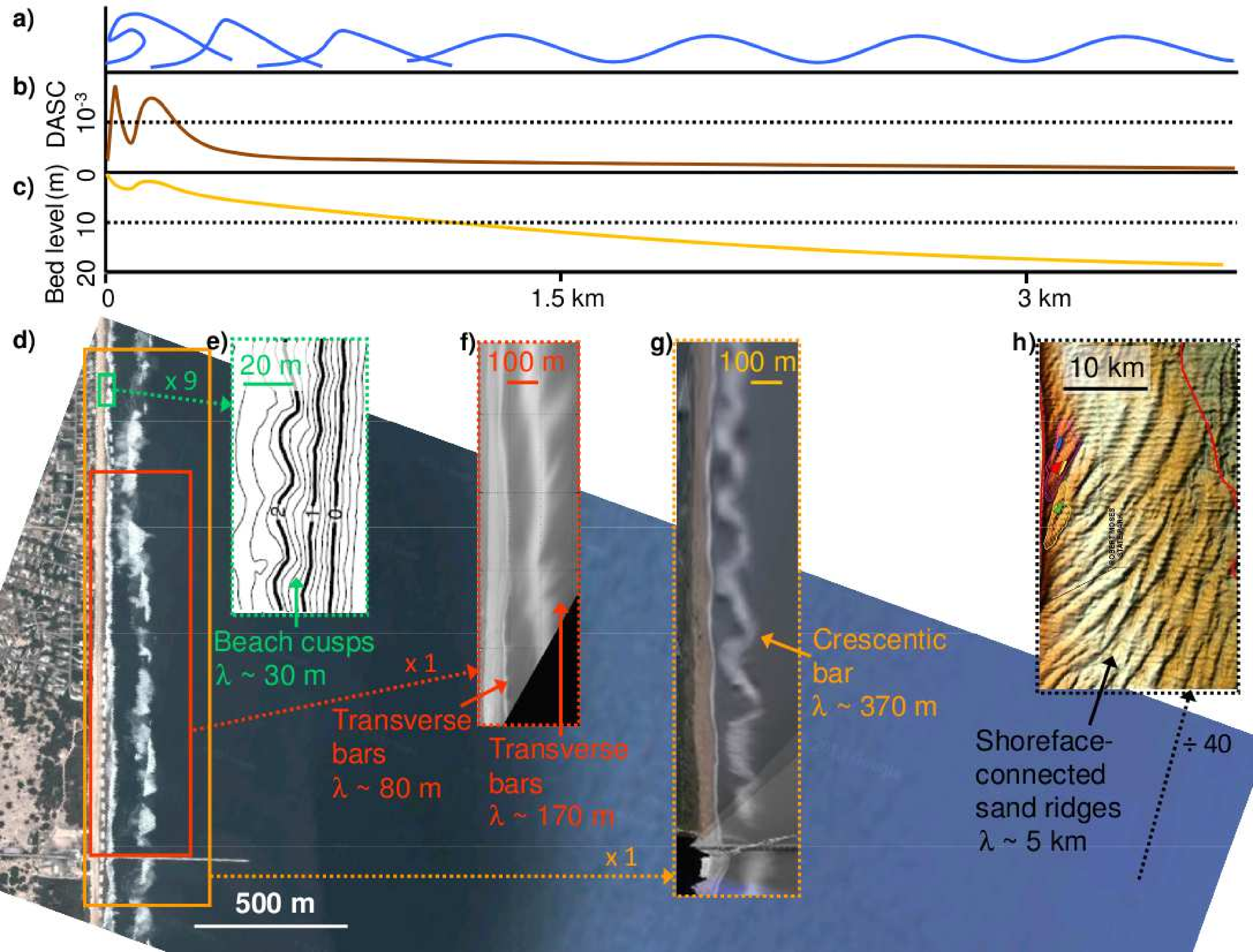

a)
b)
DASC
10^-3
10
0
c)
Bed level (m)
0
10
20
0
1.5 km
3 km
d)
x 9
e)
20 m
2
1
0
Beach cusps
λ ~ 30 m
x 1
f)
100 m
Transverse
bars
λ ~ 80 m
Transverse
bars
λ ~ 170 m
g)
100 m
Crescentic
bar
λ ~ 370 m
x 1
500 m
h)
10 km
Shoreface-
connected
sand ridges
λ ~ 5 km
÷ 40

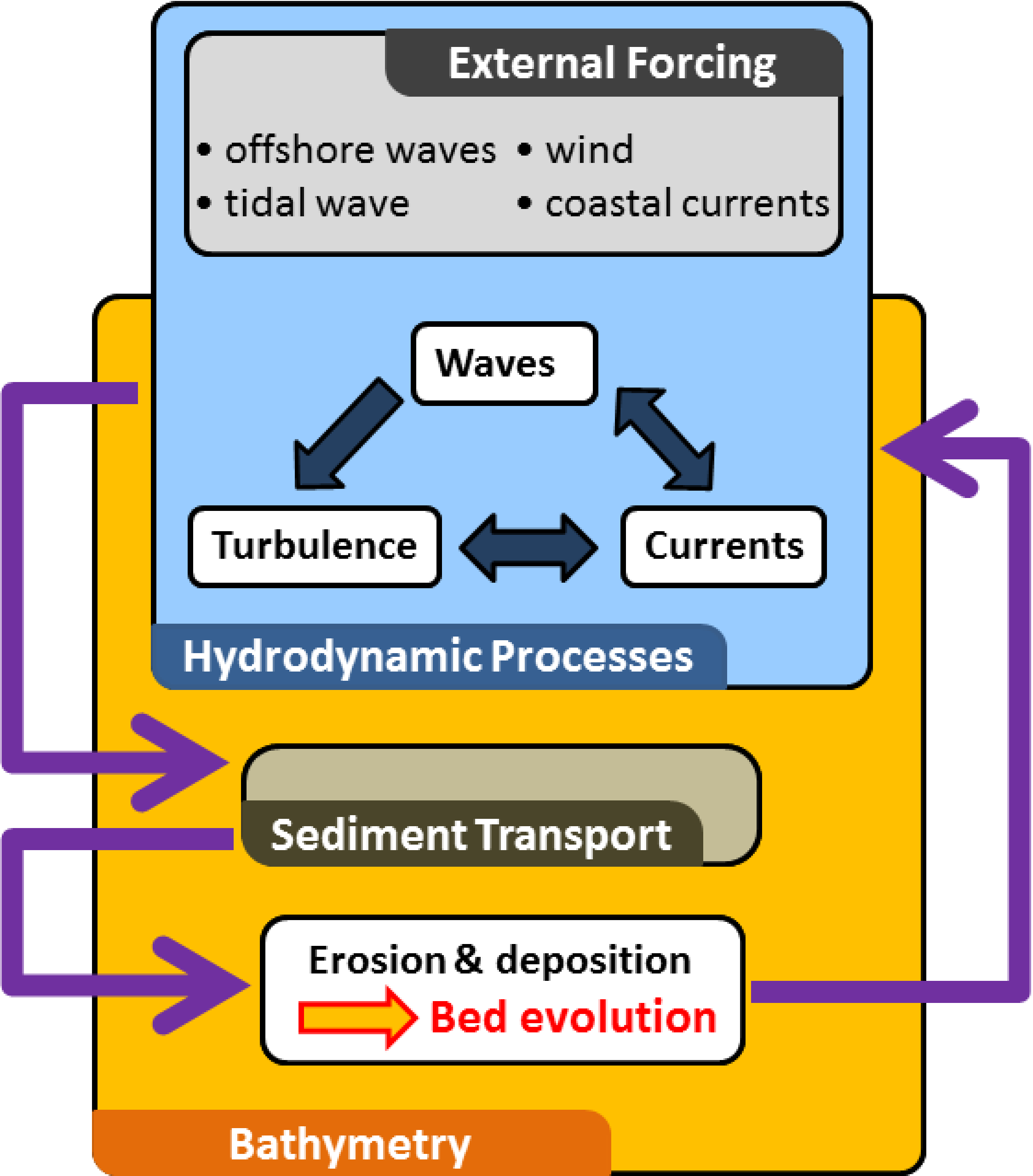
External Forcing
• offshore waves
• wind
• tidal wave
• coastal currents
Waves
Turbulence
Currents
Hydrodynamic Processes
Sediment Transport
Erosion & deposition
Bed evolution
Bathymetry

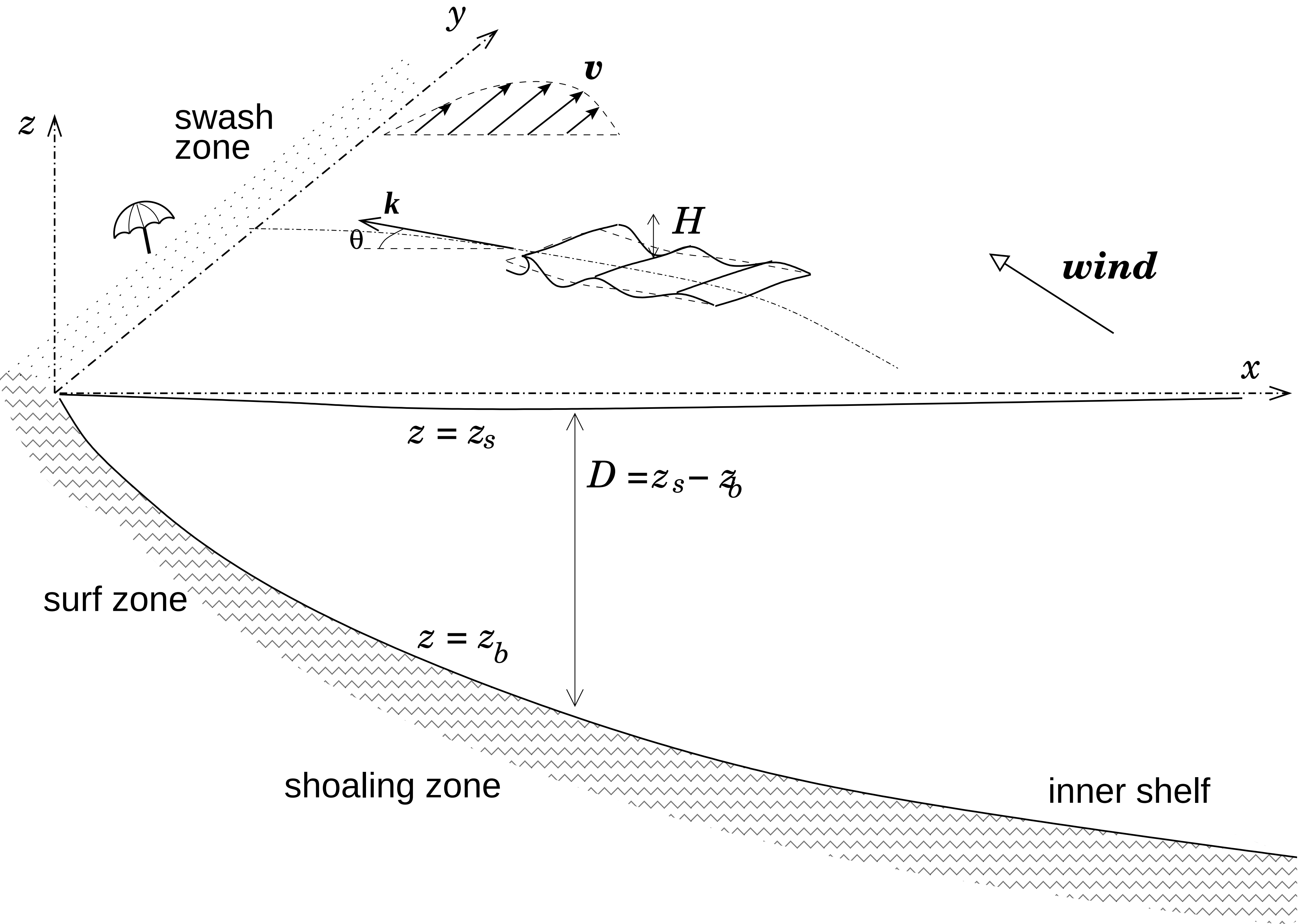

y
v
z
swash zone
k
H
θ
wind
x
z = z_s
D = z_s − z_b
surf zone
z = z_b
shoaling zone
inner shelf

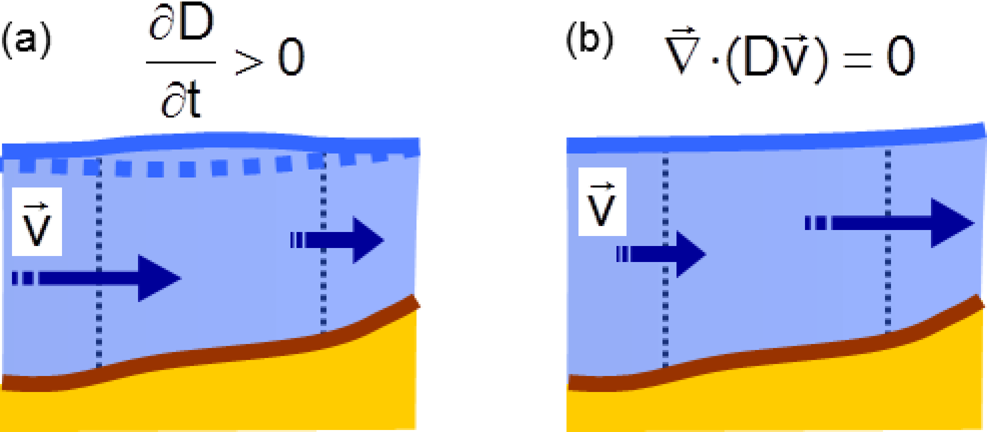

(a)
$\frac{\partial D}{\partial t} > 0$
$\vec{v}$
(b)
$\vec{\nabla} \cdot (D\vec{v}) = 0$
$\vec{v}$

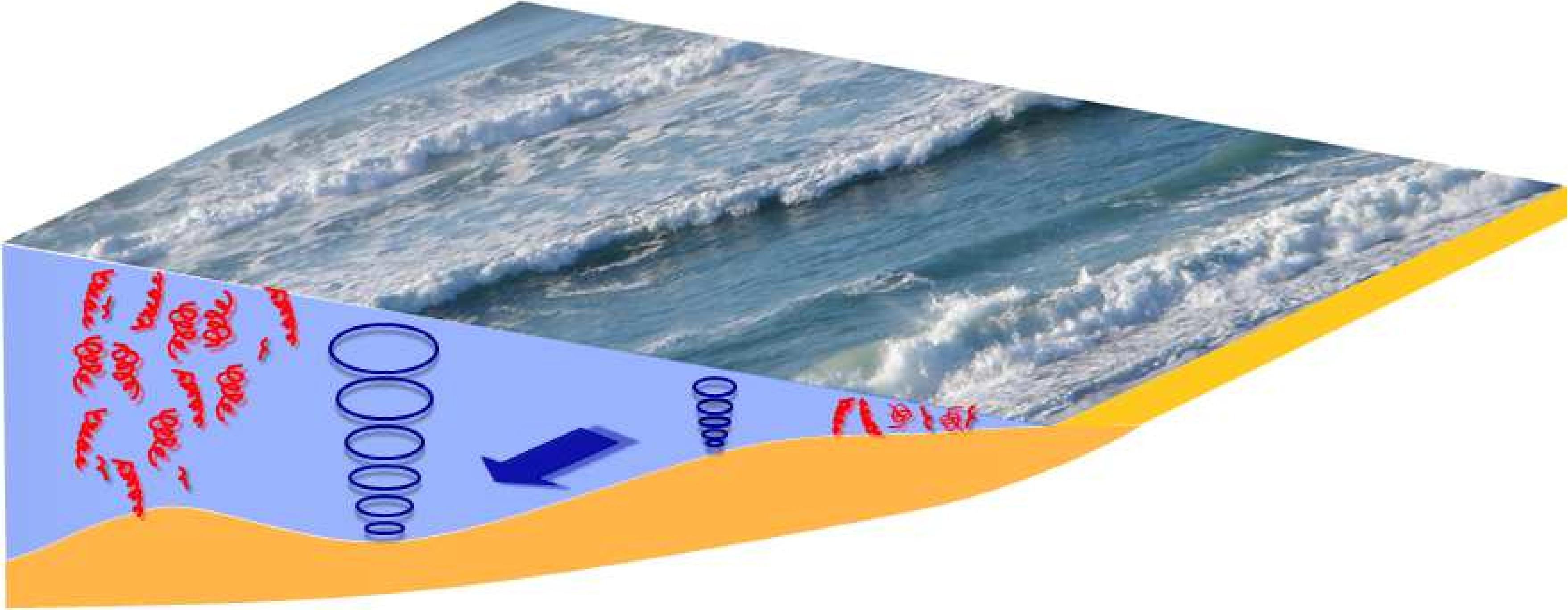

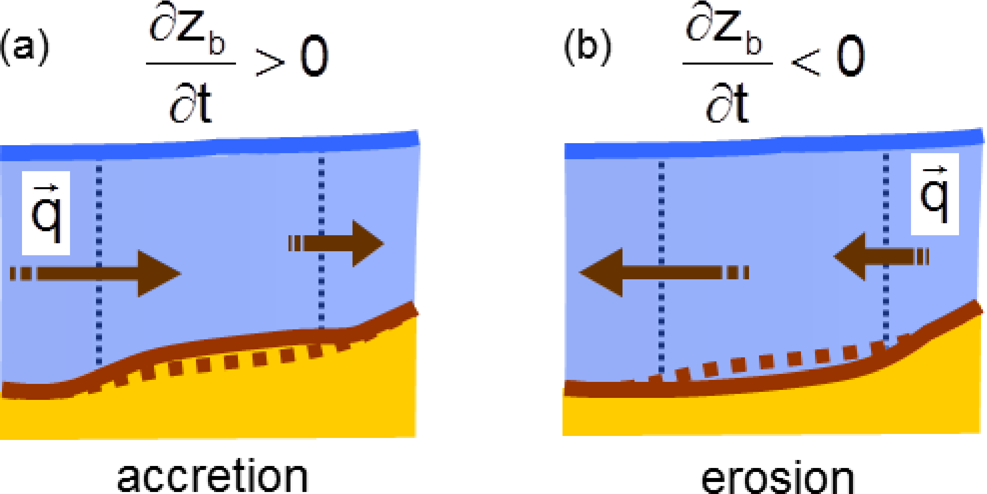
(a)
$\frac{\partial z_b}{\partial t} > 0$
$\vec{q}$
accretion
(b)
$\frac{\partial z_b}{\partial t} < 0$
$\vec{q}$
erosion

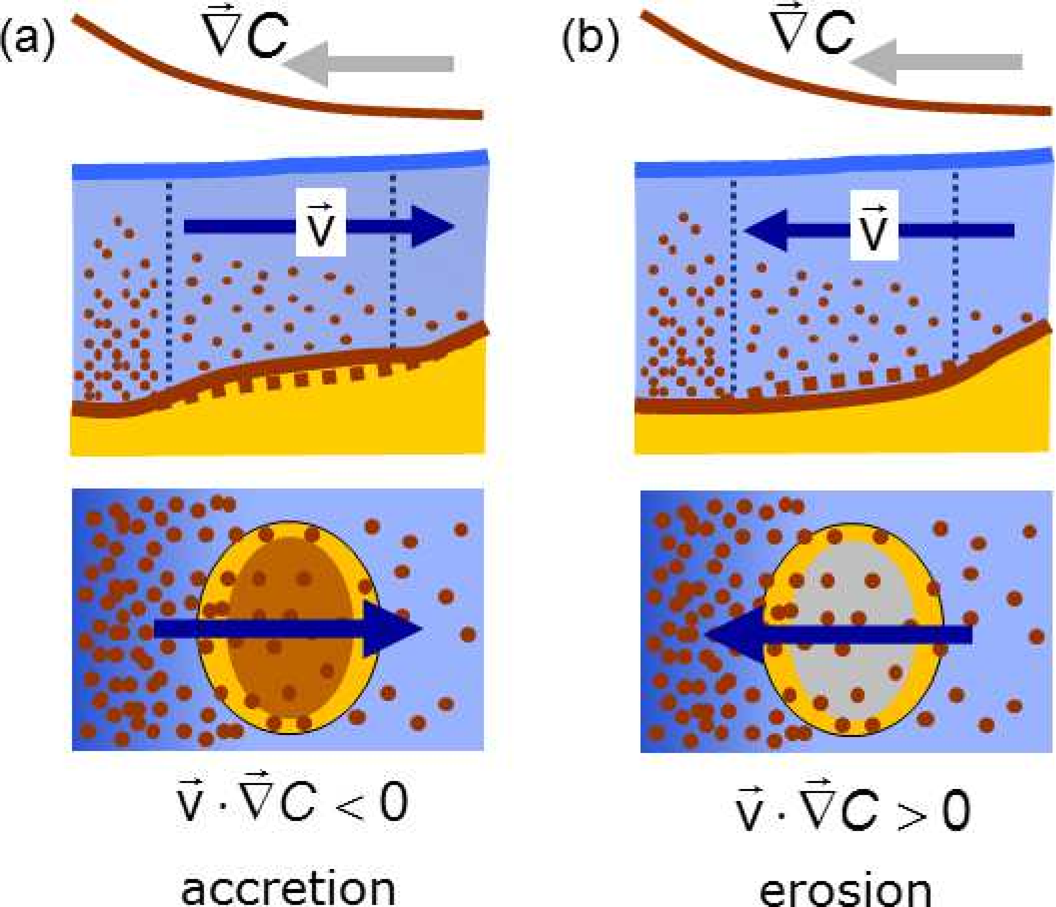
(a)
$\vec{\nabla} C$
$\vec{v}$
$\vec{v} \cdot \vec{\nabla} C < 0$
accretion
(b)
$\vec{\nabla} C$
$\vec{v}$
$\vec{v} \cdot \vec{\nabla} C > 0$
erosion

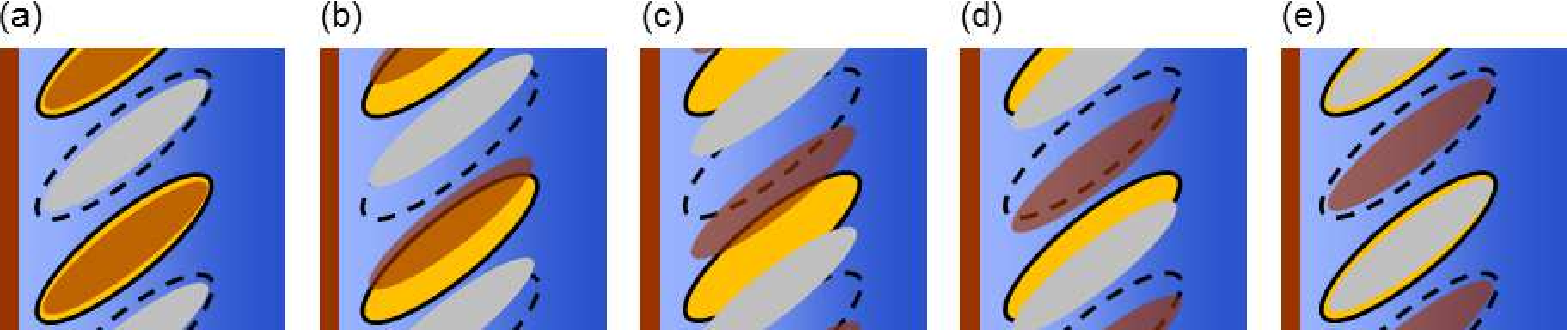

(a)
(b)
(c)
(d)
(e)

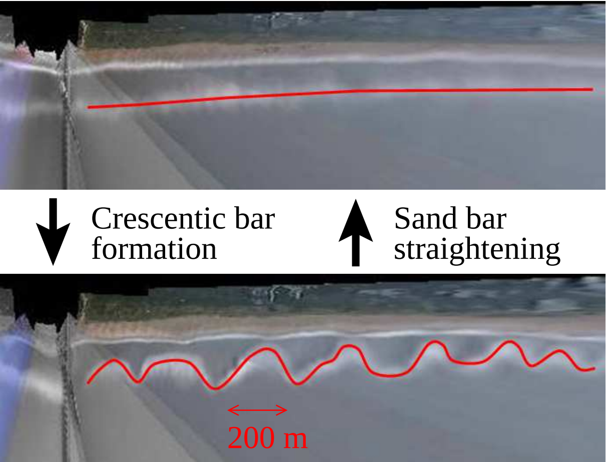
Crescentic bar
formation
Sand bar
straightening
200 m

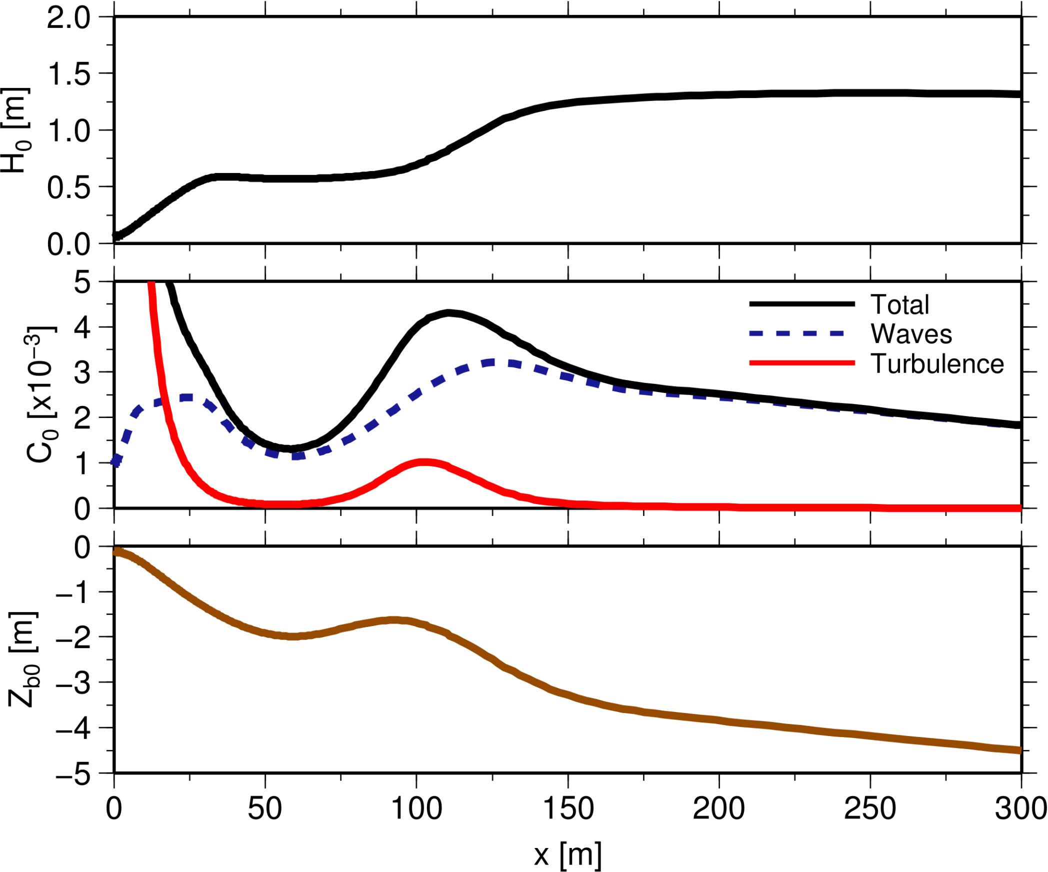

2.0
1.5
1.0
0.5
0.0
H0 [m]
5
4
3
2
1
0
C0 [x10−3]
Total
Waves
Turbulence
0
−1
−2
−3
−4
−5
Zb0 [m]
0
50
100
150
200
250
300
x [m]

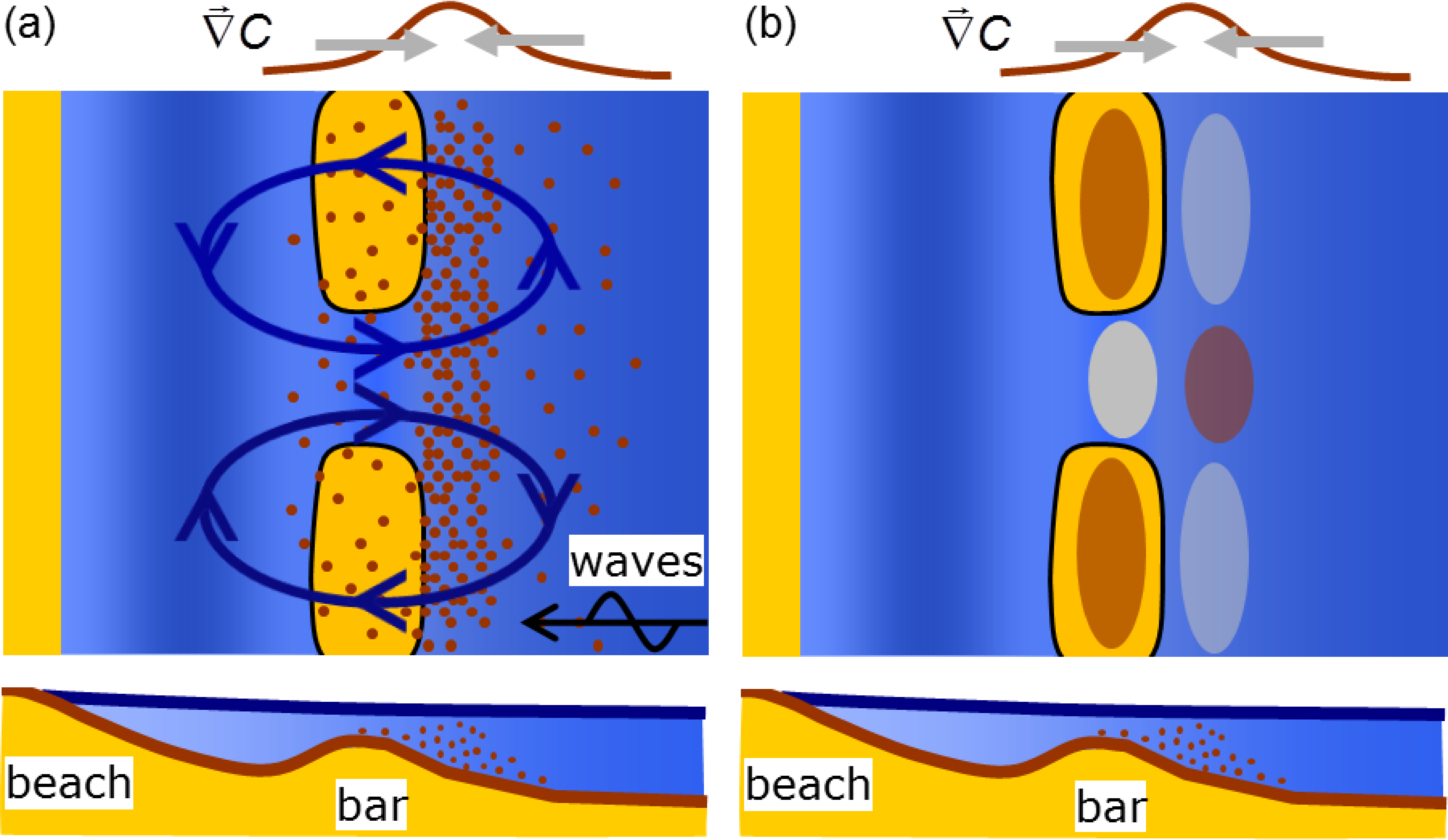
(a)
$\vec{\nabla}C$
waves
beach
bar
(b)
$\vec{\nabla}C$
beach
bar

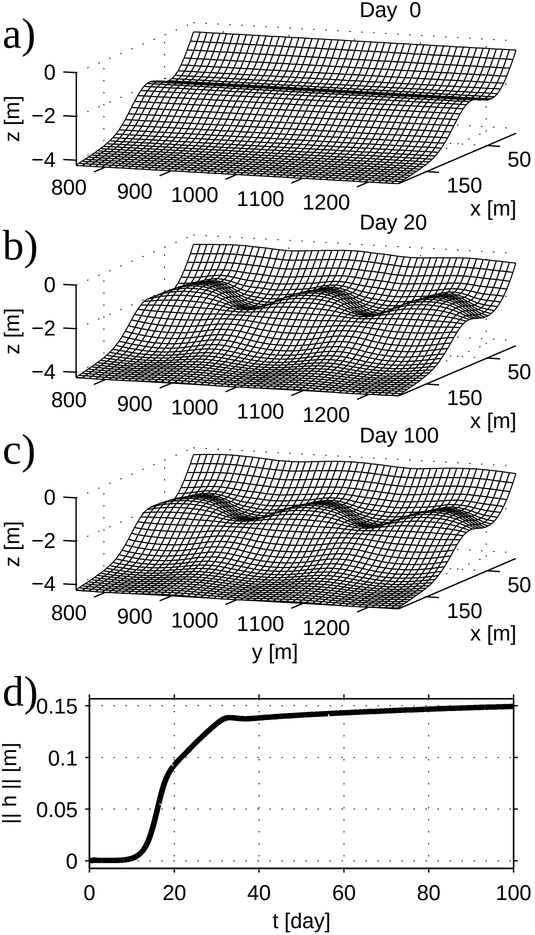

a)
Day 0
0
−2
−4
z [m]
800
900
1000
1100
1200
50
150
x [m]
b)
Day 20
0
−2
−4
z [m]
800
900
1000
1100
1200
50
150
x [m]
c)
Day 100
0
−2
−4
z [m]
800
900
1000
1100
1200
y [m]
50
150
x [m]
d)
0.15
0.1
0.05
0
|| h || [m]
0
20
40
60
80
100
t [day]

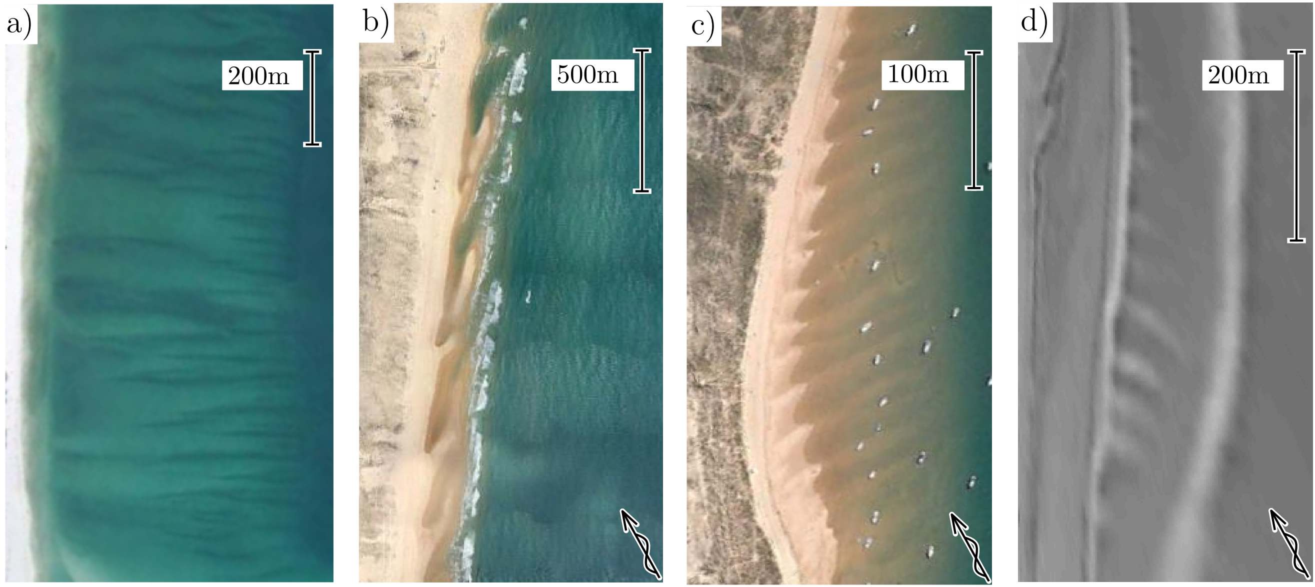
a)
200m
b)
500m
c)
100m
d)
200m

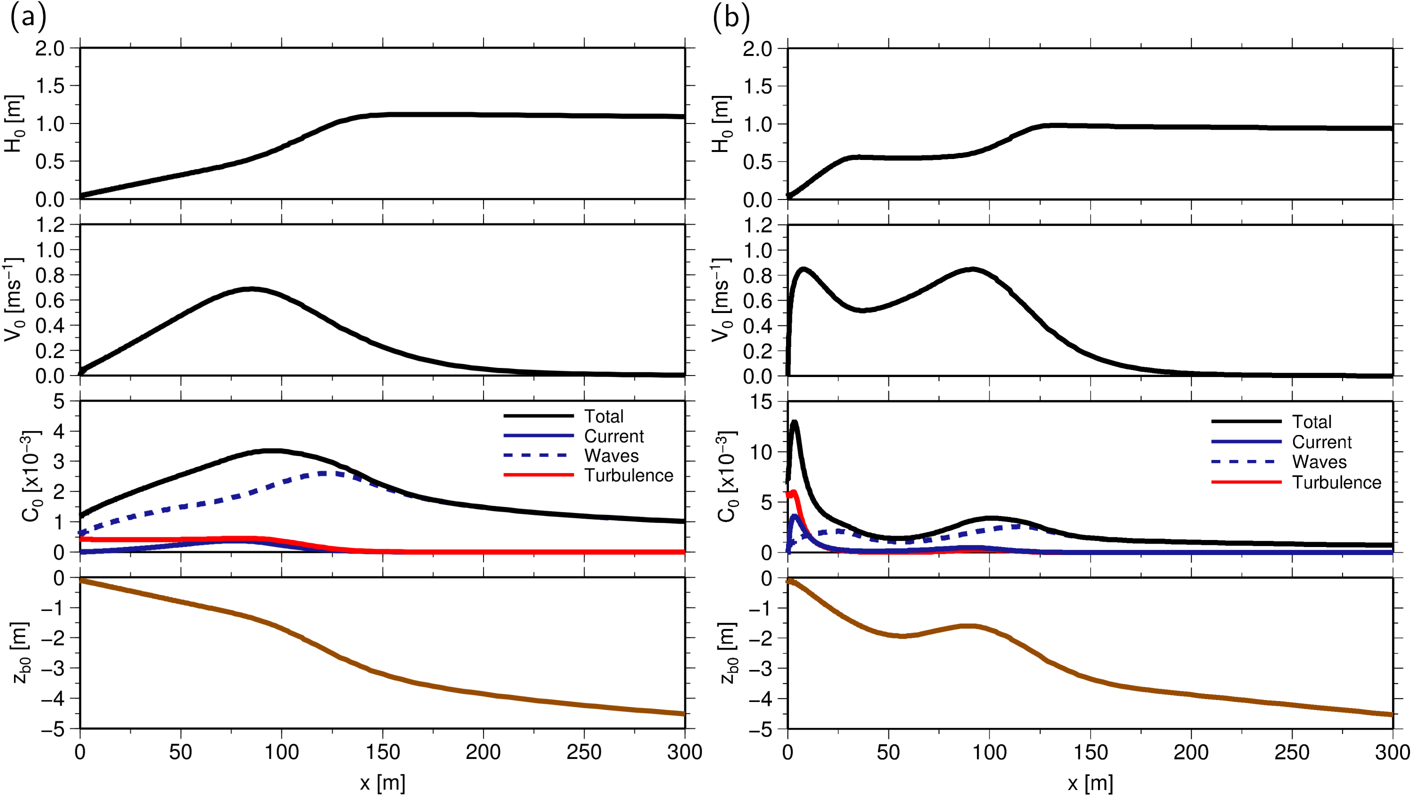

(a)
(b)
H0 [m]
V0 [ms−1]
C0 [x10−3]
zb0 [m]
Total
Current
Waves
Turbulence
x [m]

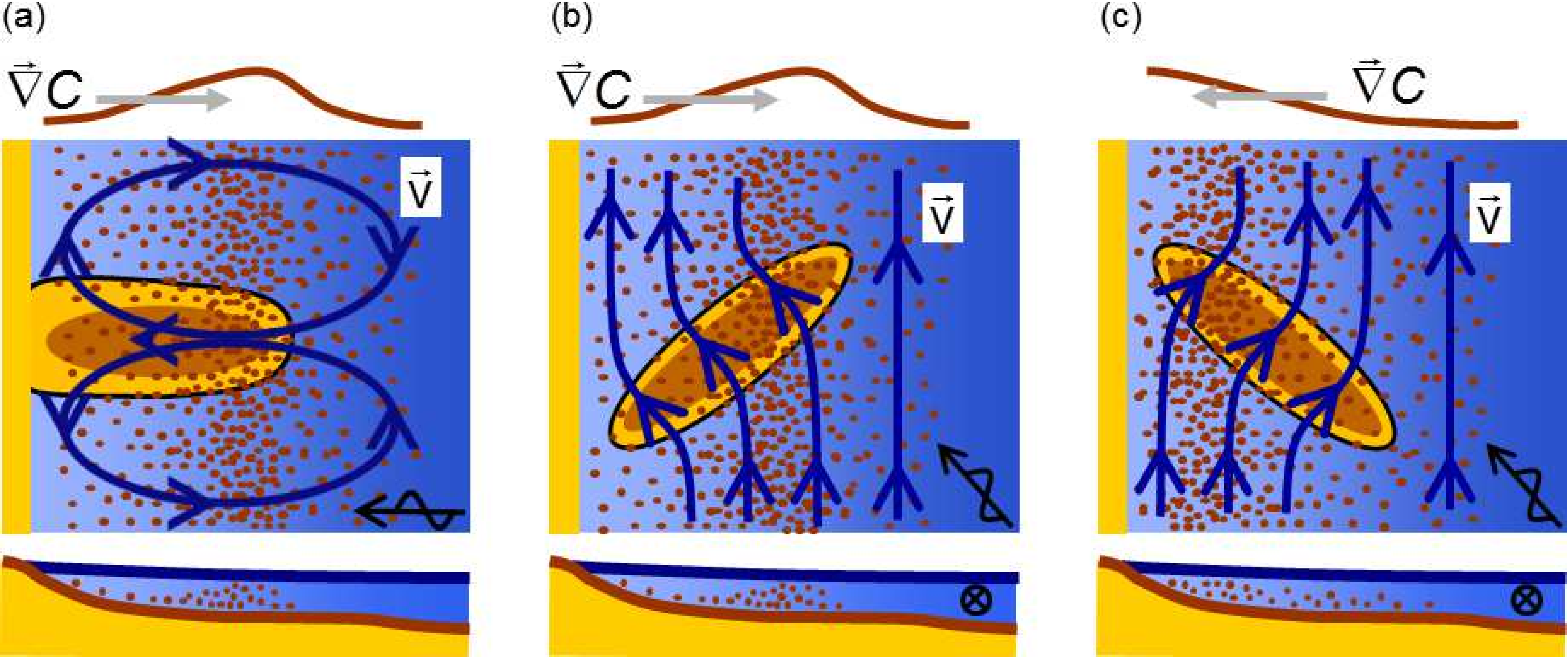

(a)
(b)
(c)
$\vec{\nabla}C$
$\vec{\nabla}C$
$\vec{\nabla}C$
$\vec{v}$
$\vec{v}$
$\vec{v}$

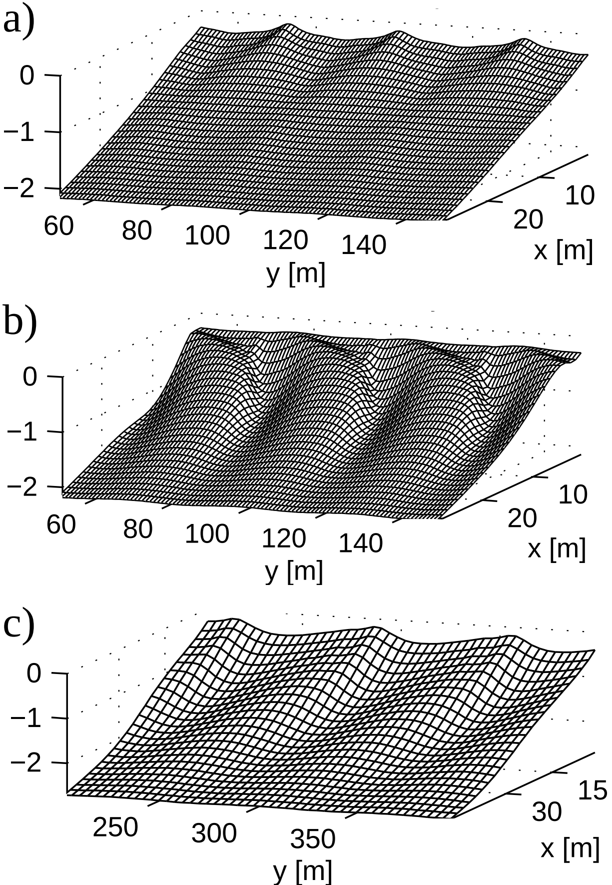

a)
0
−1
−2
60
80
100
120
140
y [m]
10
20
x [m]
b)
0
−1
−2
60
80
100
120
140
y [m]
10
20
x [m]
c)
0
−1
−2
250
300
350
y [m]
15
30
x [m]

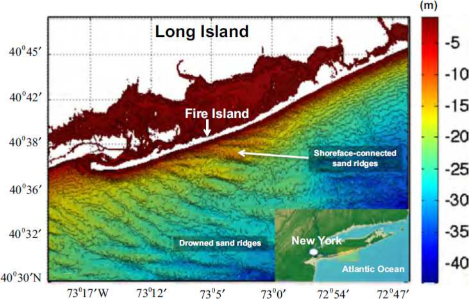

Long Island
Fire Island
Shoreface-connected sand ridges
Drowned sand ridges
New York
Atlantic Ocean
40°45′
40°42′
40°38′
40°36′
40°32′
40°30′N
73°17′W
73°12′
73°5′
73°0′
72°54′
72°47′
(m)
-5
-10
-15
-20
-25
-30
-35
-40

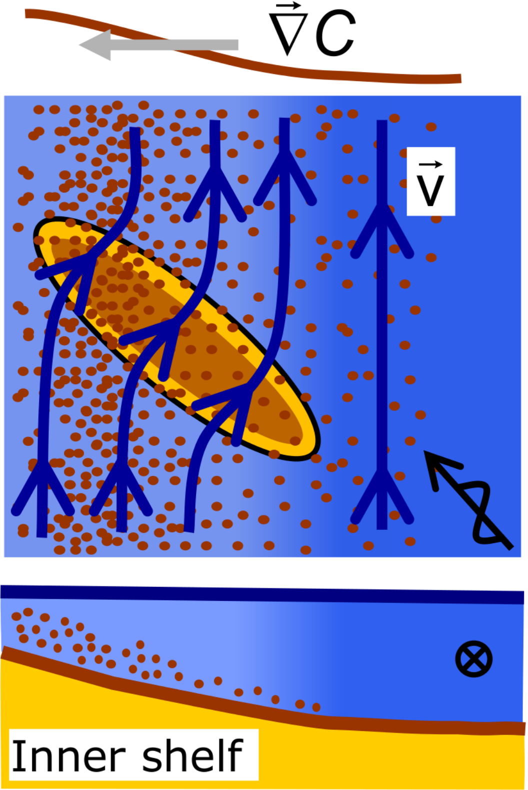

$\vec{\nabla} C$
$\vec{V}$
Inner shelf

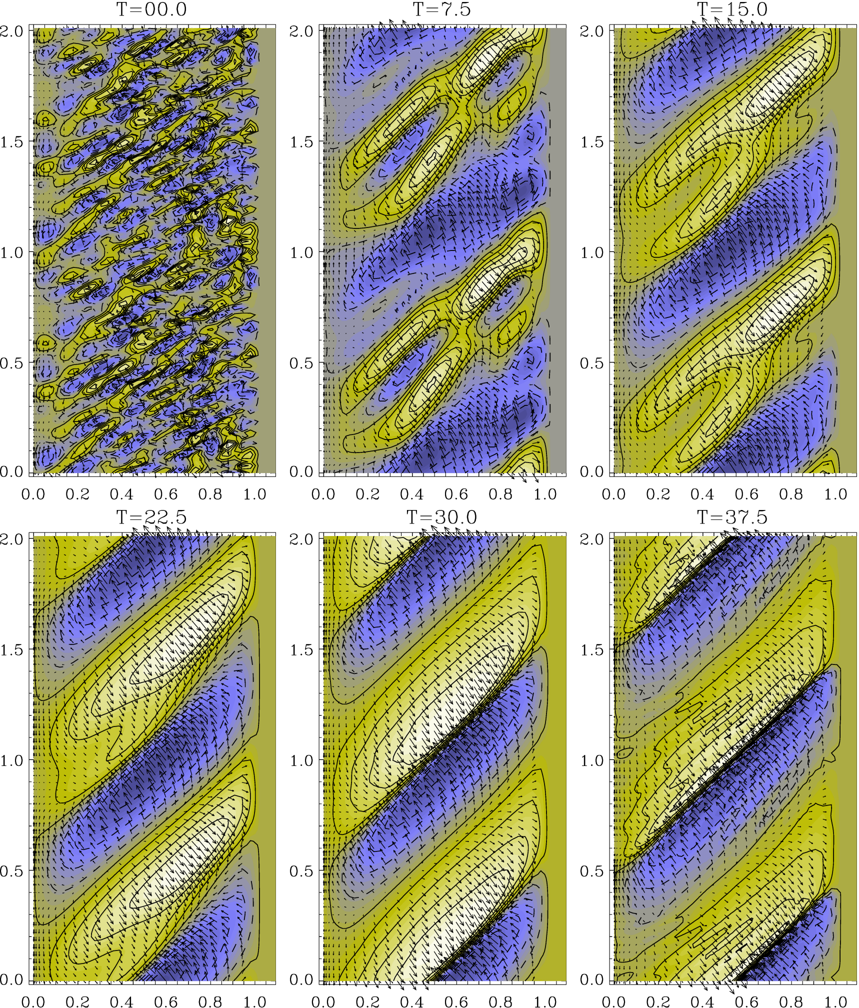

T=00.0
T=7.5
T=15.0
T=22.5
T=30.0
T=37.5
2.0
1.5
1.0
0.5
0.0
0.0
0.2
0.4
0.6
0.8
1.0

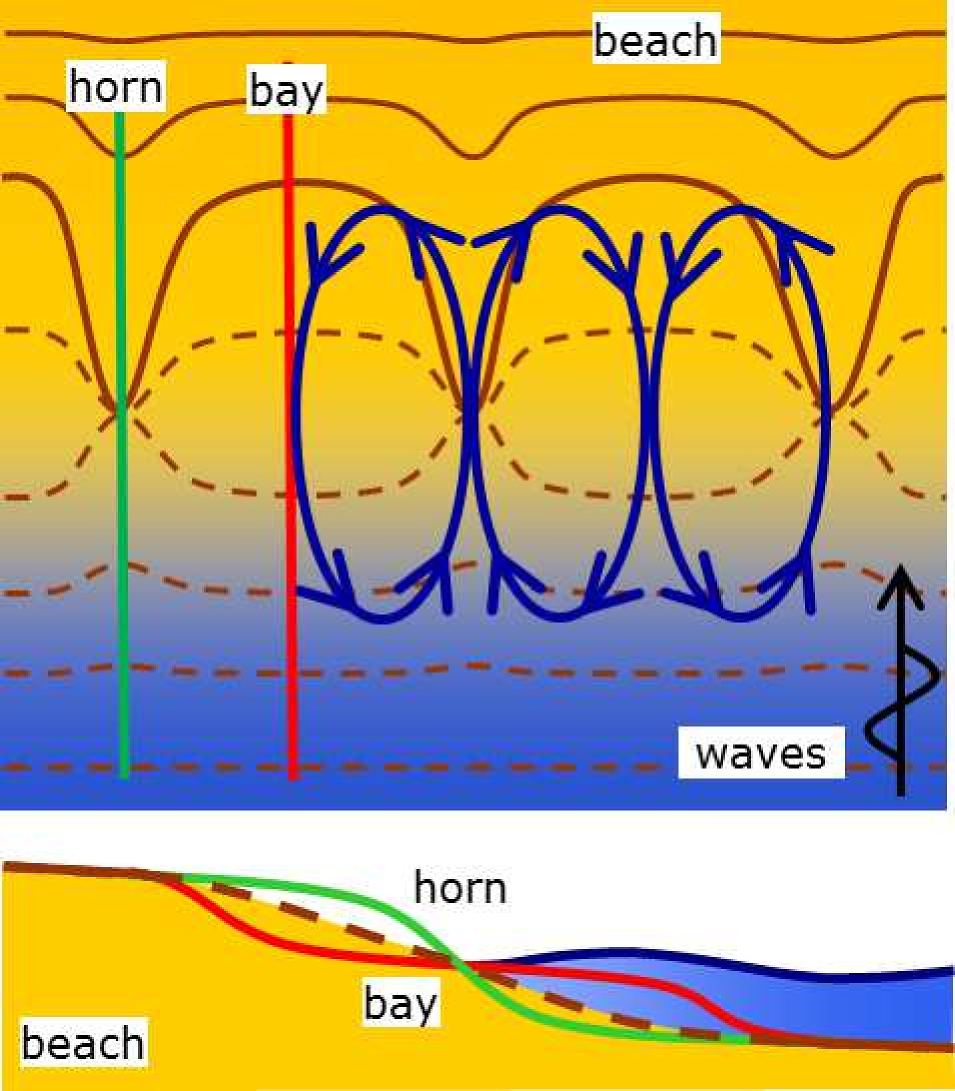
beach
horn
bay
waves
horn
bay
beach

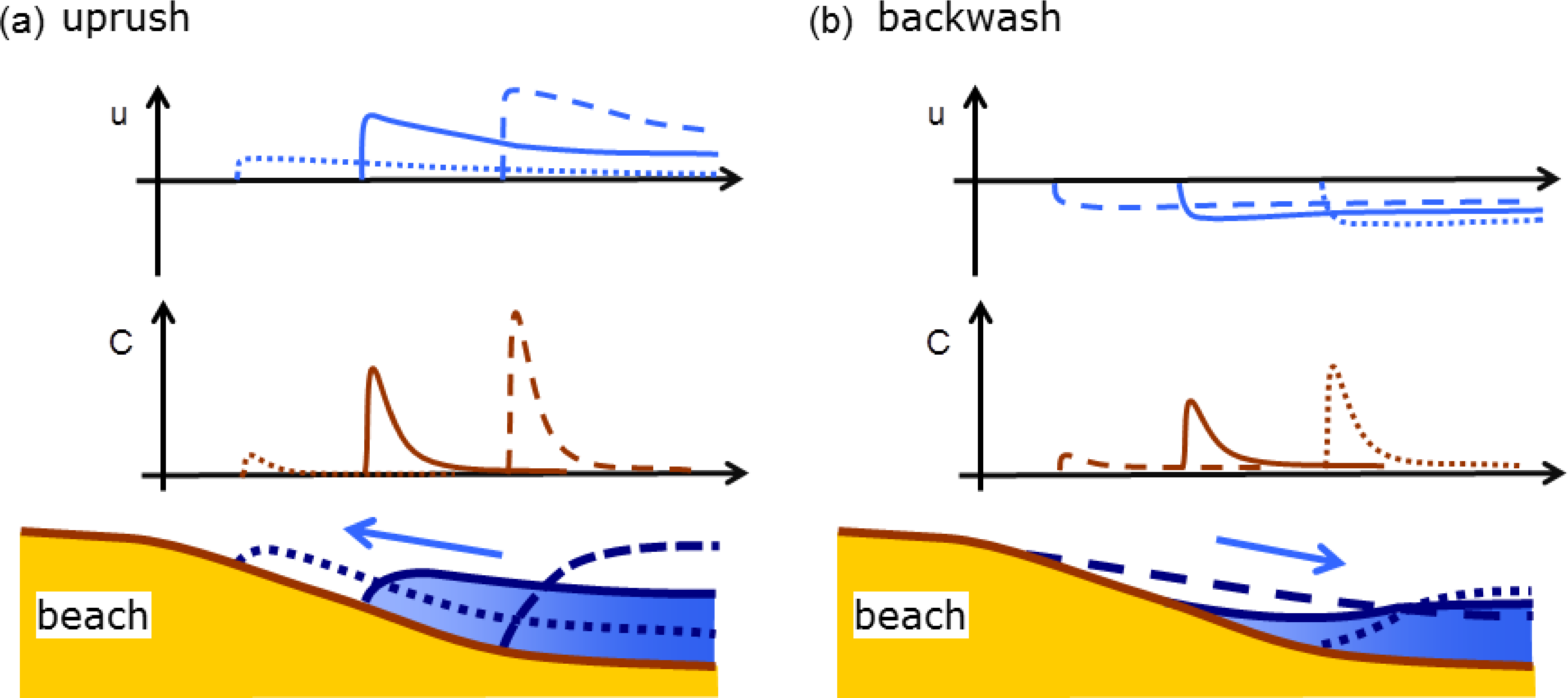

(a) uprush
(b) backwash
u
C
beach
u
C
beach

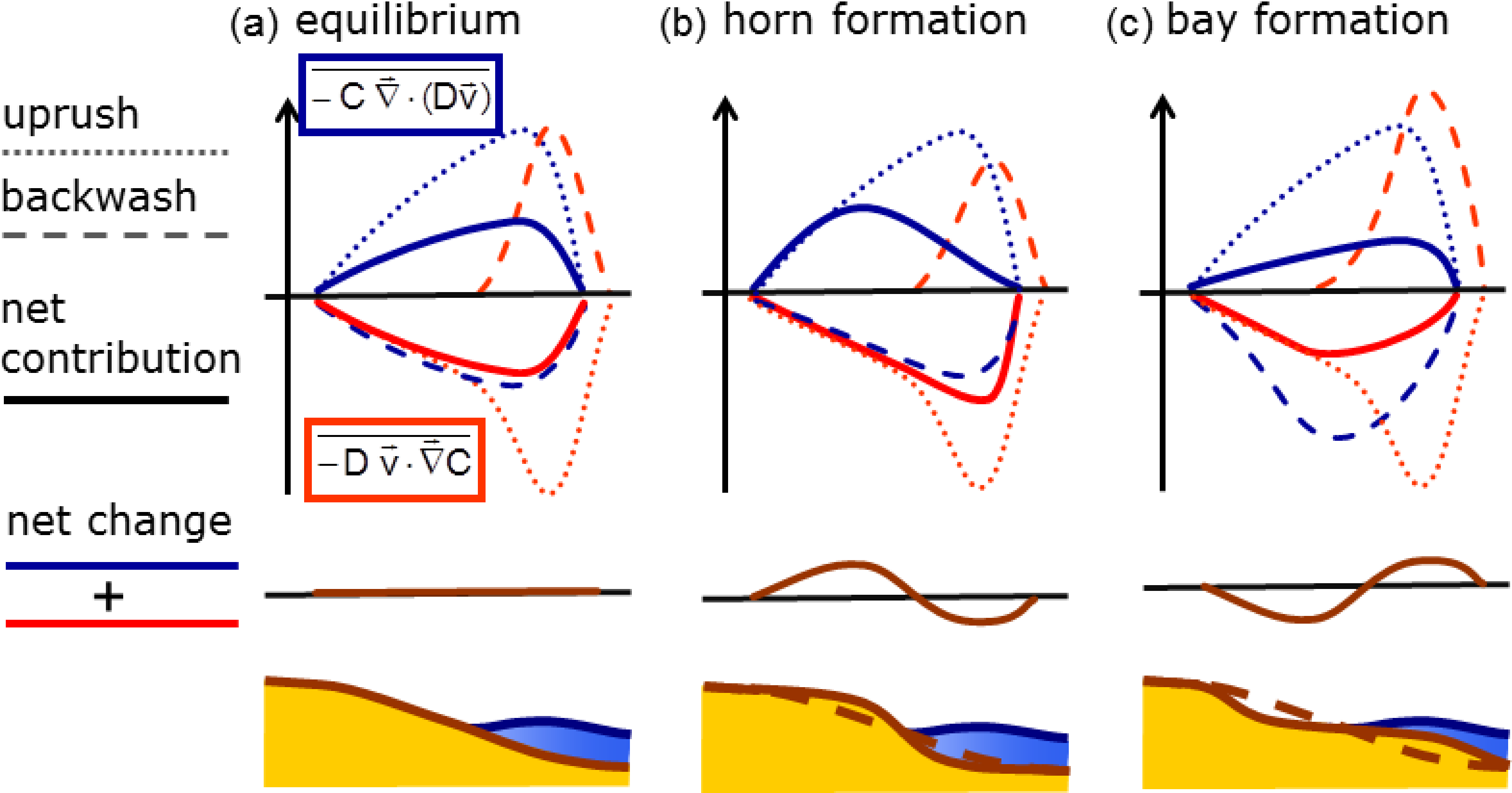

(a) equilibrium
(b) horn formation
(c) bay formation
uprush
backwash
net contribution
net change
+
$\overline{-C\,\vec{\nabla}\cdot(D\vec{v})}$
$\overline{-D\,\vec{v}\cdot\vec{\nabla}C}$

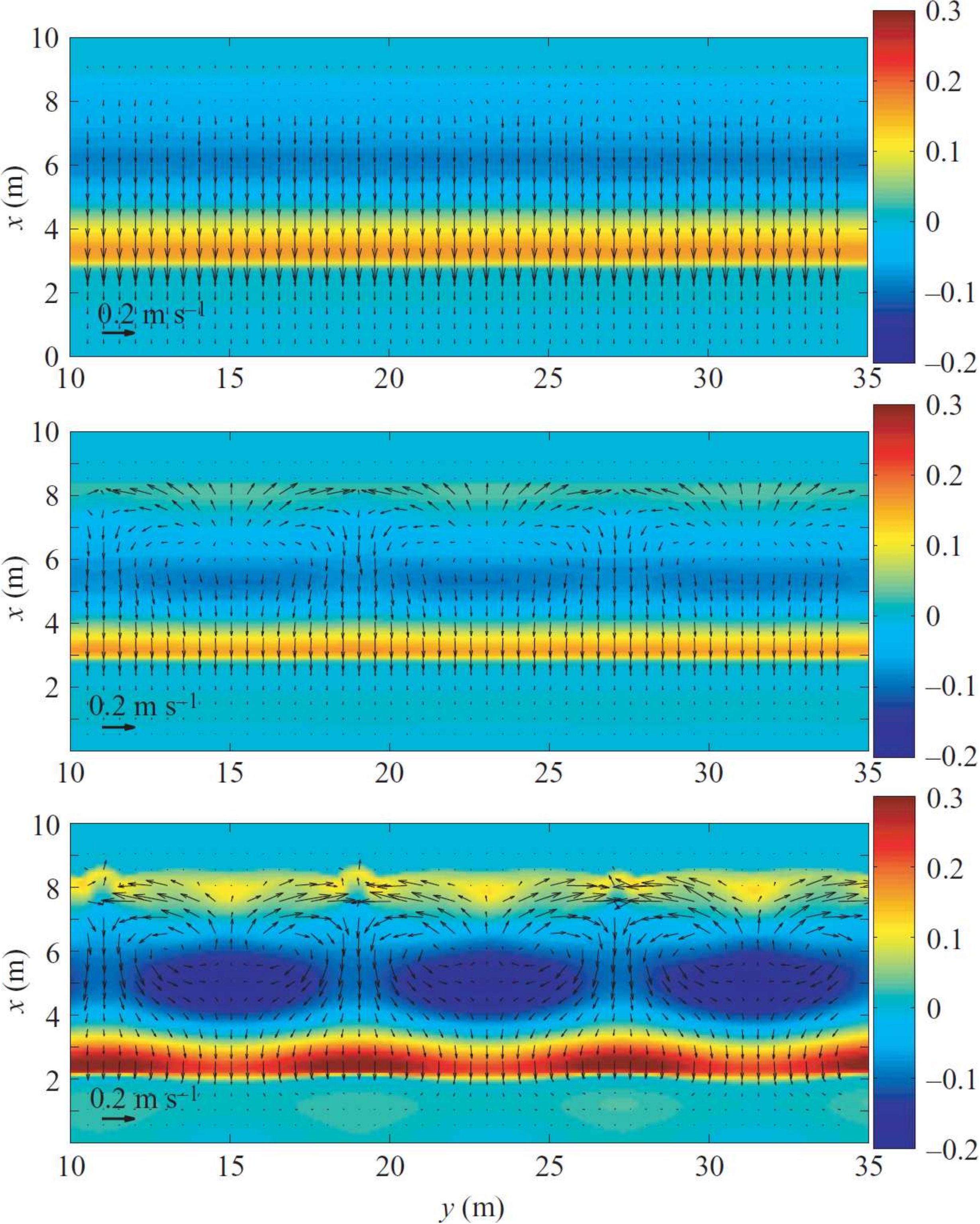

0.2 m s^{-1}
0.2 m s^{-1}
0.2 m s^{-1}
x (m)
y (m)
10
8
6
4
2
0
10
15
20
25
30
35
0.3
0.2
0.1
0
−0.1
−0.2

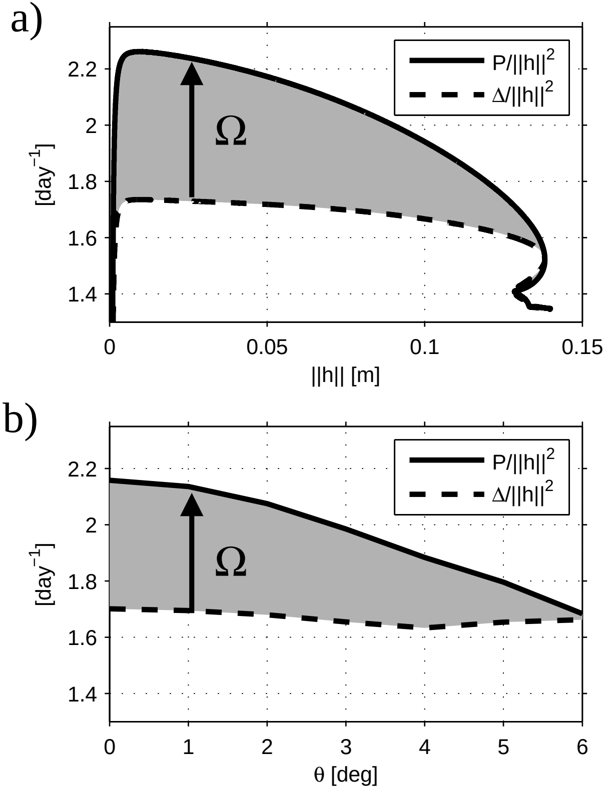

a)
P/||h||^2
Δ/||h||^2
Ω
[day^{-1}]
2.2
2
1.8
1.6
1.4
0
0.05
0.1
0.15
||h|| [m]
b)
P/||h||^2
Δ/||h||^2
Ω
[day^{-1}]
2.2
2
1.8
1.6
1.4
0
1
2
3
4
5
6
θ [deg]